ANNUAL REPORT

Nuclear Physics Laboratory

University of Washington

April, 1989

DISCLAIMER

DISCLAIMER

**Portions of this document may be illegible
in electronic image products. Images are
produced from the best available original
document.**

Cover Photo

Our cover photo is a monochrome montage of two touch-screen color displays that are part of the control system for our booster. When the cover is opened one sees on the upper left of the back cover the injector deck where two of the ion sources are now located. Also indicated below the tandem injection line is the new polarized ion source. On the front cover the booster itself is seen. The beam completes a loop starting at upper left and eventually exiting to the experimental areas (not shown) above the crossover. Touching any of the elements seen, such as cryostats, magnets, pumping stations or diagnostic elements, calls up new display pages which enable one to check the status of or change the parameters of the elements involved.

The display was generated by Mark Howe and photographed by Mary Levine. The cover was designed by Michael Strong of the Office of University Publications.

INTRODUCTION

Our new superconducting booster has been in operation now for over a year. It has proven to be quite reliable—no resonators have had to be replaced this past year and no scheduled runs had to be cancelled because of booster failures. Examples of performance achieved include the acceleration to 14 MeV/nucleon for oxygen and 16 MeV/nucleon for helium. Booster beams have been utilized in a variety of studies including the production of high energy photons, the emission probabilities of single-nucleon and complex-fragment pre-equilibrium particles, in sub-barrier fusion reactions, and in a study of ^{127}Xe in relation to its use in a neutrino detector.

A comparison of the hard photon yield in heavy ion reactions for several different isotopic projectile-target combinations has been used to try to isolate collective effects in the production mechanism. For most comparison systems the isotopic dependence is much closer to that expected for a nucleon-nucleon bremsstrahlung production mechanism than for a collective nucleus-nucleus mechanism.

We have been pursuing the issue of shape changes of highly excited nuclei by looking at the spectrum shape and angular distribution of high energy gamma rays from the decay of the giant dipole resonance built on excited states. Measurements in highly excited compound nuclei near mass 90 show that the γ-ray anistropy (a_2 coefficient) increases with spin, and is nearly zero at low spin, demonstrating that the nuclear shape changes from spherical to deformed (most likely oblate). We have also been using statistical GDR decay to probe isospin purity at high excitation energy in light N=Z nuclei. There appears to be more mixing than expected in ^{28}Si in the E_x=47-63 MeV region.

An array of phoswich detectors has been constructed and used in an experiment with a 14 MeV/A oxygen beam to determine the dependence of the ratio of pre-equilibrium protons to alphas on impact parameter. Impact parameter ranges are defined by fission and evaporation residue tags, exploiting the angular momentum dependence of fission-evaporation residue competition.

The sensitivity of the "Eöt-Wash" rotating torsion balance has been significantly improved so that we now resolve differential acceleration down to 4 x 10^{-14}g. No evidence for a fifth force coupled to isospin has been observed. Short-range violations of the equivalence principle have also been searched for.

The new polarized ion source has also been in use for over a year now. We have recently measured and optimized the polarization of deuteron beams. Polarized protons from the source were used in the continuation of an experiment begun last year to study the low energy structure of ^{14}N in the ^{13}C($\vec{p}, p$) reaction.

A project to measure the polarization of protons produced in the ^{59}Co(^{3}He,$\vec{p}$) reaction has yielded data which is rather unusual in that the polarization values are quite large, about 0.3, and fairly constant with respect to both reaction angle and excitation energy. We have some ideas about the reaction mechanism that might be responsible for this polarization and are currently trying to understand the data quantitatively.

Electron-positron pairs produced in heavy ion collisions near the Coulomb barrier at GSI may result from decay of a neutral particle. We are developing a time projection chamber (TPC) in

order to directly reconstruct the trajectories of these lepton pairs and so test the neutral particle hypothesis. Following extensive simulations we have chosen methane as the chamber medium and are developing a prototype wire chamber readout system in a departure from the standard pad-array readout system. In the near future we plan to use our prototype TPC without magnetic field to look at leptons produced in ^{58}Ni+^{238}U near the Coulomb barrier to assess the quality of kinematic information available from this system under real conditions.

Last September the new PS196 (precision measurement of the antiproton mass) beamline was commissioned at LEAR. A beam profile monitor and energy degrader system developed here were installed and successfully tested. A precision superconducting solenoid and trap system was then installed, and in subsequent runs a record number of $\bar{p}$ were trapped and then cooled. Work continues this spring to refine cooling techniques to bring trapped antiprotons down to 4K and permit the start of mass measurements this summer. A spinoff of this program was the first measurement of the charge dependence of particle ranges (Barkas effect) for the $p - \bar{p}$ system.

An experiment to measure the γ-ray branching ratio of the unbound 5.17 MeV level of ^{14}O has been completed. This quantity can be used to determine the ^{13}N(p,γ) cross section at stellar energies and to establish the temperature/density conditions required for the 'hot' or β-decay limited CNO cycle.

We continue our collaboration in the Pegasys project at SLAC. This project proposes to place a target in the PEP ring in order to study deep inelastic scattering of electrons on nuclei. The Pegasys project passed several major milestones this past year. We participated in a new magnet design which provides an acceptance of $\pm19°$ and $\pm43°$ in the vertical and horizontal planes, centered on the beam axis. The cold cluster target will create a beam of mini condensates of 10^5 molecules of the target gas (H, D, N$_2$, Ne—Xe) in a 1 cm region along the beam. A draft proposal was presented to the SLAC nuclear physics advisory committee in January 1989.

The analysis of the data from the comparison of inclusive scattering of positive and negative pions from medium and heavy nuclei has been completed. For calcium, the cross sections and spectra are rather similar for both charges, but for lead the cross section for scattering negative pions is substantially larger than that for positive pions. For the lead target the spectra for negative pions are shifted to higher residual excitations from those of the positive pions. Both these observations are qualitatively consistent with a quasi-elastic picture for the scattering.

In the accelerator mass spectrometry (AMS) program we have continued our collaboration in a world-wide study of sources and sinks for methane, an important "greenhouse" gas, by measuring ^{14}CH$_4$ concentrations in methane from northern wetland environments and (most recently) in atmospheric methane. Preliminary results for atmospheric methane indicate a slight increase in ^{14}CH$_4$ with time but suggest that there is not a significant interhemispheric gradient. Further analysis of our ^{14}C tree ring profiles for the years 1962-63-64 suggests that CO$_2$ from biospheric decomposition plays a significant role in the photoassimilation of carbon by a tree, and that mixing within the tree stem of photosynthate from different branches is limited.

We close this introduction with a reminder that the articles in this report describe work in progress and are not to be regarded as publications or quoted without permission of the investigators. In each article the names of the investigators have been listed alphabetically, but where appropriate the names of those primarily responsible for the report have been underlined.

As always, we welcome applications from outsiders for the use of our facilities. As a convenient reference for potential users, the table on the following page lists the vital statistics of our accelerator. For further information please write or telephone Dr. W.G. Weitkamp, Technical Director, Nuclear Physics Laboratory, University of Washington, Seattle, WA 98195; (206) 543-4080.

We thank Maria Ramirez and Ida Tess for producing this report and Richard Seymour and Pamela Readdy for their assistance in typesetting this report.

Robert Vandenbosch
Editor

THREE STAGE TANDEM VAN DE GRAAFF ACCELERATOR

A High Voltage Engineering Corp. Model FN purchased in 1966 with NSF funds; operation funded primarily by the U.S. Department of Energy. See W.G. Weitkamp and F.H. Schmidt, "The University of Washington Three Stage Van de Graaff Accelerator," Nucl. Instrum. Meth. **122**, 65 (1974).

Available Energy Analyzed Beams

Ion	Max. Current (pμA)	Max. Practical Energy MeV
p,d	10	18
polarized p,d	0.1	18
He	2	27
Li	1	36
C	3	63
O	2	72
Si	0.3	90
Ni	0.2	99
I	0.01	108

BOOSTER ACCELERATOR

Our linac Booster Accelerator has become operational during the past year. We have successfully accelerated p, ^{4}He, ^{7}Li, ^{12}C, ^{16}O and ^{28}Si. We give in the following table maximum beam energies and expected intensities for these and several other representative ions.

Available Energy Analyzed Beams

Ion	Max. Current (pμA)	Max. Energy (MeV)
p	> 1	35
d	> 1	37
He	0.2	65
Li	0.1	94
C	0.6	170
N	0.03	198
O	0.2	196
O	0.1	217
Si	0.1	302
Cl	0.02	303
Ni	0.001	340

Contents

13 APPENDIX 74

1 ASTROPHYSICS

1.1 Gamma-Decay of the Unbound 5.17 MeV Level in ^{14}O

E.G. Adelberger, P.B. Fernández,[*] and A. García

The gamma width Γ_γ of the unbound first excited state in ^{14}O has astrophysical significance: it plays a major role in the determination of stellar environments where the hot CNO cycle can occur.[1] Since 1985 we had been pursuing an experiment to determine this gamma width through a γ-ray branching ratio measurement.[2] We used the ^{12}C(^{3}He,nγ)^{14}O reaction, and searched for 5.17 MeV γ-rays in coincidence with neutrons populating the first excited state in ^{14}O. During 1988 we concluded taking data with our improved apparatus and target,[3] and we finalized the analysis of the data. We obtained a value for the branching ratio $\frac{\Gamma_\gamma}{\Gamma} = (7.2 \pm 3.5) \times 10^{-5}$, which corresponds to $\Gamma_\gamma = (2.7 \pm 1.3)$ eV. This result is in good agreement with the range of expected values from theoretical calculations,[1] $\frac{\Gamma_\gamma}{\Gamma} = (3-6) \times 10^{-5}$.

We performed the final analysis of our n-γ coincidence data using a fitting function that had four components: accidental coincidences; the contribution due to the target gold backing; the remaining neutron scattering background[3]; and the ^{14}O decays. The random and backing contributions were kept fixed, while the amount of neutron scattering background and the number of ^{14}O decays were adjusted to minimize χ^2. We fitted our four sets of n-γ coincidence data simultaneously, to obtain $\frac{\Gamma_\gamma}{\Gamma} = (7.2 \pm 3.5) \times 10^{-5}$, with a reduced chi-squared $\chi^2 = 1.106$ for 186 degrees of freedom, $P_{\chi^2} = 16.4\%$. The major difference with our preliminary analysis[3] was the use of a narrower fitting region, prompted by the presence of unexplained yield in the n-γ coincidence spectra. Restricting the fitting region increased our value of the branching ratio by a factor of 2, and at the same time lowered the reduced chi-squared from its previous value of $\chi^2 = 1.282$ for 467 degrees of freedom, $P_{\chi^2} < 0.1\%$.

We performed several tests to check the consistency of our result. In particular, we repeated the analysis of the data assuming different energies for the coincident neutron and gamma ray; in this way, we checked whether our fitting code found n-γ coincidence strength regardless of the neutron and γ-ray energies. The tests that we performed indicated that our data was consistent (with non-negligible probability) *only* with the occurrence of n-γ coincidences originating in the decay of the first excited state in ^{14}O. Extensive details on the experiment and the data analysis can be found elsewhere.[4] We are currently preparing a paper for publication.

[*]Argonne National Lab, Physics Division, Bldg. 203, Argonne, IL.

[1]C. Funck and K. Langanke, Nucl. Phys. A **464** 90 (1987).

[2]Nuclear Physics Laboratory Annual Report, University of Washington (1986) p. 1.

[3]*Ibid.*, (1988) p. 1.

[4]P.B. Fernández, Ph.D. thesis, University of Washington (1989) unpublished.

1.2 ^{37}Ca β^+ Decay and the Efficiency of the ^{37}Cl Detector for Supernova Neutrinos

E.G. Adelberger, A. García, T. Lang,* and D. Moltz*

In order to estimate the flux of neutrinos incident on the earth using the Davis ^{37}Cl detector, one needs the Gamow-Teller strength distribution ($B(GT)$) for the ^{37}Cl(ν, e^-)^{37}Ar reaction. The best estimate of this $B(GT)$ has been obtained from the measured beta-delayed proton spectrum from the mirror decay: ^{37}Ca $\rightarrow$ ^{37}K $\rightarrow$ $p+^{36}$Ar. At high excitation energies the inferred $B(GT)$ strongly disagrees with the results of a 0° ^{37}Cl(p,n) measurement, the β-decay results show no evidence for the strong peak at $E_x \approx 8$ MeV seen in the (p, n) measurement. The delayed proton measurement, however, was interpreted on the assumption that all protons leave ^{36}Ar in its ground state.[1] Indeed, Adelberger and Haxton[2] have shown that high energy states in ^{37}K have a strong tendency to decay to the first excited state in ^{36}Ar. This would imply that a strong peak in the $B(GT)$ at high excitation energies in ^{37}K (consistent with the one seen in the (p, n) measurement) would not be identifiable in the $B(GT)$ deduced from the delayed proton measurement unless one can distinguish beta-decayed protons feeding the ^{36}Ar first excited state from those feeding the ^{36}Ar ground state. A measurement of the beta-delayed proton spectrum in coincidence with a ^{36}Ar (first excited $\rightarrow$ ground state) γ-ray is clearly necessary in order to estimate the flux of high energy neutrinos. Although the correction for delayed proton decays to the ^{36}Ar first excited state is expected to have only a small ($\approx 5\%$) effect on the efficiency for detecting the (relatively low-energy) solar neutrinos, it will have a much more pronounced effect for supernova neutrinos which have considerably higher average energies.

We have already made an exploratory run and we are soon going to perform the final experiment at Lawrence Berkeley Laboratory to measure the branching ratio of levels in ^{37}K that decay to the first excited state in ^{36}Ar. ^{37}Ca ($\tau_{\frac{1}{2}} = 175$ $msec$) is produced via the reaction ^{40}Ca(^{3}He,$\alpha 2n$) and brought to a remote counting station using a He-jet system. It is then deposited on a tape that carries away the long-lived radioactivities while letting us count the ^{37}Ca decays. Two NaI's and a telescope (gas counter for Δ E and silicon detector for E) will allow us to measure the desired branching ratios. In our exploratory run the main problems we solved were: 1) to get enough ^{37}Ca transported through the long capillary from the reaction site to the counting station; 2) to reduce the background from long lived radioactivities that saturated the NaI's. We are confident that our newly-designed counting station and tape drive unit will allow us to make a good determination of the branching ratios.

*Lawrence Berkeley Laboratory, Berkeley, CA, 94720.

[1] R.G. Sextro *et al.*, Nucl. Phys. **A234**, 130 (1974).

[2] E.G. Adelberger and W.C. Haxton, Phys. Rev. **C36**, 882 (1987).

1.3 Angular Momentum of Low Lying States in ^{127}Xe

E.G. Adelberger, A. Charlop, <u>A.García</u>, S. Gil,* J. Gundlach and S. Kailas

Spectroscopic information about levels below $E_x = 680$ keV in ^{127}Xe is important to determine the efficiency of an ^{127}I solar neutrino detector recently proposed by Haxton.[1] This ^{127}I detector is expected to have a capture cross section about ten times bigger than the ^{37}Cl detector. This led us to perform a $\gamma - \gamma$ angular correlation experiment to study low lying levels in ^{127}Xe. Last year we presented[2] results of our exploratory run where we showed that we were able to prepare a ^{127}Cs source (which β^+ decays to ^{127}Xe with a half life of 6.25 hs) strong enough to do the angular correlation. Our analysis of the test run data showed that many corrections that are often not very important turn out to be essential when dealing with a source with a rather short half life such as ^{127}Cs, due to rapid variations in the counting rate. In our final run we corrected for dead-time and pile-up effects in the three GeLi detectors using pulsers triggered by a small NaI detector viewing the same source. We were able to fit our angular correlations with χ^2's per degree of freedom of about one in every case. The feasibility of determining the efficiency of the neutrino detector via the $0°$ ^{127}I$(\frac{5}{2}^+)(p,n)^{127}$Xe reaction depends on which one of two possible assignments $(\frac{1}{2}, \frac{3}{2})^+$ is correct for two states lying at 321 keV and 412 keV. The angular correlation measurement allows us to exclude the I=$\frac{1}{2}$ possibility for the 321 keV level and the I=$\frac{3}{2}$ possibility for the 412 keV level (see Figure 1.3-1). Further analysis to obtain ft values for ^{127}Cs β-decays and mixing ratios of diverse electromagnetic transitions in ^{127}Xe is in progress. This latter information is useful for determining the efficiency of the neutrino detector using a ^{65}Zn neutrino source.

Figure 1.3-1. a_2 coefficient as a function of the mixing ratio for the first transition (δ_{01}). The full curve is calculated with $I_0 = \frac{1}{2}$ and the dotted with $I_0 = \frac{3}{2}$. The mixing ratio for the second transition (δ_{12}) has been obtained from Geiger's data.[4] The only possible assignment consistent with the data is $I_0 = \frac{1}{2}$.
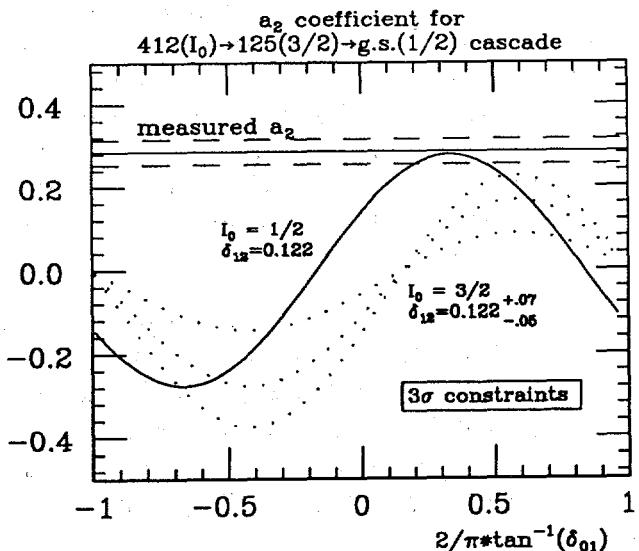
*Present Address: TANDAR, Comisión de Energía Atómica, Av. de Libertador 8250, Buenos Aires, Argentina 1429.

[1] W.C. Haxton, Phys. Rev. Lett. 60, 768 (1988).

[2] Nuclear Physics Laboratory Annual Report, University of Washington (1988) p. 3.

[4] J.S. Geiger et al., Ark. Fys. 36, 197 (1967).

2   GIANT RESONANCES

2.1   Deformation from GDR Decay Angular Distributions in Rapidly Rotating Nuclei Near A=40

J.H. Gundlach and <u>K.A. Snover</u>

Recently the spectral shapes and angular distributions of high energy gamma rays emitted in the statistical decay of hot, rapidly rotating compound nuclei near A=40 have been measured in this laboratory by M. Kićinska–Habior et al.[1,2]   Here we present results of calculated angular distribution anisotropies compared with the data, which provide evidence for deformed nuclear shapes, most likely oblate.

The sensitivity of the emission process to deformation arises from the dominance of the giant dipole resonance (GDR), which splits into several components in a deformed nucleus. The measured spectral shapes for the same temperature and different spin were found to broaden rapidly with spin, most likely due to increasing oblate splitting. This splitting is, however, not resolved in the strength function, due in part to the large contribution of thermal shape fluctuations.

An angular distribution anisotropy, on the other hand, provides model–independent evidence of deformation splitting of the GDR. The measurements (figure 2.1-1) show clear evidence for a negative a_2 coefficient on the low–energy side of the GDR, $E_\gamma \sim 11 - 17$ MeV, which is characteristic of either oblate noncollective or prolate collective rotation.

We have calculated the anisotropy expected for a rotating deformed liquid drop. The method, described earlier,[3] involves thermal averaging over a potential energy surface which in this case we assume to have a parabolic shape in the deformation parameters $(x,y) = (\beta\cos\gamma, \beta\sin\gamma)$ with a minimum located on the oblate noncollective axis ($\gamma = 60°$). The surface is then defined by β_o, the deformation at the minimum, and the curvature, the latter being fixed at 30 MeV, which is approximately correct for nuclei of this mass and temperature. Calculations of this type show that the anisotropy is a strong function of β_o, while for fixed β_o the anisotropy depends only weakly on spin and temperature.

Calculated results are shown in figure 2.1-1. Here β_o has been adjusted to match the data for $E_\gamma \geq 12$ MeV. For lower gamma ray energies, differences between data and calculation occur in part due to the fact that first chance γ–emission no longer dominates as assumed in the calculation. The inferred deformations are comparable or somewhat smaller than expected from the systematics of cold rotating liquid drops.[4] However, the values inferred here should be regarded as lower limits, since these same calculations fail by $\sim$30% to reproduce the large widths observed for the strength distributions.

---

[1] Nuclear Physics Laboratory Annual Report, University of Washington (1988) p. 5.

[2] *Ibid.*, (1987) p. 5.

[3] *Ibid.*, (1988) p.6; *Ibid.*, (1987) p.16; K.A. Snover, Cocoyoc '88; "Contemporary Topics in Nuclear Structure Physics," R.F. Casten *et al.*, eds., World Scientific, 1988, p. 251.

[4] S. Cohen *et al.*, Ann. Phys. **82**, 557 (1974).

4
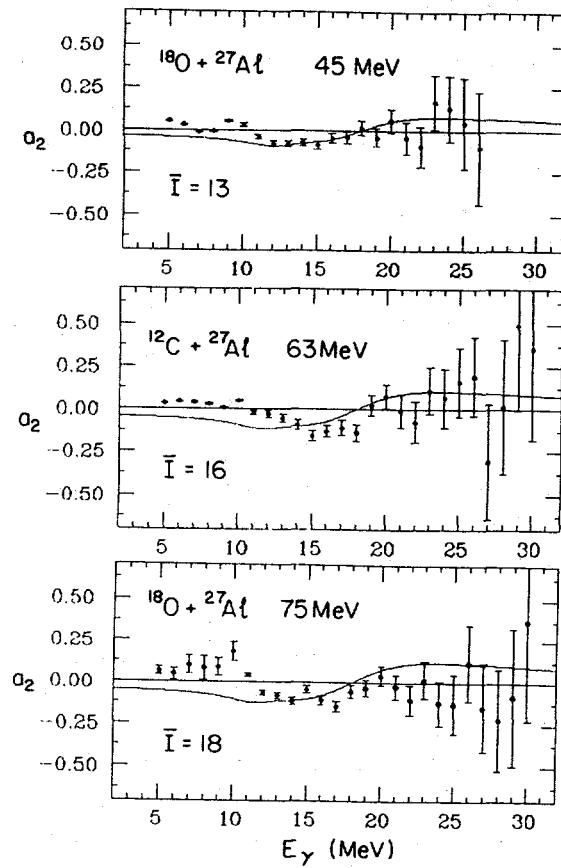
Figure 2.1-1. Measured a_2 coefficients (in the center–of–mass) for high energy γ emission in three different reactions, from Ref. 1. The curves are calculations (see text) with oblate deformation β_o = 0.10 (top), 0.13 (middle) and 0.15 (bottom). The mean final–state spins $\bar{I}$ are indicated on the figure.

2.2 Giant Dipole Gamma-Rays and Dynamic Shape Changes in Highly Excited Nuclei near A=90

J.A.Behr, C.A. Gossett, <u>J.H. Gundlach</u>, M. Kicinska-Habior,[*] K.T. Lesko,[†] K.A. Snover

We have used giant dipole resonance (GDR) γ-decay to probe the nuclear shape at moderate temperature and spins. Gamma-ray spectra and angular distributions from heavy ion fusion reactions using $^{18}O+^{72}Ge \rightarrow\ ^{90}Zr^*$ at $E_{proj} = 50$ and 74 MeV at this lab and from $^{28}Si +^{64}Ni \rightarrow\ ^{92}Mo^*$ at $E_{proj}=137$ MeV at LBL were measured. We used a 10"x15" and a 10"x10" NaI detector here and at LBL, respectively. Both detectors were gain stabilized, anticoincidence shielded, and passively shielded. Pulsed beam was essential for TOF neutron supression. Fixed GeLi detectors were used for an independent normalization check. The Ni target was self supporting while the Ge-target was backed and cooled. These reactions produced compound nuclei with average initial spins of $\overline{I} = 10\hbar, 23\hbar$, and $38\hbar$ and average temperatures (after GDR decay) of $\overline{T} \approx 1.6, 1.7$, and 2.0 MeV, respectively.

The measured spectral shapes were fitted with the Hauser-Feshbach code CASCADE using both one and two Lorentzian GDR strength functions. In all cases a strongly broadened strength function ($\Gamma_{FWHM} \geq 9MeV$) as compared to the ground state in ^{90}Zr ($\Gamma_{FWHM} = 4.1$)[1] was found with a total width which increases with spin and temperature. Since the two Lorentzians are not resolved, the γ-ray spectrum alone does not suffice to determine the nuclear shape.

Angular distributions were deduced relative to the CM of the compound nucleus and fitted with first and second order Legendre polynomials. The $a_2(E_\gamma)$ coefficients are shown in figure 2.2-1. A strong anisotropy characterizes the angular distributions below the GDR mean resonance energy for the two higher spin cases while the low spin case is nearly isotropic. The observed patterns are characteristic of γ-decay from an oblate non-collectively or prolate collectively rotating nucleus which is aligned by the initial fusion reaction. These data are qualitatively consistent with a classical liquid drop model, in which the nuclear shape is nearly spherical at the lowest spin, and becomes progressively more oblate with increasing spin. The $a_1(E_\gamma)$ Legendre coefficients were found to be small ($a_1(E_\gamma) \approx 0$) for $E_\gamma \geq 10.5MeV$, confirming statistical decay. Small but nonzero asymmetries at $E_\gamma \leq 10.5MeV$ were found for the two higher energy cases, and are attributed to decay following projectile excitation.

[*]Institute of Experimental Physics, University of Warsaw, Poland.
[†]Lawrence Berkeley Laboratory (LBL), Berkeley, CA 94720.
[1]B.L. Berman *et al.*, Rev. Mod. Phys. **47**, 713 (1975).
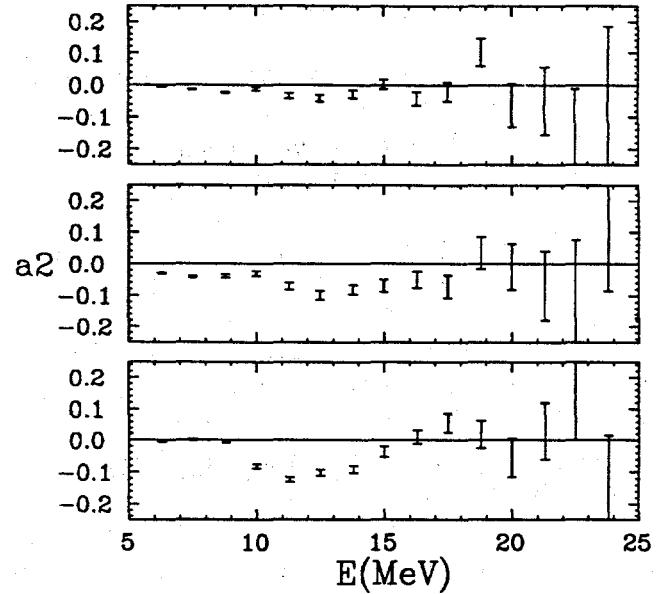
Figure 2.2-1. $a_2(E_\gamma)$ Legendre coefficients of the CM γ-ray angular distributions from the reactions $^{18}O+^{72}Ge\rightarrow$ $^{90}Zr^*$ at $E_{proj} = 50$ (top) and 74 MeV (middle) $^{28}Si +^{64}Ni\rightarrow$ $^{92}Mo^*$ at $E_{proj}=137$ Mev (bottom).

2.3 Giant Dipole Radiation and Isospin Purity in Highly Excited Compound Nuclei

J.A. Behr, C.A. Gossett, J.H. Gundlach, W.R. Hering,* and K.A. Snover

Given a compound nucleus with isospin T=0, its radiative decay through the giant dipole resonance built on lower-lying excited states will be isospin inhibited. This follows since, although γ-decay to the small percentage of T=1 final states, as well as γ-decay following nucleon emission, is isospin-allowed, γ-decay to the larger percentage of T=0 final states is isospin forbidden. We make such compound nuclei by using projectiles and targets with N=Z. By measuring the inclusive γ-ray yield in the GDR energy region, we infer the degree of isospin mixing in the compound nucleus.

For compound nuclei with sufficiently high excitation energy E^*, isospin is expected to become a better symmetry as E^* increases. Isospin mixing in the compound nucleus is related to the ratio of the Coulomb spreading width $\Gamma_{coul}^\downarrow$ to the compound nucleus decay width $\Gamma^\uparrow$. $\Gamma_{coul}^\downarrow$ is expected from sum rule arguments to be roughly constant, while $\Gamma^\uparrow$ must increase with E^*. Hence, a compound nucleus formed with a given T at high E^* will decay before the Coulomb interaction has time to mix it with states of different T. This is consistent with experiments to date.[1]

The degree of isospin mixing in ^{28}Si has been measured previously in this laboratory at low excitation energy.[2] At an initial excitation energy $E^*= 34$ MeV, the mixing was characterized by an isospin mixing parameter $\alpha^2 = 0.05$ (for small α^2, $\alpha^2 \sim \Gamma_{coul}^\downarrow/\Gamma^\uparrow$ [initial state] $+ \Gamma_{coul}^\downarrow/\Gamma^\uparrow$ [final states reached by γ decay]), so isospin was quite pure. We hope to test the theory of Reference

---

[1]H.L. Harney *et al.*, Rev. Mod. Phys., **58**, 607 (1986).

[2]M.N. Harakeh *et al.*, Phys. Lett. **B176**, 297 (1986).

1 of symmetry breaking in compound nuclear systems by extending these measurements to higher E^* and heavier N=Z nuclei.

In the present study, we have measured inclusive γ-ray cross-sections with our $10''x15''$ NaI spectrometer for the reactions $^{16}O+^{12}C$, $^{16}O+^{13}C$, $^{18}O+^{12}C$, and $^{15}N+^{13}C$ at projectile energies from 40 to 217 MeV from our Tandem and Linac, forming compound nuclei at up to $E^*= 110$ MeV and of initial isospin 0, 1/2 and 1. Pulsed-beam time-of-flight techniques were used to eliminate neutrons. The self-supporting ^{12}C and ^{13}C foils of 400-800 $\mu g/cm^2$ thickness were supplied by H. Folger of GSI. A 0.6% (atomic) stainless steel contaminant in the ^{12}C target used required a measured correction of $\leq 5\%$ to the high-energy γ spectra.

Using a version of the CASCADE statistical model code which includes mixed isospin symmetry[2], our goal is to consistently fit γ spectra near the GDR energy ($E_\gamma \approx 12$-30 MeV) from these reactions with different T to extract the isospin mixing in the T=0 ^{28}Si. We see a suppression of the GDR region γ-ray yield from the isospin-inhibited $^{16}O+^{12}C$ reaction, compared to the isospin-allowed reactions, by factors of 2-3. A comparison of the ratio of the experimental cross-sections for $^{16}O+^{12}C$ and $^{16}O+^{13}C$ with a statistical calculation using default parameters yields, for both $E^*=47$ and 63 MeV in ^{28}Si, $\alpha^2 \approx 0.15$. Thus the mixing seems, surprisingly, to be larger at higher excitation energies than at $E^*=34$ MeV. In order to be sure this result is reliable, it is particularly important that we be certain we understand the isospin-allowed emission process—to this end we are currently analyzing the $^{18}O+^{12}C$ and $^{15}N+^{13}C$ reactions.

In contrast to the lower-energy spectra discussed above, our data at the higher excitation energies of 82 and 110 MeV appear to contain contributions from nuclear bremsstrahlung at γ-ray energies above the GDR energy, and this contribution must be understood in order to extract information about isospin purity from statistical decay. We hope to do this from the systematics of the spectrum shapes as a function of projectile energy and γ-ray energy.

8

3 HEAVY ION INDUCED REACTIONS

3.1 High Energy γ Emission in C + Mo Reactions at E/A $\sim$ 10 MeV

J.A. Behr, C.A. Gossett, W.R. Hering,[*] S.J. Luke, B.T. McLain, D.P. Rosenzweig, and K.A. Snover

Hard photon production in heavy ion collisions at E/A < 20 MeV is poorly understood. We have investigated both the bombarding energy dependence and projectile/target isotope dependence of the high energy γ production for ^{12,13}C + ^{92,100}Mo reactions near E/A $\sim$ 10 MeV.

Recently, Butsch[1] and collaborators have reported that they observed a strong target isotope dependence of the high energy γ yield from ^{12}C + ^{112,124}Sn reactions at 8 and 12 MeV/A. They found that the yield of photons with E_γ > 30 MeV for the ^{124}Sn target was much larger than that for the ^{112}Sn target and they suggested that this difference could be attributed to production from a collective mechanism. One would expect collective production of γ-rays to scale as the square of the E1 effective charge, $(\frac{Z_p}{A_p} - \frac{Z_t}{A_t})^2$, leading to a ratio (^{12}C +^{124}Sn)/(^{12}C+^{112}Sn) = 3.26.

We chose to study the systems ^{12}C + ^{92,100}Mo at 9-14 MeV/A and ^{13}C + ^{92,100}Mo at 10,11 MeV/A for which large relative yields would be predicted if indeed the production mechanism were dominated by collective effects. High energy carbon beams from the NPL Superconducting Linac were incident on isotopically enriched Mo targets, and the photons were detected in the 10 in by 15 in NaI scintillator detector.[2] Angular distributions were also measured for ^{12}C + ^{92,100}Mo at 11 MeV/A.

The figure below shows the photon production cross-sections for ^{12}C + ^{100}Mo and ^{12}C + ^{92}Mo as a function of bombarding energy. The ratio of the yields, 1.6 ± 0.1, is fairly constant with beam energy and is much smaller than the 3.39 predicted for a collective production mechanism. The difference in the cross-sections is somewhat greater than the ratio of 1.06 which would be expected from a nucleon-nucleon mechanism. However, even more striking than the above comparison, are the comparisons of the yields for other projectile combinations. Ratios of yields of roughly 60 would be expected for (^{13}C+^{100}Mo)/(^{13}C+^{92}Mo) and for (^{13}C+^{92}Mo)/(^{12}C+^{92}Mo) if collective effects dominated. The measured ratios were 1.1 ± 0.1 and 1.3 ± 0.1 for these two pairs of systems, respectively, in relatively good agreement with production via a nucleon-nucleon production bremsstrahlung mechanism.

Figure 3.1-1. Production cross-sections for high energy γ-rays with E_γ >30 MeV for ^{12}C + ^{100}Mo and ^{12}C + ^{92}Mo as a function of bombarding energy for Θ_{lab} = 90°.

---
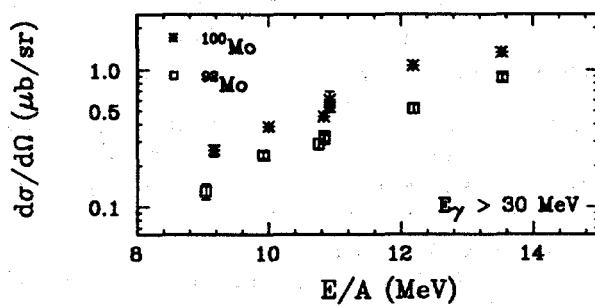
[*]University of Munich, Sektion Physik, Schellingstrasse 4 D-8000 Muenchen 40, W. Germany.

[1]R. Butsch, et al., Bull. Am. Phys. Soc. **33**, 980 (1988), and private communication.

[2]Nuclear Physics Laboratory Annual Report, University of Washington (1988) p. 82.

3.2 High Energy γ-Rays from ^{14}N + Ag at 35 MeV/A

W. Benenson,[*] J. Clayton,[*] K. Joh,[*] D. Krofcheck,[*] S.J. Luke, T. K. Murakami,[*] J. Stevenson,[*] and R. Vandenbosch

There has been a great deal of experimental investigation into the emission of high energy gamma rays from heavy ion collisions in recent years. The interesting feature of the data is that it is possible to obtain photons which have an energy greater than the energy per nucleon of the beam. This observation has raised the question as to what the mechanism is which produces these high energy photons. The mechanism which seems to be the most likely candidate is photon production through nucleon-nucleon bremsstrahlung. In this model a proton from the projectile collides with a neutron from the target (or vice versa) and produces photons through bremsstrahlung.[1] It is possible, in this model, for the nucleons in either case to couple their momentum of relative motion with their Fermi momentum to produce the highest energy gamma rays. In this spirit Randrup and Vandenbosch have extended their nucleon-exchange transport (NET) model for the the production of hard neutrons[2], to include the production of high energy photons.[3] In the past year we have began an experimental program to study the production of high energy photons, in order to determine how sensitive the model is to various components.

We chose to study the system ^{14}N + Ag at 35 MeV/A; this system was chosen for two major reasons. First, the energy of the beam was important to ensure, as much as possible, a clean nucleon-nucleon mechanism. Recent results had indicated that as the bombarding energy decreased to 10-20 MeV/A the reaction mechanism increased in complexity.[4] So we thought it important to have the beam energy high enough to be out of that energy range. Second, recent data has been taken for the neutron emission from the same system.[5] This data, along with the photon data, will give us a more complete picture of the reaction involved, helping us to refine the ingredients of the NET model. In particular we hope to get a better understanding of the appropriate nucleon-nucleon cross-section[6] to be used, since the value of the in-medium nucleon-nucleon cross-section is not understood very well. We should be aided in this determination since we will possess both the photon and neutron data.

The measurements were taken at the National Superconducting Cyclotron Laboratory at Michigan State University. We obtained a ^{14}N beam from the K-500 cyclotron and employed two detector systems in the measurements; a Čerenkov range telescope[7] and a 5 inch by 9 inch BaF$_2$ scintillation detector. We were able to take a very complete angular distribution of the photons, with measurements taken at 30°, 45°, 60°, 75°, 90°, 120°, and 150° in the laboratory system with both detectors. The motivation for the selection of these angles was to get an idea of what the production cross-section was doing in the forward hemisphere. Theory predicts that the angular distribution for a nucleon-nucleon process would possess a single maximum, be forward peaked and would turn

[*]National Superconducting Cyclotron Laboratory, Michigan State University, East Lansing, Michigan.

[1]It is, of course, also possible to produce photons from proton-proton collisions, but based on simple multipole estimates this process should be less important by a couple orders of magnitude.

[2]Nucl. Phys. **A474**, 219 (1988).

[3]Nucl. Phys. **A490**, 418 (1988).

[4]R. Butsch, et al., Bull. American Physical Society **33**, 980 (1988).

[5]H. Schelin, et al., Michigan State University Cyclotron Laboratory, preprint MSUCL-671, January 1989.

[6]The present prescription uses half of the isospin averaged free nucleon-nucleon cross-section.

[7]J. Stevenson, et al., Physical Review Letters **57**, 555 (1986).

over at very forward angles. This angular distribution is distinct from the angular distributions obtained from a collective mechanism or statistical emission from a composite system. It was hoped that we could see the this turning over in the angular distribution, to help verify a nucleon-nucleon signature.

The analysis of the data from the Čerenkov detector has been completed. Figure 3.2-1 below shows the angular distribution of photons produced above 30 MeV in this reaction. Figure 3.2-2 shows the photon energy spectrum at 90°. The solid lines in both figures are the result of a Nucleon-Exchange Transport model calculation using standard inputs into the code. The calculation is unique in that there are no adjustable parameters. The model reproduces the general trend of the angular distribution, and also the slope of the energy spectrum over most of the experimentally observed region. The model with its standard parameters underestimates the absolute cross-section by a factor of 3-4.

The angular distribution is forward peaked, with the $\frac{\sigma(30°)}{\sigma(150°)}$ ratio approximately equal to 4. This fact along with the absence of any other maximum leads to the conclusion that the production mechanism is most probably nucleon-nucleon bremsstrahlung for photon energies greater than 30 MeV. The calculation is normalized to the data at 30°, 90° and 150°; yielding a normalization constant of 3.97.
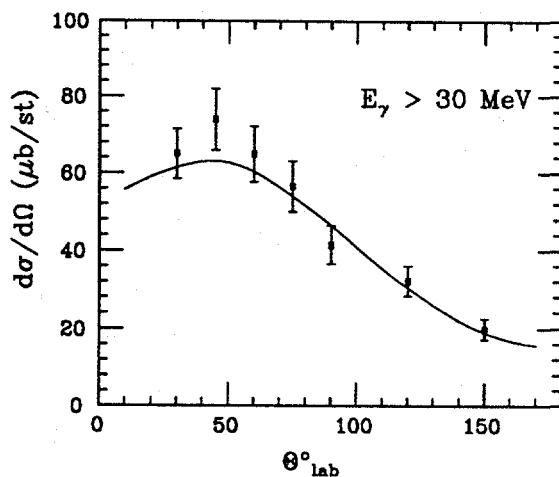
Figure 3.2-1. Angular distribution for photons from ^{14}N + Ag at 35 MeV/A. The model calculation (full curve) has been normalized to the data to show the shape comparision more clearly.
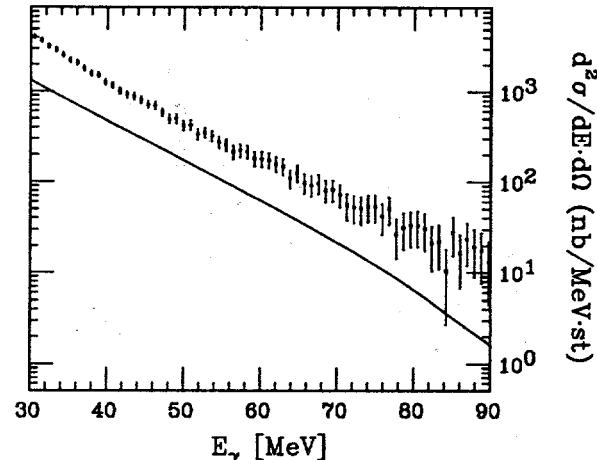
Figure 3.2-2. Photon energy spectrum at 90° in the laboratory system, from ^{14}N + Ag at 35 MeV/A.

3.3 Fusion Cross Section for the System ^{6}Li+^{28}Si at $E_{Li} = 36$ MeV

A. Charlop, A. García, S. Gil,* S. Kailas, S.J. Luke, B.T. McLain, D. Prindle
and R. Vandenbosch

The nucleus-nucleus real potentials (V_N) deduced for the projectiles ^{6}Li, ^{9}Be and ^{12}C from the analysis of their fusion excitation function data agree remarkably well with the ones determined from the analysis of their elastic scattering data.[1] It was realized[2] that in order to extend this comparison of the potentials to smaller interaction distances, R=5 fm in the case of ^{6}Li+^{28}Si system, it would be necessary to extend the measurement of the fusion cross section up to E=36 MeV. With this motivation the fusion cross section for ^{6}Li+^{28}Si has been measured at E_{Li}=36 MeV. We followed the technique of Hugi *et al.*[2] who determined the fusion cross section from the measurement of the proton and the alpha spectra at several angles followed by an analysis of these spectra using the statistical model. A detector-grade Si crystal of 2.8 mg/cm^2 thickness has been used as the target in the present measurement. The charged particles-protons, alphas, deuterons and tritons-in the energy range from 5 to 20 MeV have been detected using two Si telescopes and their spectra have been measured in the angular range 10^0 to 155^0. The data are being analysed using the statistical model code PACE.[3] The preliminary analysis indicates that the fusion cross section at E_{Li}=36 MeV is of the order of 850 mb. In figure 3.3-1 the experimental alpha and proton spectra are compared with the statistical model predictions.
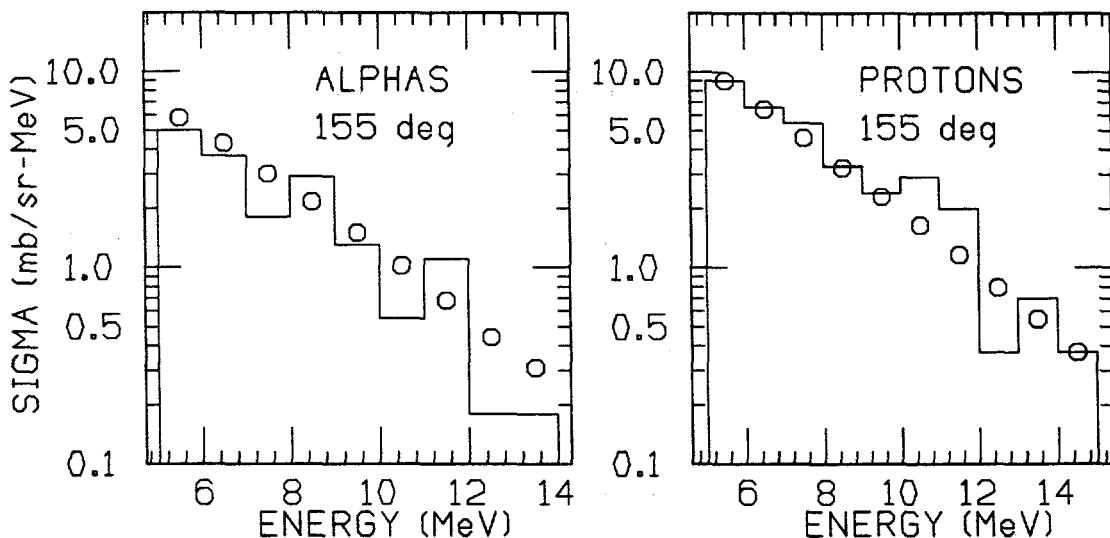
Figure 3.3-1. Comparison of the measured (open circles) and the calculated laboratory system spectra.

---

*Present address: TANDAR, Comisión de Energía Atómica, Av. de Libertador 8250, Buenos Aires, Argentina 1429.

[1]S. Kailas and S.K. Gupta, Phys. Rev. **C34**, 357 (1986).

[2]M. Hugi, J. Lang, R. Müller, E. Ungricht, K. Bodek, L. Jarczyk, B. Kamys, A. Magiera, A. Strzalkowski and G. Willim, Nucl. Phys. **A368** 173 (1981).

[3]A. Gavron, Phys. Rev. **C21**, 230 (1980).

3.4 Dispersive Contribution to ^{6}Li+^{12}C, ^{58}Ni Real Potential

S. Kailas

The anomalous increase of the heavy-ion real potential observed at barrier energies has been successfully explained in terms of the dispersion relation approach[1] which connects the imaginary and the real parts of the potential. This approach has been shown to work well[2] in explaining the data for a number of projectiles like ^{4}He, ^{16}O and ^{32}S. In the present work, the energy-dependent contribution to the real potential that arises from the imaginary potential through the dispersion relation is estimated for ^{6}Li+^{12}C, ^{58}Ni systems.

For the present analysis the volume integral per projectile-target pair of the imaginary part has been computed at several energies starting with the parameters of the imaginary potential available from the literature. In the lower part of figure 3.4-1 the volume integral of the imaginary part for Li+C system has been plotted as a function of Li energy. Using the linear schematic model of Mahaux *et al.*[2] the dispersive contribution to the real part arising due to the energy dependence of the imaginary part has been calculated. Choosing E=210 MeV as the reference energy the above calculations are suitably normalized to the value of the volume integral determined at this energy. The resultant real potential volume integrals are plotted in the upper part of figure 3.4-1. The values of the volume integrals of the real part are 30-40 % higher at low energies as compared to their respective values at E=210 MeV. It is conceivable that there is a connection between this observation and the reduced value of normalization (N= 0.6-0.7) usually found for the ^{6}Li real potential from the folding model analysis carried out at higher energies.
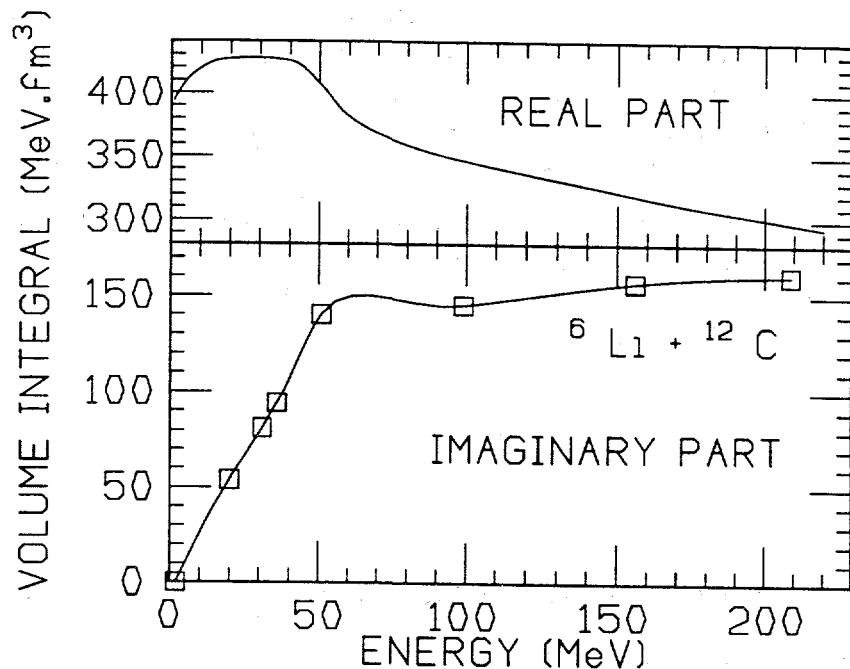
Figure 3.4-1. Volume integrals of the imaginary and the real parts for the system ^{6}Li+^{12}C

[1]M.A. Nagarajan, C. Mahaux and G.R. Satchler, Phys. Rev. Lett. **54**, 1136 (1985).
[2]C. Mahaux, H. Ngô and G.R. Satchler, Nucl. Phys. **A449**, 354 (1986).

13

3.5 Spin Distributions in Near-Barrier Fusion Reactions

A. Charlop, A. García, S. Gil,* S. Kailas, D.D. Leach,† S.J. Luke, A. Pacheco,‡ E. Renshaw and R. Vandenbosch

We have been pursuing our gamma ray multiplicity studies on several fronts during the past year. One effort has been to perform a "calibration" between multiplicity and angular momentum using the ^{166}Er (α,xn) reaction. This reaction makes the same compound nucleus as does the ^{154}Sm + ^{16}O reaction, and the excitation energies can be matched using above-barrier alpha energies where the mean spin can be deduced in a straight-forward manner from the fusion cross section. The latter has been determined on-line for the 2n and 4n channels using the intensity of the ground state rotational band transition. The 3n channel was determined using a delayed radioactivity technique. Preliminary analysis indicates our previous empirical procedure for converting multiplicity to angular momentum was quite reasonable. A more refined analysis is in progress.

We have used our new electrostatic deflector[1] and recoil detector[2] in a number of studies. A report of our previous discrete-line tagging measurements with the inclusive evaporation residue tagging technique has confirmed[3] the results reported last year obtained by summing 3n- and 4n-channel results. We have gone on to measure the gamma ray multiplicity for the ^{28}Si + ^{154}Sm reaction. The fusion cross section for this system had been measured previously at the TANDAR Laboratory in Buenos Aires. An independent measurement of the 4n channel by on-line spectroscopy is in good agreement with the earlier results. One surprisingly preliminary result is the slowness with which the gamma ray multiplicity increases for this system at above-barrier energies.

We have initiated a collaboration with the TANDAR Laboratory[3] to study fusion cross sections and gamma multiplicities for several entrance channels of varying mass asymmetry leading to the same compound nucleus ^{170}Hf. A first attempt at studying the ^{142}Ce + ^{28}Si reaction was compromised by a target obtained from another laboratory turning out to be much thinner than advertised. Other systems we plan to study are ^{32}S + ^{138}Ba, ^{48}Ti + ^{122}Sm, and ^{82}Se + ^{88}Sr.

We are also collaborating with colleagues from TANDAR on a study of the influence of hexadecapole deformation on fusion cross sections and spin distributions. We are comparing the ^{16}O + ^{154}Sm(β_4=0.083), ^{16}O + ^{166}Er ($\beta_4 = 0.002$) and ^{16}O + ^{176}Yb ($\beta_4 = -.054$) systems. All of these targets have β_2=0.27±0.01.[4] Data analysis is in progress.

---

*Present address: TANDAR, Comisión de Energía Atómica, Av. de Libertador 8250, Buenos Aires, Argentina 1429.

†John Fluke Mfr. Co. Inc., Everett, WA 98206.

‡TANDAR, Comisión de Energía Atómica, Av. de Libertador 8250, Buenos Aires, Argentina 1429.

[1] Nuclear Physics Laboratory Annual Report, University of Washington (1988), p. 73.

[2] *Ibid.*, p. 75.

[3] A. Charlop, A. García, S. Gil, S.J. Luke and R. Vandenbosch, Proceedings of the Symposium on Heavy Ion Interactions around the Coulomb Barrier, Legnaro, Italy, June 1988.

[4] T. Ichihara *et al.*, Phys. Rev. **C36**, 1754 (1987).

3.6   Impact Parameter Dependence of Pre-equilibrium Particle Emission

A. Charlop, C. Hyde-Wright, S. Kailas, D. Prindle, K. Swartz, <u>R. Vandenbosch</u>

We now have a fairly complete understanding of the mechanism for pre-equilibrium <u>nucleon</u> emission in heavy ion reactions at bombarding energies per nucleon up to about the Fermi energy.[1-3] A semiquantitative understanding of the energy spectrum, angular distribution, and absolute multiplicities has emerged by considering a nucleon exchange model where the velocity from Fermi motion in the donor nucleus is coupled to the relative motion of the projectile and target. A quantitative understanding of the angular distribution requires incorporation of nucleon-nucleon scattering in the target nucleus as projectile nucleons traverse through it. This consideration makes it difficult to understand how complex particles (e.g., d,t,α) could arise from the same mechanism. Specifically it is hard to visualize how complex particle emission can be strong at very small impact parameters. We suspect that pre-equilibrium nucleons and pre-equilibrium complex particles arise from distinctly different mechanisms and with distinctly different impact parameter dependencies. There is a hint that the impact parameter dependence is very different for protons and for alpha particles from the work of Awes *et al.*,[4] who were able to measure the multiplicities separately for the two classes of events corresponding to full and small momentum transfer.

We have initiated an experiment to further define the impact parameter within the class of full momentum transfer by exploiting the angular momentum dependence of fission competition with neutron evaporation. Depending on the fissionability of the composite system, the division of the fusion-like events into the more and less central events can be accomplished by tagging on the evaporation residues and on the fission fragments. Statistical model calculations show that the diffuseness of the ℓ-dependence of the fission-evaporation residue competition is not prohibitively large, and that the dividing ℓ can be moved throughout the fusion range by a modest variation in target Z and A. The experiment involves the measurement of light charged particles in coincidence with either fission fragments or evaporation residues. The former are detected by a semiconductor detector at 145°, and the latter by a dE/dx—E particle telescope operated in veto mode (to suppress elastic scattering events) and placed at about 20°. The light charged particles are detected in an array of phoswich detectors described elsewhere in this report.[5] We have performed an experiment with a 14 MeV/A ^{16}O beam incident on ^{159}Tb, ^{181}Ta, Ir and ^{197}Au targets. The fission cross sections have been determined to be 500, 1400, 2000 and 2000 mb, respectively. Thus the fissions from Tb tag only the highest partial waves contributing to fission, whereas fission essentially exhausts the fusion cross section for the heaviest targets. Analysis of the coincidence data is underway.

[1]J.P. Bondorf *et al.*, Nucl. Phys. **A333** (1980) 285.

[2]S. Leray *et al.*, Z. Phys. **A320** (1985) 383.

[3]J. Randrup and R. Vandenbosch, Nucl. Phys. **A474** (1987) 219.

[4]T. Awes *et al.*, Phys. Rev. **C25** (1982) 2361.

[5]This report, section 11.1.

3.7 Heavy Ion Elastic Scattering at 10-50 MeV/Nucleon

J.G. Cramer, S. Kailas, and B.T. McLain

We have been studying elastic scattering and have spent the past year analyzing data from an experiment at Michigan State and an experiment here in 1987. Our Michigan State data consists of 50 MeV/nucleon ^{12}C on ^{12}C, ^{40}Ca, ^{90}Zr, and ^{208}Pb which we obtained with the K500 cyclotron and the S320 spectrometer. We have hundreds of two dimensional spectra and we had to improve one of the lab's two dimensional display programs in order to analyze them. We also modified one of the lab's fitting routines to allow interactive fitting, in a reasonable amount of time, of functions with nearly 20 variable parameters. This was necessary because we took data for three angles at once using a triple slit aperture and we have to fit three peaks which have seven parameters each. We have been troubled for quite a while with many of our spectra in which a large number of counts appear in an area where there shouldn't be any. We have connected this to a problem with the position wire detectors but so far we can't determine the cause. Unfortunately, this may make much of our data unreliable.

Our experiment here involved 84 Mev ^{7}Li on a carbon target from 3° to 47° in the lab. The accompanying figure shows the data and an optical model fit using Woods-Saxon potentials. The fit starts to break down after 40° and we plan to investigate the changes needed in the potentials to improve the fit in this region. We will be doing more experiments this year with additional targets and different energies and we will investigate how good we can get the energy resolution to see if we can resolve low lying excited states. With the improvements in booster tuning since our last experiment we hope to get data at even larger angles and to reduce the angular errors due to beam instability.
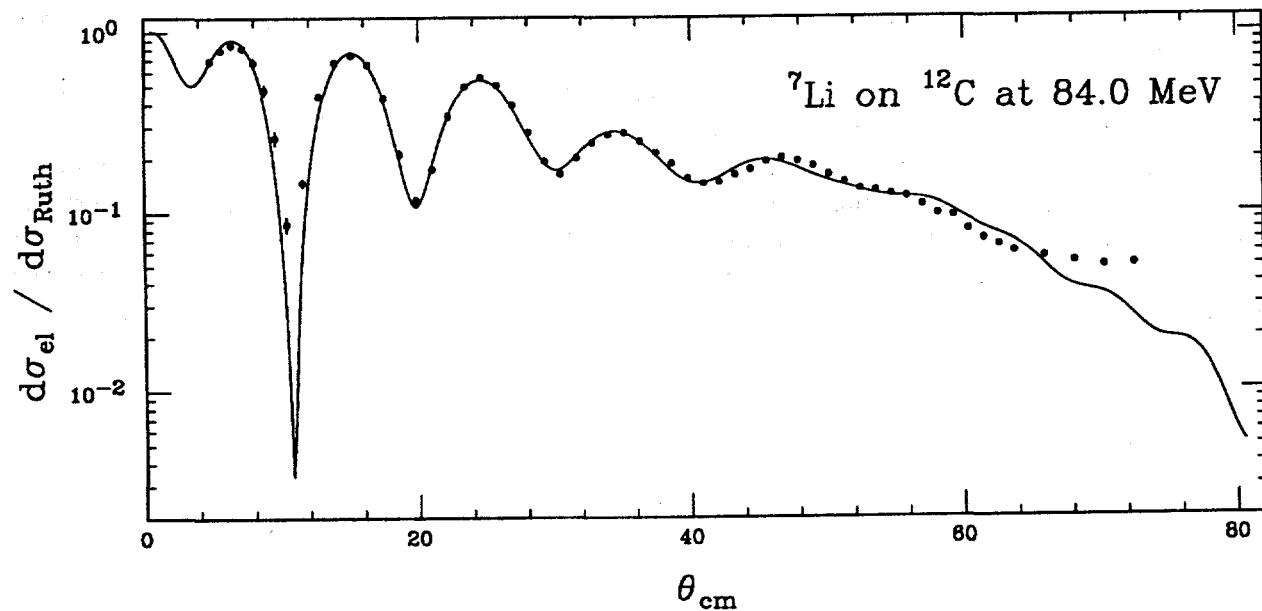
Figure 3.7-1. Elastic scattering angular distribution and optical model fit with Woods-Saxon potentials.

4 FUNDAMENTAL SYMMETRIES

4.1 Isoscalar Parity Mixing in ^{14}N

E.G. Adelberger, W.C. Haxton, C. Johnson and <u>V.J. Zeps</u>[*]

The analysis of the first round of parity violation (PV) measurements in ^{14}N has been completed, and the results disagree strongly with the predictions made prior to the experiment.[1] In conjunction with several members of the nuclear theory group, an effort has been launched to determine the source of the discrepancy. Several subsequent PV matrix element calculations have indicated a large sensitivity of the PV matrix element to the choice of the $2\hbar\omega$ interaction. Predictions range using the DDH "best value" weak coupling constants[2] from $\langle 0_2^+; 1|H_{PV}|0_2^-; 1\rangle = -1.39$ to -0.25 eV as compared to the measured matrix element of $\langle 0_2^+; 1|H_{PV}|0_1^-; 1\rangle = 0.38\pm0.28$ eV (the phases have been normalized to the strong interaction matrix elements).

The theoretical uncertainties result from the approximations made in essentially all shell model calculations of PV matrix elements, but to which the ^{14}N system is inordinately sensitive. The weak matrix element between the $0_2^+, 0_1^-; T = 1$ doublet in ^{14}N is qualitatively different from the parity-mixed doublets previously studied because the $0_2^+; 1$ level is predominantly $2\hbar\omega$ in character and the levels are unbound to proton decay. Consequently, unlike previous PV matrix element calculations, the PV matrix element in ^{14}N is potentially much more sensitive to the higher $3\hbar\omega$ and $4\hbar\omega$ excitations—calculations which up till now have not been feasible—and to the unbound character of the wave functions.

We have tested the ^{14}N wave functions of several of the $(0+1+2)\hbar\omega$ shell model calculations mentioned above by comparing the calculated electromagnetic decay rates and spectroscopic factors with the observed values. For the most part, these parity conserving properties are fairly well reproduced, with the noted exception of the spectroscopic factors for the predominantly $2\hbar\omega$ levels—such as the $0_2^+; 1$ level—which are overpredicted by factors of three to five and are anti-correlated with the size of the predicted weak matrix. The spectroscopic factor probes the $0\hbar\omega$ component of the predominantly $2\hbar\omega$ levels with relatively high precision. Since we have seen that the weak matrix element in ^{14}N is quite sensitive to the amount of $0\hbar\omega$ component of the wave function, one cannot expect to obtain a reliable weak matrix element prediction unless the predicted spectroscopic factor of the $0_2^+; 1$ level agrees with the experimentally determined value. Haxton and Johnson are presently working on this problem, first by studying the effects of $4\hbar\omega$ degrees of freedom on the level structure in ^{16}O. It is anticipated that these large model space calculations will ultimately provide more reliable wave functions for ^{14}N, since in a perturbative sense, these $4\hbar\omega$ degrees of freedom are required for a proper treatment of the $2\hbar\omega$ interaction for levels that are predominantly $2\hbar\omega$ in character.

To test the sensitivity of the predicted PV matrix element to the unbound character of the wave functions, we rewrote the code that calculates the two-body matrix elements of the parity violating operators for an arbitrary choice of basis states. We chose more realistic Woods-Saxon single particle wave functions (W-S) for the basis states, rather than the usual harmonic oscillator wave functions (HO). The W-S wave functions were obtained using the optical model code BIND, which

---

[*]Carnegie-Mellon University, Department of Physics, Pittsburgh, PA 15213.
[1]V.J. Zeps, Ph. D. thesis, University of Washington (1989), unpublished.
[2]B. Desplanques, J.H. Donoghue, and B.R. Holstein, Annals of Physics **124** (1980) 449.

solves the Shrödinger equation for a particle in W-S well, and fitting the single particle excitations in mass-17 and mass-15 with a single set of parameters (the well width is scaled by $A^{1/3}$). Several approximations were made since the levels beyond the $2s_{1/2}$ orbital were not bound in our W-S well. We found that the approximations of neglecting configurations beyond the $2s - 1d$ shell, and artificially binding the $1d_{3/2}$ orbital resulted in only about a 20% change in the calculation. The net result of reevaluating the PV operator with W-S wave functions was to reduce the PV matrix element prediction by roughly 50%, bringing the measured and predicted values more in agreement.

Using more realistic W-S single particle wave functions and anticipating better wave functions from the shell model calculations, we can soon expect to use the results of the PV measurement in ^{14}N to set reliable constraints on the isoscalar weak ρ−exchange coupling constant of the DDH meson exchange theory. Furthermore, the techniques developed as a result of this study should establish a framework for improved analysis of other parity doublets as well.

4.2 Preliminary Work on a Device to Detect the PNC Spin Rotation of Cold Neutrons Transmitted Through Parahydrogen

E.G. Adelberger, B.R. Heckel,* S.K. Lamoreaux,* D.M. Markoff, and S. Saha*

We have progressed on the design and development of an experiment to probe the weak interaction between nucleons. The experiment measures the parity non-conserving (PNC) spin rotation of transversely polarized neutrons transmitted through a parahydrogen target. Theoretical calculations of the low energy neutron-proton scattering interaction show the dominance of the isovector pion exchange term.[1] Experiments in light nuclei indicate a value of the corresponding scattering amplitude, F_π, that is less by an approximate factor of 3 than the theoretical prediction of Desplanques, Donoghue, and Holstein[2] (referred to as DDH best values). The extent of neutral current enhancement of F_π is not known. The direct measurement of this PNC n-p observable will provide a definitive experimental determination of the weak pion exchange scattering amplitude, F_π.

A general description has been given previously of how the experiment will transmit and detect cold neutrons emitted from the ILL reactor in Grenoble, France.[3] The cryogenic system necessary to sustain and transfer the liquid parahydrogen between two target chambers has been developed. The cryopump liquefication system is able to liquefy the hydrogen gas and maintain the system at sufficiently low temperatures. Liquid hydrogen tests of the centrifigal pump demonstrated its ability to displace the fluid. With the use of a capacitive liquid-level detection and feedback system, the liquid hydrogen level in the vessel was successfully maintained or changed as desired.

Monte-Carlo computer simulations are now being developed to optimize the target and beam size for maximum experimental sensitivity to the spin rotation measurement.

---

*Department of Physics, University of Washington, Seattle, WA.
[1]Y. Avishai and P. Grange, J. Phys. G: Nucl. Phys. **10**, 449 (1984).
[2]B. Desplanques, J.F. Donoghue, B.R. Holstein, Ann. of Phys. **124**, 449 (1980).
[3]Nuclear Physics Laboratory Annual Report, University of Washington (1987) p. 27.

4.3 Searching for New Macroscopic Interactions

E.G. Adelberger, J.H. Gundlach, B.R. Heckel, G. Smith, C.W. Stubbs, H.E. Swanson, P. Williams and S. Yu

Our 'Eöt-Wash' rotating torsion balance experiment is exploring the possible existence of new macroscopic interactions that would appear as a violation of the equivalence principle. The device is described in previous Annual Reports. Over the last year we have exploited the significant improvement in performance that has resulted from increased sensitivity and better control of potential sources of systematic error. We have added two new layers of magnetic shielding and have surrounded the apparatus with an azimuthally symmetrical copper isothermal shield. The gravity gradient compensation scheme has been refined as well.

In order to assess the viability of a recent suggestion[1] of a 'fifth force' coupled to isospin we have used 1.3 metric tons of lead as the attractor, rather than the hillside as in our previous runs. We have established an upper limit on the differential acceleration of Be and Al towards the lead of $\Delta a = (0.15 \pm 1.31) \times 10^{-10}$ cm s^{-2}. This null result[2] precludes (at 2σ) a reconciliation of the positive 'fifth force' observations of Thieberger[3] and Boynton et al.[1] with our data in terms of a coupling to isospin, for all ranges over which the positive results have been interpreted.

We recognized that our early hillside results[4] could constrain the possibility that the tower data of Eckhardt et al. and the mineshaft data of Stacey et al. are consistent with the quantum gravity model of Goldman, Nieto and Hughes. This model predicts scalar and vector partners of the graviton that mediate interactions (coupled to B) of gravitational strength, but of short range (up to a few thousand km.). These two interactions are presumed to predominantly cancel, but any small difference in the range or coupling strength of the two Yukawa interactions could give rise to an observable effect. At our experimental site the horizontal direction of a non-Newtonian force is a strong function of its range λ, sweeping through 60° as λ ranges from 10 to 1400m. Since forces that are not parallel cannot cancel, this allows us to set stringent limits on the parameters of the quantum gravity model: the joint 2-Yukawa fit to the tower and mineshaft data is inconsistent with the constraints[5] from our experiment.

We have just completed a preliminary run again using the hillside as the attractor, after replacing the turntable with a precision commercial device. The new turntable is a significant improvement, with better tilt characteristics and a smoother rotational drive. The preliminary results from this run show no evidence for any anomalous effects, at the level of 4×10^{-14} in $\delta a/g$.[6] This represents a 25-fold improvement over our earlier hillside data. This represents by far the most sensitive test to date for short-range violations of the equivalence principle and is within a factor of three of Dicke's celebrated result, while extending this limit to ranges less than 1 AU.

---

[1]P. Boynton et al., Phys. Rev. Lett. **59**, 1385 (1987).

[2]C.W. Stubbs et al., Phys. Rev. Lett. **62**, 609 (1989).

[3]P. Thieberger, Phys. Rev. Lett. **58**, 1066 (1987).

[4]C.W. Stubbs et al., Phys. Rev. Lett. **58**, 1070 (1987).

[5]C.W. Stubbs, E.G. Adelberger and E.C. Gregory, Phys. Rev. Lett **61**, 2401 (1988).

[6]E.G. Adelberger, Proceedings of 1989 Moriond Workshop, to be published.

4.4 Precision Measurement of the Antiproton Mass–Progress Report

X. Fei,[*] G. Gabrielse,[*] J. Haas,[†] H. Kalinowsky,[†] W. Kells,[‡] L.A. Orozco,[*] S.L. Rolston,[§] R.L. Tjoelker,[*] and <u>T.A. Trainor</u>

The purpose of this program is to measure the mass of the antiproton relative to that of the H^+ or H^- ion to a precision of $10^{-6} - 10^{-9}$ as a test of CPT invariance for hadrons. This is to be accomplished by determining the cyclotron frequency ω_c for antiprotons captured in a Penning trap. Measurements at the 10^{-6} level will be made with clouds of ~ 1000 $\bar{p}$. Refinement of technique should finally permit measurements on single $\bar{p}$ at the 10^{-9} level.

$\bar{p}$ slowed to 105 MeV/c in the LEAR facility at CERN are provided in slow extraction mode ($\sim 10^4$Hz) for tuning purposes or in fast extraction mode (10^9 $\bar{p}$ in 200 ns) for trapping. Particles are further slowed in a degrader adjusted to coincide with the range of the $\bar{p}$. Emerging $\bar{p}$ up to 2.5 keV in energy are captured by an anharmonic 3 kV trap. These are then electron cooled to a few eV and drop into a precision harmonic trap. The $\bar{p}$ are then resistor cooled to 4K in preparation for the ω_c measurement.

In 1986 we demonstrated the feasibility of the degrader scheme, trapping $100 - 1000$ $\bar{p}$ in a crude trap at 10K. Last year (1988) in September we demonstrated the operation of the new PPAC beam profile system,[1] and carefully measured the range of protons in aluminum with a TOF system. In October we successfully trapped 5×10^4 $\bar{p}$ in a new anharmonic trap with a lifetime of hours and measured the range of $\bar{p}$ with the same system. The range measurements have provided a precision determination of the Barkas effect for the $p - \bar{p}$ system.[2]

In December trapped $\bar{p}$ were cooled to 5eV, but the details of the cooling mechanism are not completely understood. In April, 1989 we expect to perfect electron cooling and attempt resistor cooling. The first precision mass measurements may be possible during the summer.

[*]Department of Physics, Harvard University, Cambridge, MA 02138.
[†]Institut für Physik, Universität Mainz, BRD.
[‡]Institute for Boson Studies, Pasadena, CA.
[§]National Institute of Standards and Technology, Gaithersburg, MD.
[1]Section 11.5, this report.
[2]Section 4.5, this report.

4.5 Measurement of the Barkas Effect in the $p - \bar{p}$ System

X. Fei,[*] G. Gabrielse,[*] J. Haas,[†] H. Kalinowsky,[†] W. Kells,[‡] L.A. Orozco,[*] S.L. Rolston,[§] R.L. Tjoelker,[*] and <u>T.A. Trainor</u>

A difference in the range of 5.9 MeV protons and antiprotons in a degrader composed primarily of aluminum has been observed. The fractional change in range is 5.6 ±1.4% with antiprotons having the greater range.[1]

These observations were made with 105 MeV/c p and $\bar{p}$ beams from the LEAR facility at CERN, and extensive calibration runs and systematic error checks were done with a proton beam at this laboratory. The range measurement system consisted of a PPAC beam profile monitor (BPM) used as a start detector and active collimator,[2] an assortment of gas and solid energy degraders and a channel plate detector (MCP). The gas degrader consisted of an adjustable mixture of helium and SF_6 used to make fine adjustments to the overall degrader thickness. The last 70% of the energy loss occurred in the last half of the degrader which was composed of aluminum.

The transmission through the degrader is defined as BPM·MCP/BPM. This ratio falls from some constant value near unity to zero (or a pion background in the case of $\bar{p}$) as the degrader thickness is varied across the range of 5.9 MeV p or $\bar{p}$. The relative shift of this transmission curve between p and $\bar{p}$ gives the fractional difference in range or Barkas effect.

The stopping power can be written as

$$\frac{dE}{dx} = \frac{4\bar{n}e^4 N_o}{mV^2 A} Z^2 Z_T (L_0 + L_1 Z + L_2 Z^2 + ...)$$

L_1 and higher odd coefficients represent the projectile charge sign dependence, or Barkas effect. They depend on the projectile speed and the nature of the degrader material. The observed fractional change in range agrees within a factor of two with several theoretical calculations. More recent theories are in good agreement with the observed effect (~6.4% vs. the observed 5.6 ±1.4%).

---

[*]Department of Physics, Harvard University, Cambridge, MA 02138.

[†]Institut für Physik, Universität Mainz, BRD.

[‡]Institute for Boson Studies, Pasadena, CA.

[§]National Institute of Standards and Technology, Gaithersburg, MD.

[1] "Direct Observation of the Barkas Effect Using Antiprotons and Protons," G. Gabrielse *et al.*, accepted by Physical Review A.

[2]Section 11.5, this report.
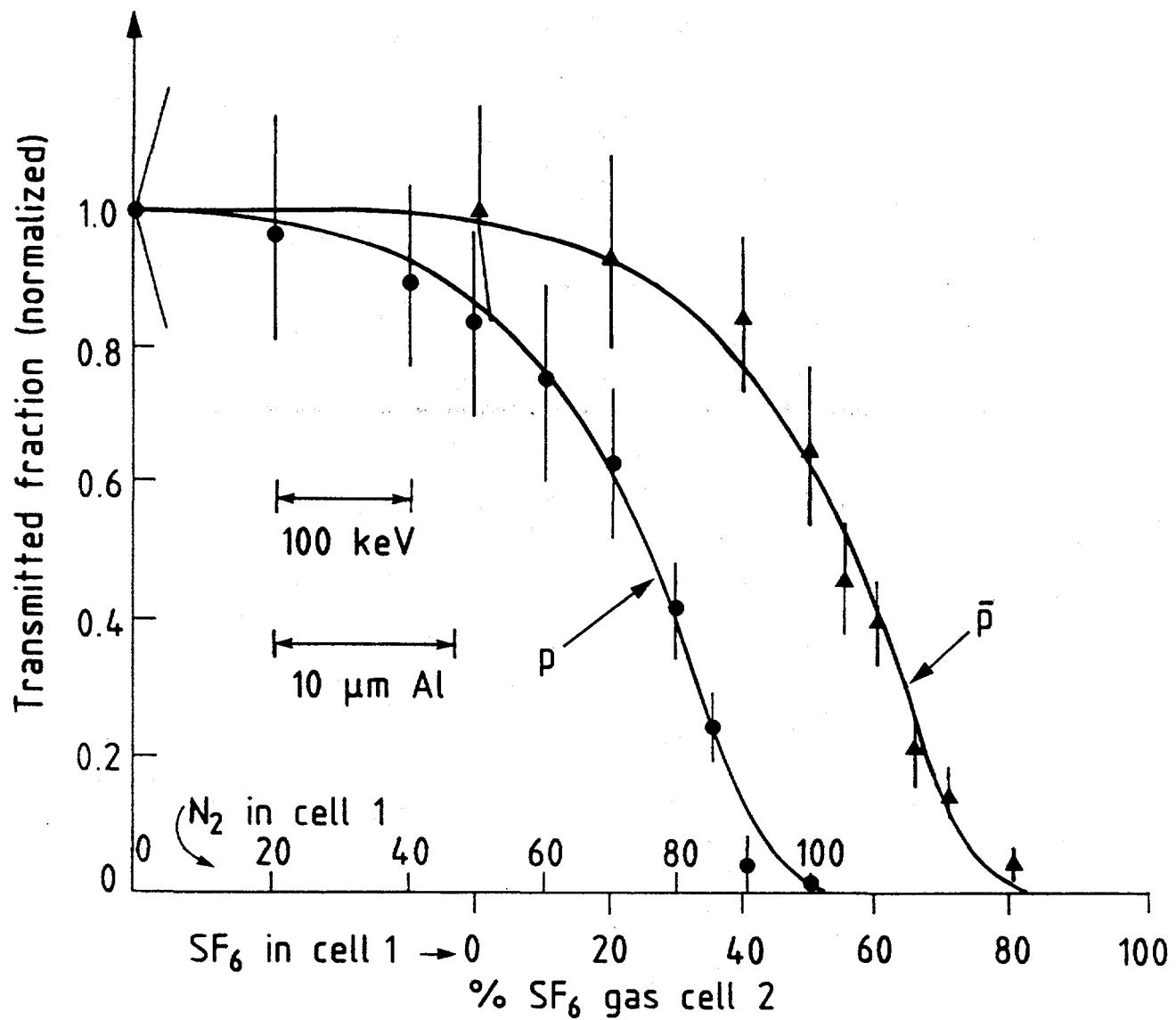
Figure 4.5-1. Transmission of protons and antiprotons vs. degrade and thickness showing the Barkas effect.

4.6 H-atom Experiment Progress Report: Survey of Systematics

T.A. Trainor and P. Wong

This year was spent characterizing systematic effects which would adversely affect the objective of this experiment, which is to place an improved upper limit on parity violation (PV) in atomic hydrogen due to the neutral weak current.

The magnetic field was trimmed successfully to less than ± 50 milligauss in 600 gauss. The field strength was monitored by its effect on resonances, and the data interpreted using revised algorithms.[1] The computer fit allowed us to determine the B-field profile and the necessary coil corrections. They also enabled us to explain various anomalies noted by Chupp *et al.* in 1982.

The B-field current control system was updated, reducing its noise by a factor of five, corresponding to B fluctuations < 1 part in 100,000.

Scans were made across the $\alpha_+\beta_0$ resonance. Spurious results were traced to improper choice of lock-in frequencies. For a triple demodulation experiment, Trainor[2] has shown that the frequencies must be chosen very carefully to reduce crosstalk between harmonics. Recently we performed a systematic search to determine an appropriate set of frequencies.

One remaining anomaly allowed the strong E-motional amplitude (non-zero v x B due to finite beam emittance) to be incorrectly demodulated due to incomplete common mode rejection. This was traced to differential quenching of the metastable beam in the two polarities of the applied electric field.

Current work is focusing on the buildup of space charge which occurs in the RF cavities in one polarity of the applied electric field. Under this condition, the axial potential well in the RF cavity and the magnetic field create a large anharmonic Penning trap. This space charge is the source of the differential quenching described earlier and introduces an inherent asymmetry in a critical parameter of the experiment. We are trying to understand the nature of the space charge and exploring possiblities to reduce it.

No other spurious amplitudes were found in either the $\alpha_+ \rightarrow \beta_0$ or $\alpha_0 \rightarrow \beta_0$ resonances to the present sensitivity of the apparatus. Metastable yield and detector efficiency are being optimized preparatory to final determination of a PV upper limit.

Figure 4.6-1. Metastable Hydrogen yield vs. time after turning on a trapping potential in cavity I. The yield changes as charges accumulate in the trap. Notice the reproducible manner (a,b) in which the charge buildup affects the beam intensity.

---
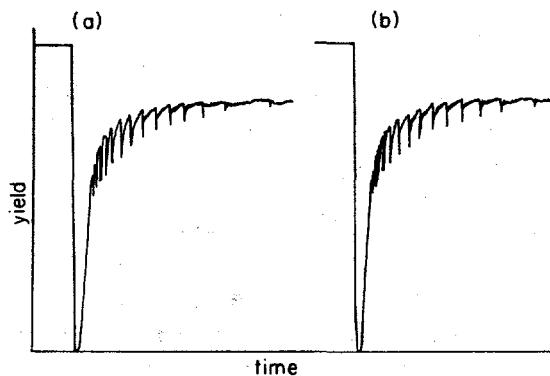
[1] Nuclear Physics Laboratory Annual Report, University of Washington (1988) p. 26.
[2] *Ibid.*, (1982) p. 77.

23

5 NUCLEAR REACTIONS—POLARIZATION

5.1 Polarized Protons from the $^{59}\text{Co}(^3\text{He},\vec{p})$ Reaction

K. Sagara,* S. Kailas, W.G. Weitkamp, D. Will and H. Willmes[†]

We have continued our study of the $^{59}\text{Co}(^3\text{He},\vec{p})$ reaction at 27 MeV incident energy as part of a general study of the mechanisms contributing to outgoing proton polarization in reactions and scattering.

To measure the outgoing polarization, we are using a vane-type high-pressure helium polarimeter at the final focus of the magnetic spectrograph/momentum filter. To reduce background a coincidence is obtained between pulses from a ΔE detector in front of the polarimeter and from detectors detecting protons scattered from helium. Earlier problems with a gas-filled ΔE detector[1] have been resolved by replacing it with a thin solid state detector. The maximum proton energy which can be measured has been increased from 25.5 to 30.5 MeV by revising the control system and some wiring of the momentum filter.

During the year we have taken measurements of the polarization, increasing our data set to 39 points at outgoing proton energies from 17.67 MeV to 30.5 MeV (the ground state reaction gives an outgoing proton energy of 36.3 MeV) and at angles from 18° to 42°. The data are similar to those reported last year[3] with an average uncertainty of about ±0.1. Rather surprisingly, the data show little variation in magnitude with respect to energy and angle. The value is always about 0.3 except at the lowest energies, where it decreases somewhat.

To assist in the interpretation of these data, we have measured the $^{59}\text{Co}(^3\text{He},p)$ cross section at 27 MeV incident energy. Preliminary data from the first run are shown in figure 5.1-1. A second run has been completed to reduce statistical uncertainties and to verify the absolute calibration.

Three different reaction mechanisms operate in the outgoing proton energy region of the cross section and polarization data. The first, evaporation, is predominant at large angles, represented in figure 5.1-1 by the data at 60°. Proton polarization from evaporation is expected to be very small. Evaporation may account for the decrease in polarization at the lowest proton energies.

The second reaction mechanism is breakup, which is expected to be forward peaked and to show a broad peak at a proton energy of about 1/3 of the incident beam energy. The broad peak in the 12° data in figure 5.1-1 is probably due to breakup.

The third reaction mechanism is deuteron stripping, which should predominate at higher proton energies. Our cross section data are consistent with a smooth transition from breakup to stripping as the proton energy increases.

The way in which breakup and stripping produce a proton polarization with a constant magnitude of about 0.3 is not clear. The strength of both of these mechanisms vary with angle and energy. Presumably in both cases the ^3He dissociates into a proton and deuteron during the reaction process. If this deuteron experiences a strong spin-orbit force in interacting with the target

---

*Kyushu University, Fukuoka 812 Japan.
†University of Idaho, Moscow ID 83843.
[1]Nuclear Physics Laboratory Annual Report, University of Washington (1988) p. 32.

nucleus, the associated proton would tend to be polarized. Measurements of deuteron scattering from targets in this mass range do show spin-orbit effects, but analyzing powers tend to be small at small scattering angles.[2]
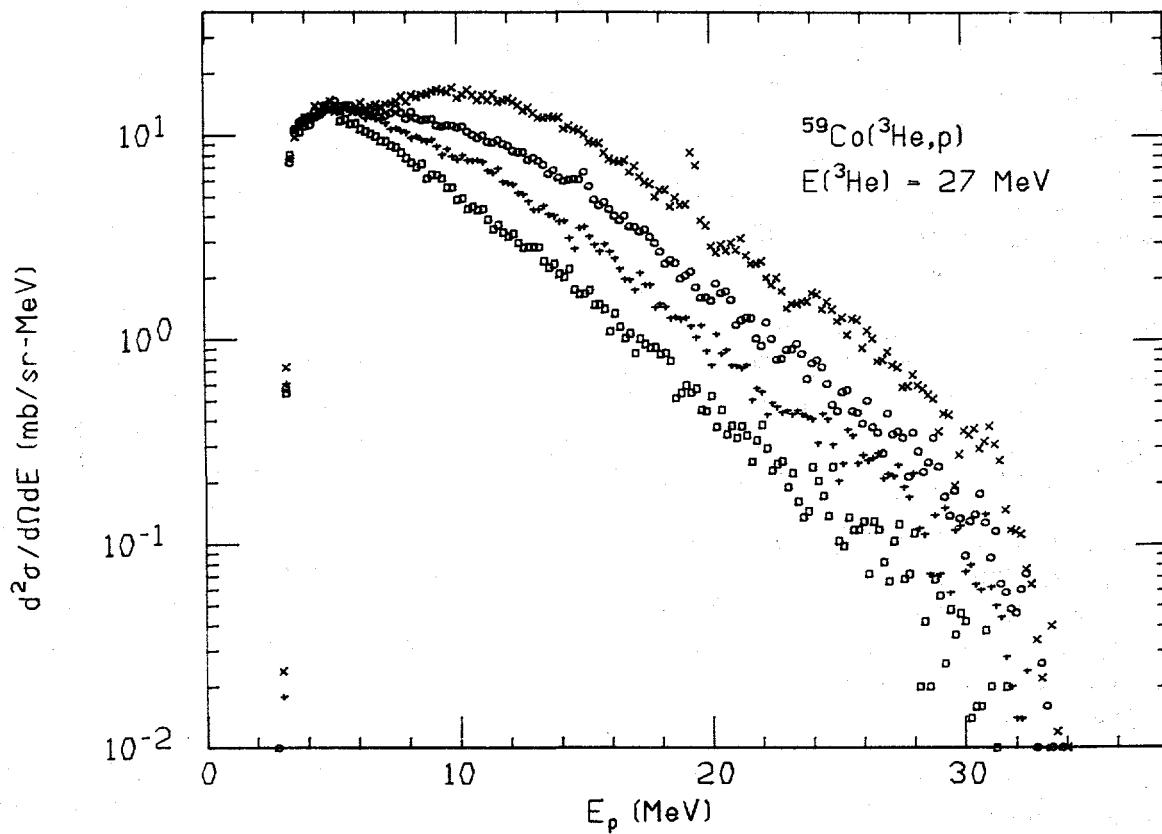
Figure 5.1-1: Cross section for the ^{59}Co(^{3}He,p) reaction. Lab reaction angles: (from top to bottom) 12°, 30°, 42°, 60°.

[2]Y. Tagishi, Deuteron Involving Reactions and Polarization Phenomena, World Scientific, Singapore, 1986, p. 79.

5.2 Low Energy Structure in ^{14}N Studied with ^{13}C$(\vec{p}, p)$

D.R. Balsley, A. García, <u>C.A. Gossett</u>, S. Sutlief, H.E. Swanson and V.J. Zeps[*]

The low energy structure of ^{14}N was studied with polarized proton elastic scattering from ^{13}C from $E_p = 1$ to 3.5 MeV. Our interest in ^{14}N stems, in part, from our recent measurement of isoscalar parity mixing of the $0^+, 0^-$ resonances in ^{14}N observed at $E_p \sim 1.15$ MeV (see Section 4.1). There the experimental result and the theoretical prediction for the parity violating longitudinal analyzing power are in strong disagreement. A phase shift analysis of the cross section and parity-conserving transverse analyzing power for proton elastic scattering from ^{13}C over wide angular and excitation energy ranges may provide clues to possible problems with the theoretical description of the parity-mixed resonances.

The cross section and analyzing power for ^{13}C$(\vec{p}, p)$ were measured simultaneously at nine laboratory angles from 36.5° to 170°, and in general the statistical uncertainties in the measured yields were $< 1\%$. The proton energy was varied from 1 to 3.5 MeV in steps as small as 0.2 keV in the regions of sharp resonances and in steps as large as 15 keV in other regions. The relative solid angles of the detectors were determined using Rutherford scattering from a gold target.

Great care was taken to have good energy resolution in backward counters in order that elastic scattering from ^{13}C and ^{12}C could be resolved. The relative percentage of ^{13}C and ^{12}C as a function of time could thus be determined in combination with separate measurements of elastic scattering from ^{12}C using a natural carbon target in the same detection geometry as the ^{13}C measurements. These results will allow us to make corrections, if necessary, to the ^{13}C scattering data to account for ^{12}C contributions.

The thickness of the ^{13}C and ^{nat}C targets were measured using the extremely narrow, $\Gamma \sim 135 eV$, 2^+ resonance in $^{13}C(p, \gamma_0)$ at $E_p = 1.75$ MeV. The fraction of ^{13}C present in the ^{nat}C target was sufficient to measure the thickness of the target in this manner.

Data analysis is in progress and a phase shift analysis of the measured cross sections and analyzing powers is planned.

---
[*]Present address: Carnegie-Mellon University, Department of Physics, Pittsburgh, PA 15213.

5.3 The Scattering of Polarized Protons to the Continuum

I. Halpern, D.R. Rosenzweig, T.A. Trainor

Some years ago we made some measurements of analyzing powers of proton scattering from nuclei into the continuum.[1] An analysis[2] of these results and of results obtained elsewhere[3] at higher proton energies suggested that, at the higher energies ($\sim$65 MeV), most of the protons which scatter into the back hemisphere have large impact parameters and orbit all the way around the downstream side of the nucleus, being emitted from the opposite side of the nucleus from the side on which they arrive.

We abandoned our own experimental work in 1981 because the proton energies then available at our local tandem accelerator were too low for useful studies of these orbiting effects. (At tandem energies, the protons can be very strongly deflected in the nuclear potential and some of the orbiting path lengths are consequently long and particle emissions are therefore very smeared out in angle.) With the advent of the booster we decided to make some calculations to see whether the now-available proton energies ($\sim$ 35 MeV) were high enough to exhibit clean versions of the orbiting effect leading to backward emissions with large analyzing powers. These analyzing powers arise from the opposing effects of the spin-orbit potential on polarized protons which arrive on opposite sides of the nucleus. We remain interested in these effects since they offer a unique opportunity to study surface reactions in nuclei (The peripherally orbiting projectiles spend an unusually long time in the nuclear surface).

Our calculations indicate that for medium weight nuclei, the positive backward analyzing powers should be large enough to allow one to study some interesting features of the orbiting process. Among features which we are looking into further are:

1. The dependence of the analyzing powers on outgoing energy. The protons which are incident on that side of the nucleus where the spin-orbit interaction increases the effective radius of the overall nuclear potential reach considerably further back in angle than the protons which are incident on the other side of the nucleus. They travel, however, in a region of lower nuclear density. This leads one to expect that two-step reactions will have analyzing powers which are substantially less than those for one step reactions. The evidence from $(\vec{p}, p')$ reactions with large energy loss and the fact that the analyzing powers are lower in $(\vec{p}, {}^3\text{He})$ than in $(\vec{p}, \alpha)$ support this expectation, but the issue needs further study.

2. The implication of the orbiting picture that the character (oscillatory or smoothly varying) of the angular distributions for polarized protons will differ, left vs. right, at certain energies.

We look forward to studying these and other effects.

---

[1] Nuclear Physics Laboratory Annual Report, University of Washington (1976- 1981).

[2] H.C. Bhang et al., Phys. Lett. **112B**, 299 (1982).

[3] H. Sakai et al., Nucl. Phys. **A344**, 41 (1980).

6 MEDIUM ENERGY REACTIONS

6.1 Photoproduction of π^+ on a Variety of Nuclei

M. Doss,[*] I. Halpern, D.P. Rosenzweig, and <u>D.W. Storm</u>

We have shown that many features of inclusive pion scattering at energies near the (3,3) resonance can be understood in terms of a model based on nuclear geometry and single scattering of the pion by a nucleon. This scattering either leads to the pion leaving the nuclear volume or it may lead to absorption of the pion. Multiple scattering leading to pion escape is suppressed for several reasons, including the strong likelihood of absorption.[1] The details of scattering reactions are not sensitive to the mean free path of pions in the nucleus, provided the mean free path is short compared to the nuclear radius. The situation is very different for pions made by photoproduction. When the residual nucleus is left in the continuum, the pions are presumably photoproduced uniformly throughout the nucleus on single nucleons. Except for smearing out due to Fermi motion and some effects of the optical potential, the pion energy spectrum and angular distribution are expected to be the same as those for photoproduction on free nucleons. Because of the spherical symmetry of the distribution of the production sites, the attenuation of the pions traveling through the nucleus should be angle independent, and can be measured by comparing the cross section for π^+ photoproduction on nuclei with that on protons. Thus in studying how pions propagate through nuclear matter, photoproduction provides complementary information to scattering.

Our proposal to measure photoproduction of π^+ on various nuclei has been approved at the Saskatchewan Accelerator Laboratory. We plan to use the tagger in conjunction with the new pulse stretcher ring to provide monochromatic photons with energies from 200 to above 250 MeV. We plan to detect the π^+ in a $\Delta E - E$ plastic scintillator, which will be large enough to stop 100 MeV pions. We will identify π^+ by observing the decay muons in the E scintillator. These are 4 MeV muons which appear with a mean delay time of 26 nsec, set by the pion lifetime. This technique has been used successfully at Mainz[2] for 30 MeV pions, and it has been used at TRIUMF[3] for pions up to 100 MeV. Our goal is to obtain reasonable quality spectra for continuum photoproduction of π^+ at several angles and with several targets in the mass range from carbon to lead.

We have designed and are building a counter holder. A cylinder of BC 408, 12 inches long by 6 inches in diameter, is being prepared for us by Bicron.[4] This scintillator will be viewed by a Hamamatsu 1250 phototube, which should be capable of delivering a fast enough signal to permit observation of the decay muons from more than half the π^+ decays. The detector will be ready for tests during June. At Saskatoon we will study the ability of the detector to identify π^+ and will study the backgrounds associated with the tagger. We plan to study the efficiency of the detector as well as its spectral response to various energy π^+ at TRIUMF. Actual measurements of photoproduction will be done during the summer or fall.

[*]University of Saskatchewan, Saskatoon, S7N 0W0 Canada.

[1]K. A. Aniol, *et al.*, Phys. Rev. **C33**, 208 (1986).

[2]R.W. Gothe, *et al.*, Nucl. Instr. and Meth. **A276**, 233 (1989).

[3]D. Axen, *et al.*, Nucl. Instr. and Meth. **118**, 435 (1974).

[4]Bicron Corporation, 12345 Kinnsman Rd, Newbury, Ohio, 44065.

6.2 The Pegasys Project at SLAC

C.E. Hyde-Wright and the Pegasys collaboration*

We have analyzed the feasibility of measuring virtual Compton scattering $(e, e'\gamma')$ with the proposed Pegasys facility on the PEP ring at SLAC. In this reaction, the target radiation (Compton) and electron radiation (Bethe-Heitler) amplitudes interfere coherently. In the deep inelastic limit (large energy and momentum transfer) the reaction takes place on a single quark. As a result, the cross section has the simple form:[1]

$$d\sigma = d\sigma_0 \left[T_{BH} U^{(2)}(x_C) + T_{Int} U^{(3)}(x_C) + T_C U^{(4)}(x_C) \right],$$

$$U^{(n)}(x_C) = \sum_a \lambda_a U_a(x_C)$$

$$x_C = Q_C^2 / 2M\nu_C$$

The only dependence on the target is contained in the structure functions $U^{(n)}$. The factors $d\sigma_0$, T_Λ are determined by kinematics. The variables ν_C and Q_C^2 are the net energy transfer and invariant momentum transfer squared, respectively. $U_a(x_C)$ is the probability of finding a quark of flavor a and charge $e\lambda_a$ in the target with 'momentum fraction' x_C.

The structure function $U^{(2)}(x) = F_2(x)/x$ is measured in deep inelastic electron (or muon) scattering. The Bethe-Heitler cross section is just the radiative tail of electron scattering. The structure function $U^{(3)}(x_C)$ is of particular interest because it measures the valence quarks in the target. Thus inclusive Compton scattering is complementary to the Drell-Yan process which measures the anti-quark sea.

We have estimated the ability of the Pegasys experiment to isolate the structure functions, on the basis of the kinematic weights T_Λ. The experiment is limited by statistics, by the background of photons from decays of hadrons, and by the resolution of the electromagnetic calorimeter that measures photon momenta. The $\pi^0 \to \gamma\gamma$ decay is the dominant background. Approximately two thirds of these decays are fully reconstructed and can be vetoed. We assume that the residual statistical background can be determined with 10% precision. In addition, we impose a cut on photon transverse (to the virtual photon) momentum squared, requiring that it be greater than 1 GeV^2. For these conditions, the Bethe-Heitler, Compton, and interference cross sections are everywhere greater than twice the uncertainty in the statistical background.

Systematic errors are estimated by smearing pseudo-data by the shower counter resolution of $\sigma_k/k = 0.1\sqrt{1\text{GeV}/k}$, $\sigma_\theta = 0.001$. We simulated a 90 day run on H_2 at the design luminosity of $1.6 \cdot 10^{32}/\text{cm}^2/$ sec. The structure functions $U^{(n)}$ are extracted in the simulation with a precision of $\pm 20\%$ for $0.1 \leq x_C \leq 0.6$.

*R.G. Arnold, P.E. Bosted, S.E. Rock, and Z. Szalata, *American University*, L. Dennis, J.D. Fox, and K. Kemper, *Florida State University*, J. Lambert, *Georgetown University*, F.S. Dietrich, K. van Bibber, and J.D. Molitoris, *Lawrence Livermore National Laboratory*, C.C. Chang and H.H. Holmgren, *University of Maryland*, R. Hicks, R. Miskimen, G. Peterson, S.H. Rokni, and H. Baghaei, *University of Massachusetts*, R. Finlay, and K. Hicks, *Ohio University*, K.A. Giffioen, *University of Pennsylvania*, A. Hirsch, N. Porile, and R. Scharenberg, *Purdue University*, G. Adams, P. Stoler, and P.F. Yergin, *Rensselaer Polytechnic Institute*, G.G. Petratos, *University of Rochester*, R.A. Gearhart, W. Langeveld, M.L. Perl, E.M. Riordan, and Y.S. Tsai, *Stanford Linear Accelerator Center*, Z.E. Meziani, and S.E. Kuhn, *Stanford University*, E. Piesetzsky, *Tel Aviv University*, R.C. Minehart and O. Rondon, *University of Virginia*

[1]S.J. Brodsky, J.F. Gunion, R.L. Jaffe, Phys Rev **D6** (1072) 2487.

6.3 Magnetic Optics of the 1.6 Gev/c SLAC Spectrometer

C. Hyde-Wright, <u>K. Swartz</u>

For a recent experiment at SLAC (NE11) the acceptance of the 1.6 GeV/c spectrometer was increased by the removal of the entrance defining slits and the addition of two quadrupoles between the existing spectrometer and the target. This meant that the electron trajectories entering the spectrometer had a larger emittance than previously and that there were no well defined apertures. Therefore a more detailed knowledge of the electron trajectories and in turn of the magnetic field is needed to calculate the new acceptance of the spectrometer. For this purpose a magnetic field map of the spectrometer was made from which a TRANSPORT [1] model of the spectrometer of the spectrometer was constructed.

The 1.6 GeV/c spectrometer is a one-element dipole with entrance and exit pole face rotations as well as curved pole faces for second order focusing. Only first order optics are being used until these are fully understood; second order contributions to the acceptance are small. Only the entrance and exit fringe fields were measured since the rest of the magnet is a dipole to first order. From the field measurements a multi-element model of the magnet is calculated with each element being small enough that electron trajectories are almost straight in each element. From the multi element model the acceptance is found by tracking an ensemble of electrons through the magnet and checking that they do not collide with the beam pipe before and after each element. This procedure is done by the program TURTLE [2], whose input is a TRANSPORT model.

The entrance and exit fringe fields were measured using a Hall probe. The field measurements were done in a one inch grid in the magnetic midplane, measuring only the large dipole component (the other components should be zero in the magnetic midplane). The reasons for this choice were; In measuring the non-dipole field component small rotations of the probe contribute relatively large offsets in field measurements due to the much larger dipole field. Errors in position and in rotation of the probe only contribute in second order to the dipole field. A much larger range of data points can be taken since the beam pipe is larger in the bend plane. A second order fit was done to these measurements from which the TRANSPORT parameters for a dipole wedge magnet were extracted for each element. These values together with the position of the central ray with respect to the beam pipe are the TRANSPORT parameters used as inputs to TURTLE.

A comparison of the model and a more accurate wire float that was previously done largely agree. The values of the over all matrix elements (in the TRANSPORT notation) from the raytrace is given below. The acceptance and optics of the 1.6 GeV/c spectrometer will be studied from the NE11 data as well. Using the NE11 data and previous measurements a consistent and improved model of the spectrometer will be constructed.

First order optics of the SLAC 1.6 GeV/c spectrometer

$< x|x > \ = -.686 \pm .04$ $\qquad < x|\theta > \ = .002 \pm .002 \ cm/mr$

$< \theta|x > \ = -4.52 \pm .1 \ mr/cm$ $\qquad < \theta|\theta > \ = -1.45 \pm .06$

$< y|y > \ = .12 \pm .03$ $\qquad < y|\phi > \ = .828 \pm .03 \ cm/mr$

$< \phi|y > \ = 1.01 \pm .2 \ mr/cm$ $\qquad < \phi|\phi > \ = 1.31 \pm .09$

$< x|\delta > \ = 4.23 \pm .09 \ cm/\%$ $\qquad < \theta|\delta > \ = 6.74 \pm .25 \ mr/\%$

---

[1] K. Brown, SLAC Report No. 75. 1967.
[2] D. C. Carey, SLAC Report No. 246. 1982.

6.4 Inclusive Scattering Spectra for $\pi^{\pm}$ at 100MeV from a Variety of Nuclei

J.F. Amann,[*] R.L. Boudrie,[*] M. Doss,[†] D. Drake,[*] I. Halpern, J. Nelson,[‡]
M. Khandaker,[§] D.P. Rosenzweig, D.W. Storm, D.R. Tieger[‡] and S.A. Wood[¶]

The analysis of our measurement of inclusive pion inelastic scattering spectra has been completed, and we are now in the process of interpreting the results. Excitation spectra have been obtained at several angles from ^{12}C, ^{40}Ca, ^{120}Sn, and ^{208}Pb,[1] where the π leaves up to 80 MeV in the target nucleus. The pion energy was measured using the Clamshell magnetic spectrometer at LAMPF in three overlapping momentum bites. All spectra are fairly broad, and we are currently trying to understand the systematics of these spectra in terms of a quasi-elastic description of the inelastic reaction. Such a description suggests a ratio near 2 for the π^- to π^+ cross section from Pb, but a value near 1 for Ca. This expectation disagrees with previous data[2] which showed little difference between the π^- and π^+ reaction cross-sections for scattering from Pb. Our measurements show a large ratio (2.1) for the π^- to π^+ cross-section in Pb, (see figure 6.4-1) and a small ratio (1.1) in Ca, in line with expectation. The enhancement in the π^- cross-section and an associated shifting of the spectra towards higher excitation energy are the result of Coulomb effects and of the neutron excess in Pb. The π^+ spectra and angular distributions agree with earlier data taken with a germanium telescope.[3]

The main uncertainties associated with the measured cross-sections arise from a) the efficiency variation across the spectrometer focal plane, b) the copious μ background, c) the absolute normalization to πp cross-sections, and d) the run-to-run normalizations required to merge the three bites into one spectrum. The total uncertainty in the data is $\approx$5-10%. Our most sensitive technique for differentiating the μ from the π exploits the difference in energy deposited in a ΔE scintillator for π's and μ's of the same momentum. At the lower momenta, where the muons are numerous, this difference is greater than 30%. To obtain the relative efficiency function across the focal plane, two separate techniques were brought to bear. These were 1) measuring the elastic cross-sections from ^{1}H at a given energy for several magnetic field settings, and 2) comparing overlapping regions of the cross-section obtained from two neighboring momentum bites. Both techniques produce satisfactorily similar functions.

We are attempting to calculate the features of the spectra (both magnitude and shape), using a classical model of the inelastic process in which the pion collides with a single nucleon with the free nucleon cross-section. The target nucleus enters into our calculation in three fundamental ways. First, it acts as an absorber of the incoming and outgoing projectile. Second, it provides the source for the scattering, which is taken to be a Fermi-gas of nucleons. Third, the Coulomb and nuclear fields of the target alter the projectile's kinetic energy and flux at the impact site (and therefore its dynamics). The folding together of these components leads to estimates of cross-section and back-angle scattering spectra which reproduce at least qualitatively the main features present in the data.

[1]Nuclear Physics Laboratory Annual Report, University of Washington (1988) p. 36.

[2]D. Ashery *et al.*, Phys. Rev. C **23**, 2173 (1981).

[3]K. Aniol *et al.*, Phys. Rev. C **33**, 208 (1986).
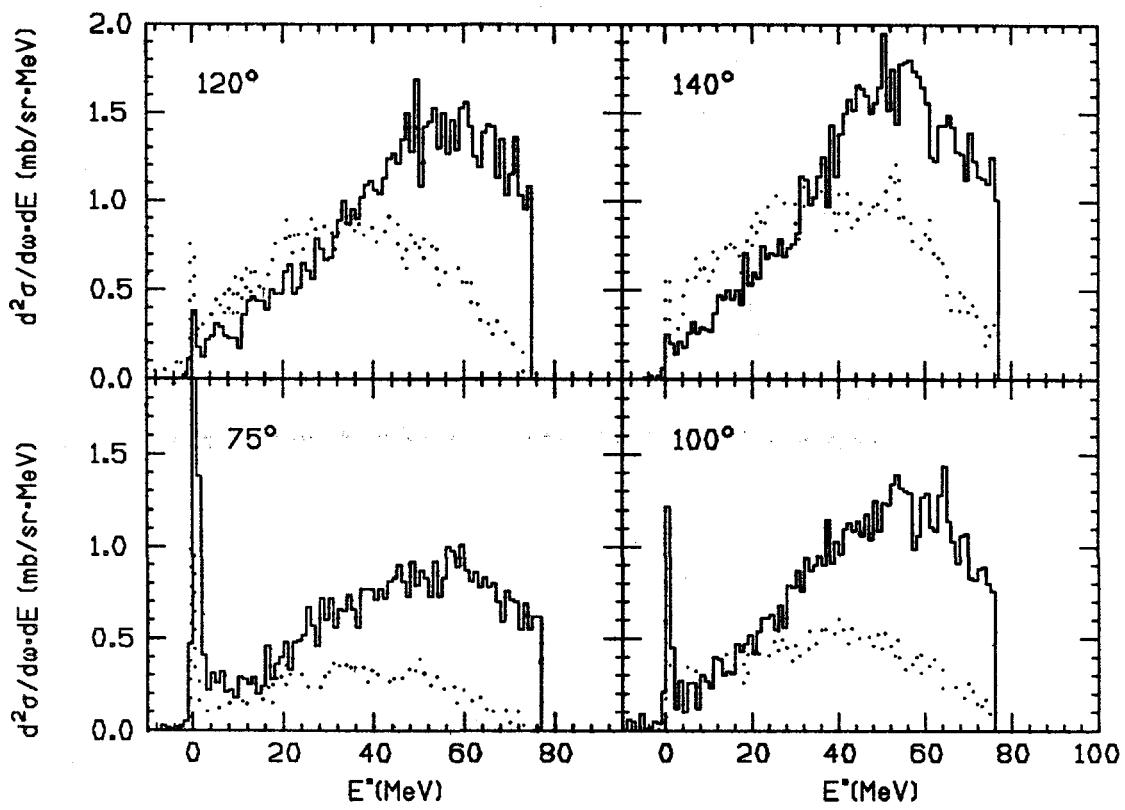
Figure 6.4-1. Excitation spectra for 100 MeV π scattering from Pb at four spectrometer angles. Each plot compares data for π^- (solid) and π^+ (dotted) beams. There is a clear enhancement in the π^- cross-section and a shift to higher excitation energy. The cut-off at ≈ 75 MeV is the limit of acceptance of the lowest momentum bite.

6.5 Electron Scattering from the Proton and the Deuteron

C.E. Hyde-Wright, K.Swartz,
R.G. Arnold, P.E. Bosted, S.E. Rock, and Z. Szalata,[*]
F.S. Dietrich, K. van Bibber,[†]
C.C. Chang[‡]
R. Hicks, R. Miskimen, G. Peterson, S.H. Rokni,[§]
K.A. Giffioen,[¶]
G.G. Petratos,[∥]
R.A. Gearhart,[**]
S.E. Kuhn,[††]
J. Alster, J. Lichtenstadt,[‡‡]

Data taking on experiment NE-11 at the Stanford Linear Accelerator Center (SLAC) was completed in January 89. Elastic electron scattering data were obtained on the proton for 1.75 $GeV^2 \leq Q^2 \leq 6.0$ GeV^2. In the same kinematics, quasi-elastic scattering data were obtained on the deuteron for 1.75 $GeV^2 \leq Q^2 \leq 4.0$ GeV^2. Data were taken with two spectrometers simultaneously in the End Station A. The 1.6 GeV/c spectrometer was fixed at 90° and the 8 GeV/c spectrometer was placed at angles from 17° to 90°. At $Q^2 = 6.0$ GeV, the 8 GeV/c spectrometer was at 17°. At all other Q^2 values, data were taken with the 8 GeV/c spectrometer at least three different angles.

The $n(e, e')n$ contribution to the $D(e, e')$ data will be extracted by subtracting the $p(e, e')p$ and $p(e, e')N\pi$ contributions. The proton contributions are calculated from the measured $H(e, e')$ spectra, folded over the deuteron wave function. The proton data will extend the range of separation of the charge and current scattering, independent of any scaling assumption that $G_{M,p}(Q^2) = \mu_p G_{E,p}(Q^2)$. The data on deuterium reach a value in Q^2 where the neutron electric form factor $G_{E,n}$ is predicted to be be equal or larger than the magnetic form factor $G_{M,n}$.[1]

---

[*]*American University*, Washington, DC 20016.

[†]*Lawrence Livermore National Laboratory*, Livermore, CA 91550.

[‡]*University of Maryland*, College Park, MD 20902.

[§]*University of Massachusetts*, Amherst, MA 01003.

[¶]*University of Pennsylvania*, Philadelphia, PA 19104.

[∥]*University of Rochester*, Rochester, NY 14627.

[**]*Stanford Linear Accelerator Center*, Stanford, CA 94305.

[††]*Stanford University*, Stanford, CA 94205.

[‡‡]*Tel Aviv University*, Tel Aviv, ISRAEL.

[1]M. Gari and W. Krümpelmann, Z. Phys., **A322** 689 (1985).

7 ACCELERATOR MASS SPECTROMETRY (AMS)*

7.1 AMS: Scientific Program*

T.A. Brown, J.A. Caggiano, <u>G.W. Farwell</u>, P.M. Grootes, and F.H. Schmidt

During the past year our program has again been centered on radiocarbon (^{14}C) studies.

1. <u>Tree ring ^{14}C profiles.</u> Further analysis of the data on tree ring profiles for 1962 – 63 – 64 (the "bomb spike" years) in Sitka spruce has been accomplished and a paper was presented at the 13th International Radiocarbon Conference at Dubrovnik, Yugoslavia (June, 1988); publication will occur in Radiocarbon [1] (an earlier paper is still in press[2]). Our results suggest that CO_2 from biospheric decomposition plays a significant role in the photoassimilation of carbon by a tree, and that the mixing within the tree stem of photosynthate from different branches is limited. If these conclusions are correct one would then expect to find a vertical ^{14}C gradient in the 1963 ring for a tree growing in a deep forest canopy: the canopy creates a progressive lowering of the ^{14}C contribution from biospheric decomposition from forest floor to the top of the tree, and the disequilibrium between tropospheric and biospheric ^{14}C concentrations was most severe during 1963 due to the rapid rise of the former.

   In contrast, the 1963 ring for a relatively isolated tree growing in a wind-washed location on (for example) the Pacific Coast should show no such gradient. Additionally, neither tree should show such a gradient if, as some believe, carbon incorporated in tree stem growth comes from what amounts to a pool of photosynthate generated by photosynthesis at all levels of the tree crown. We are planning measurements to resolve these issues, which are important in the paleoenvironmental intepretation of tree–ring isotope studies as well as in the fuller understanding of the formation of cellulose from photosynthate.

2. <u>Pollen studies in lake sediment cores.</u> One of us (T.A. Brown) has been a principal in a collaborative effort with the Simon Fraser University–McMaster University AMS group to use AMS in the radiocarbon dating of pollen concentrates from lake sediment cores. The dates obtained by AMS for pollen concentrates differ significantly from those obtained through the conventional radiocarbon dating of bulk sediments.[3] These results offer the promise of more reliable chronologies for important paleoenvironmental events. We are preparing for a series of AMS radiocarbon measurements in this laboratory on pollen concentrates, and possibly on separated pollen grains, with this purpose in mind.

3. <u>Studies of ^{14}C in methane.</u> We have continued our collaboration with P.D. Quay (School of Oceanography) in the NASA–supported study of atmospheric methane (CH_4) and methane

[1] "Importance of Biospheric CO_2 in a Subcanopy Atmosphere Deduced from ^{14}C AMS Measurements," P.M. Grootes, G.W. Farwell, F.H. Schmidt, D.D. Leach, and M. Stuiver, Radiocarbon 30, No. 3 (1989), in press.

[2] "Rapid Response of Tree Cellulose Radiocarbon Content to Change in Atmospheric $^{14}CO_2$ Concentration," P.M. Grootes, G.W. Farwell, F.H. Schmidt, D.D. Leach, and M. Stuiver, Tellus (1989), in press.

[3] "Radiocarbon Dating of Pollen by Accelerator Mass Spectrometry," T.A. Brown, D.E. Nelson, R.W. Mathews, J.S. Vogel, and J.R. Southon, Quaternary Research (submitted).

released from wetlands.[4,5] Our most recent AMS measurements on $^{14}CH_4$ give the following results:

(a) Atmospheric methane from the Olympic Peninsula, Washington, shows a slight increase in $^{14}CH_4$ with time.

(b) There appears not to be an interhemispheric gradient in $^{14}CH_4$, based on the first two measurements; we will soon have a better estimate.

(c) The presence of nuclear–weapons–test–related ^{14}C in the CH_4 flux from all wetlands tested indicates that the cycling time between carbon fixation in plants and methane production is short (less than ~30 years). In the Amazon floodplain and the Minnesota peatbogs the methane ^{14}C concentration was similar to the present ^{14}C concentration in atmospheric CO_2, suggesting an annual cycling of plant carbon into CH_4.

These studies are continuing and form part of a world–wide study of methane, an important "greenhouse" gas.

7.2   AMS: Technical Highlights

T.A. Brown, J.A. Caggiano, G.W. Farwell, P.M. Grootes and F.H. Schmidt

A. Advances in carbon-sample making
Last year we reported that new equipment was being designed to permit preparation of very small tantalum-encapsulated graphite samples. The required jigs, presses, etc., have now been constructed, so we are able to make graphetized samples weighing from 300 to 400 micrograms imbedded in a Ta well 0.028 inches (0.071 cm) in diameter. These samples produce from 200 to 400 thousand ^{14}C counts for contemporary carbon.

B. Improved carbon beam intensity and stability
General improvement in the modified UNIS sputter ion source has raised the useful $^{12}C^-$ beam to 60-80 μA or ~ 1 μA ^{13}C to the image Faraday cup. This increase raised our ^{14}C detection rate for contemporary carbon to as high as 160 per second. For carbon from a 1964 tree ring the rate is ~ 300/sec. The high rate makes it possible to tune the tandem by observing the ^{14}C counts on a rate meter connected to a chart recorder.

C. A 39 second fluctuation
Study of the ^{14}C count rate disclosed a very surprising variation of 20 to 30% with a regular period of 39 seconds. Subsequent investigations revealed the cause to be an incredible coupling between the Generating Voltmeter period, 60 Hertz line frequency, and the Tandem belt period. The implications for AMS are very serious, because our normal unknown-to-standard cycle period is 41 seconds. The GVM-60 hertz-belt coupling phenomenon has implications for general Tandem energy regulation, and is reported in Section 9.7. It has been eliminated.

D. Side Faraday Cup Alignment
Proper positioning of the side Faraday cup, which is used to monitor the ^{12}C beam when

[4]Nuclear Physics Laboratory Annual Report, University of Washington (1988), p. 38.

[5]"An Isotopic Biogeochemical Study of Tundra Methane and its Exchange with the Atmosphere," P. Quay, S. King, J. Staley, P. Grootes, G. Farwell, and R. Gannon, NASA Upper Atmosphere Research Program: Research Summaries, 1986–1987, pp. 317 – 318.

^{14}C is being injected into the Tandem, has been a problem. We devised a new technique for adjustment based on the $(^{12}CH_2)^-$ and the $(^{13}CH)^-$ contaminant beams, the masses of which are known to high precision. The difference in mass between these ions is equivalent to 27 volts change in acceleration potential (85 kV). We measured 40 ± 10 volts. The ^{14}C then lies 56 volts above the setting for the weighted average for $^{12}CH_2$ and ^{13}CH. ^{13}CH is 80% of the total CH component. The procedure has improved normalization by the ^{12}C beam to the side Faraday cup.

E. New Computer Installation

The replacement of the PDP 11/60 with a VAX 3200 and the installation of XSYS as the data acquisition system required the revision of the AMS experiment-control program. Major changes were made to the subroutines which allow computer control of the inflection and analyzing magnets through an IEEE bus and communication with the 5TI Controller. Additional changes were made to the data acquisition sections of the AMS program to make it compatible with XSYS.

F. Sputter Source LN$_2$ trap installation

The improvements in UNIS performance described above are in part, due to the addition of a LN$_2$ trap to the source vacuum system. The addition of the trap has decreased the base vacuum of the source by a factor of 3, has significantly increased the stability of the source at the high output settings, and has decreased the sample-change turn around time from $\sim$4 hours to <1 hour. In addition, significant improvements have been reported in the performance of the Alpha Source because of the LN$_2$ trap.

8 RESEARCH BY OUTSIDE USERS

8.1 Hard Errors Generated in EEPROM's by Heavy Ions

D.L. Oberg,* J.L. Wert,* and P.R. Measel*

Nonvolatile memory is an important component of most computerized systems. There are many types of nonvolatile memory devices: ROM ("read-only memory"), UVPROM ("ultraviolet programmable read-only memory"), EAPROM ("electrically alterable read-only memory"), and EEPROM ("electrically erasable read-only memory") to name just a few.

EAPROM's and EEPROM's are of special interest as they can be re-programmed while in-circuit thus making software modifications possible for systems in physically inaccessible locations. These devices are erased by internally applying a voltage across the thin gate insulator at each memory cell. This allows the charge stored in the memory cell to be bled off. Unfortunately, this also results in a large voltage gradient across the insulator during the write or erase cycle. It has been previously seen that permanent damage can be caused in MNOS ("metal-nitride-oxide semiconductor") devices by the combination of high voltage gradient and heavy ion tracks.[1]

These devices are to be used in systems where heavy ions are probable; thus, any NVRAM application should be viewed as suspect. The EEPROM's we are interested in are somewhat different from the devices previously tested. While EEPROM's do not have an external voltage supply for writing/erasing, they do use an internal charge pump to generate the required higher voltage from TTL levels. Also many EEPROM's are designed with extra bits in each word for EDAC ("error detection and correction") to provide for long-term reliability. The present work is to determine if EEPROM's would be subject to observable damage from heavy ions.

We used 98 MeV chlorine ions from the Van de Graaff to irradiate several EEPROM's. The devices were preprogrammed using a Tektronix 3295 VLSI test system at the Boeing Radiation Effects Laboratory. Testing at the NPL was done with a pattern generator which is a part of the Boeing portable SEU ("single event upset") test system. This is a different application of the same system used for previous tests at the Nuclear Physics Laboratory.[2] This system repeatedly reads the devices and when errors are detected the device is reset and the error is logged.

Hard errors (permanent damage) were seen in these tests. This indicated the internal voltage levels were sufficient to cause damage when an ion strikes and that the internal EDAC was not fully effective in correcting this type of damage. Further tests and analyses are being conducted.

---

*Boeing Aerospace Company, Seattle, WA 98124-2499.

[1] "Hard Error Generation by Neutron-Induced fission Fragments", J.S. Browning *et al.*, IEEE Trans. Nuc. Sci., NS-34, Dec 1987.

[2] Nuclear Physics Laboratory Annual Report, University of Washington (1988) p. 43.

8.2 Charged Particle Detector Development

E.D. Franco* and A. Milgram*

We are developing a threshold ionization particle detector based on metal-insulator-silicon capacitor (MISC) thin film technology. These detectors act as compact Geiger counters responding only to particles with stopping powers above a well-controlled threshold. Our primary research goal is to develop the proper MISC architecture to expand the sensitivity to encompass a range of stopping power from 1 to 50 MeV-cm^2/mg in SiO_2. We are using attenuated ^{252}Cf fission fragments to determine the functional dependence of the stopping power threshold required to produce a count and the applied electric field across the MISC between 15 to 40 MeV-cm^2/mg. These fission fragment studies were confirmed and extended by a series of experiments at the University of Washington Van de Graaff Facility. The response of the detector was measured with essentially monoenergetic carbon and silicon ions with stopping powers comparable to those attainable with heavily attenuated fission fragments. The results verified our 252Cf experimental results and the fission fragment correction factors that determine the magnitude of the ionization energy loss in the structure.

8.3 Thin Layer Activation Analysis for Application to the Study of Erosion-Corrosion in Feedwater Pipes

J.T. Stanley[†]

Irradiation of a second set of 2.5 inch diameter pipes was carried out for continuation of the erosion-corrosion studies described in last year's report.[1] An interesting development in this work is that calibration experiments to determine the distribution of radioactive ^{56}Co below the surface showed considerably deeper penetration than had been anticipated. Furthermore, the amount of extra penetration varied for different samples in a way that was consistent with the amount of beam heating of the samples. This suggests that diffusion of the radioactive Co occurs because of the temperature increase produced by the proton beam. This is an unexpected result because of the short times and moderate temperatures involved. A possible explanation is that the point defects introduced by the proton interactions with the lattice atoms enhance the rate of diffusion.

*Advanced Research and Applications Corporation, Sunnyvale, CA 94086.
†Chemical Engineering Department, Arizona State University, Tempe, AZ, 85287-6006.
[1] Nuclear Physics Laboratory Annual Report, University of Washington (1988) p. 41.

9 VAN DE GRAAFF AND ION SOURCES

9.1 Van de Graaff Accelerator Operations and Development

C.E. Linder, F.H. Schmidt, T.A. Trainor, and W.G. Weitkamp

During the year from April 16, 1988 to April 15, 1989 the tandem operated 3925 hours. Additional statistics of accelerator operations are given in Table 1. During the year, 30% of the available operating time was lost to maintenance and development activities. Principle problems involved the drive motor and the charging system. We replaced two drive motors during the year, including one brand-new one which ran only 524 hours before burning up. The charging system activities are described in Sec. 9.8 and below.

For the past several years, we have had sporadic difficulty with the high energy column current rising to a value 5 to 30 % higher than the low energy column current. This was accompanied by a shift in the position of the beam as it left the tandem and an increase in the belt charge required to maintain the terminal voltage. Clearly, either the belt has been losing charge to the column or the effective column resistance has been changing. Several times we have been able to temporarily reduce this effect by cleaning the belt guides on the column where the charged belt first enters the column. In January we observed that when one abruptly turned off the belt charge, the high energy column current dropped immediately to the same value as the low energy column current and then decreased in the normal way as the terminal charge bled off on the column resistors, indicating definitely that charging current was rubbing off on the column. Inside the tank, inspection of the belt guides outside the belt showed nothing unusual. However, some of the belt guides inside the belt were out of position. The inside belt guide is held by a screw in a slot. The misaligned belt guides, some shifted by as much as 0.2 inch, were forcing the belt outward against the outside belt guides. Using a simple gauge, we realigned all the inside belt guides. The effect disappeared for two months but then reappeared in April. Further investigation will be required.

In 1975 we installed a new set of resistor assemblies in the tandem. The assemblies were built in-house and consisted of PVC tubes with 4-100 MΩ RPC resistors held in end-to-end contact with a spring.[1] The parts for these assemblies cost $12 each (in 1975). Over the years a fraction of the resistors have failed and we have used up our spares. RPC resistors are no longer available so we have had to look for a substitute. We tried 10 assemblies in which the RPC resistors were replaced with Caddock MG815 resistors. Caddock resistors have been used successfully in other tandems in geometries in which the resistors are well shielded from sparks. Apparently our PVC tubes do not give enough protection however, because the resistors quickly degenerated. The first one opened after 3 months in the machine, and all were removed after 4 months because the average resistance had increased by 40%. The Caddock MG815 is a non-inductive resistor; it may be that inductive resistors are more tolerant of the column environment. We have begun testing other resistors in hopes of finding ones which are both inexpensive and reliable.

For many years, an ion pump has pumped the low energy beam tube. While maintaining a satisfactory vacuum, this type of pump suffers from several deficiencies such as a poor pumping speed at pressures in the 10^{-4} Torr region, poor pumping speed for helium and moderately high maintenance requirements. We have replaced the ion pump with a turbomolecular pump. This has overcome the pumping speed problems and required no maintenance so far.

Improvements to the tandem generating voltmeter are described in Section 9.7.

---

[1] Nuclear Physics Laboratory Annual Report, University of Washington (1975) p. 5.

Table 1
Tandem Accelerator Operations
April 16, 1988 to April 15, 1989

Activity	Days Scheduled	Percent
A. Nuclear Physics Research		
Light Ions	37	10
Polarized Ions	15	4
Heavy Ions	27	7
Booster Beams	70	19
Accelerator Mass Spectrometry	24	7
Subtotal	173	47
B. Outside Users		
Advance Research and Applications Corp.	1	<1
Arizona State University	1	<1
Boeing Aerospace Corporation	5	1
Subtotal	7	2
C. Other Operations		
Tandem Development	36	10
Tandem Maintenance	71	20
Booster Development	16	4
Unscheduled Time	62	17
Subtotal	185	51
Total	365	100

9.2 Polarized Ion Source

D.R. Balsley, C.M. Bitz, J.K. Eisenberg, A. García, <u>C.A. Gossett</u>, G.C. Harper, J.A. Rogers, K. Swartz and V.J. Zeps*

A crossed-beams polarized ion source based on the design of Ref. 1 has been in operation for nuclear physics experiments since late 1987. Thermal beams of polarized atomic hydrogen or deuterium are ionized by charge exchange in collisions with a collinear fast neutral cesium beam. Negative ions are extracted and the polarization symmetry axis may be precessed into any desired direction by a crossed-fields spin precessor. Polarized beam currents as high as $1\mu A$ have been recently observed, although more typical long term operation has generally been at the level of ~300nA.

The polarization of deuterons has been studied and optimized in the last year. A good deal of tuning of the rf transition cavities for deuterium, ($2\to6$, 455 MHz) and ($3\to5$, 330 MHz) (see for example Ref. 2), including adjustments of physical components, was required in order to allow the cavities to be driven with sufficient detected power within the cavity. In particular the resonant frequency of the $3\to5$ transition was initially too low for that transition to be driven. A trim coil was constructed around one half of the strong field transition magnet in order to allow simultaneous optimum performance of both the $2\to6$ and $3\to5$ transitions. Vector polarization of $it_{11} = 0.46$ was measured using deuteron elastic scattering from ^{4}He at 13 MeV. The measured value of the polarization corresponds to only $\sim80\%$ of the maximum possible value, 0.57, and we plan to investigate whether the deuteron polarization could be improved. For protons we quite typically measure polarizations greater than 0.90 (1.0=maximum).

A major effort was spent on optical alignment of the atomic beam and H$^-$ beam formation components of the source. We found initially that the axes of the atomic hydrogen beam and the neutral cesium beam were far from parallel, and that the beams did not have a large intersection region within the volume of the solenoid. We also found large variations in the relative alignment of the elements of the H$^-$ beam extraction system and that many components were not initially constructed in order to allow for reliable, self-aligning reassembly. Considerable effort was also spent in establishing fixed reference points within the accelerator vault in order to facilitate future alignment work. In overall performance, the H$^-$ current output of the source increased by approximately a factor of 2 and the transmission of the beam through the low energy beamline and through the tandem each improved by 50%, thereby increasing the available beam intensity for experiments.

The closed-loop chilled water system for the polarized ion source was completely rebuilt. The original water pump for the system provided insufficient flow rate and output pressure in order to adequately cool all components of the source and was replaced. The pressure regulation and water flow interlock systems were also improved.

As described in more detail in the following report, the development of the control system has steadily progressed. The interlock systems for the atomic beam and cesium beam systems, including all vacuum, high voltage and cooling controls, are completely under computer control

---

*Present address: Carnegie-Mellon University, Department of Physics, Pittsburgh, PA.

[1]W. Haeberli, *et al.*, Nucl. Instrum. and Methods, **196**, 319 (1982).

[2]W. Haeberli, Ann. Rev. Nucl. Sci. **17**, 372 (1967).

and have performed quite reliably. The hardware and software for both remote and local analog control of source parameters through "knob boxes" connected via the Linac μvax have been designed and are under construction and development.

9.3 Polarized Ion Source Computer Control System

C.M. Bitz, C.A. Gossett, G.C. Harper, M.A. Howe, and H.P. Readdy

Work has continued on the control system for the polarized ion source in an effort to place it completely under computer control with both remote and local access. Progress has been made toward this goal and some new enhancements have been added to this project.

The interlocks for the atomic beam system and the cesium beam system, two independent processors on the polarized ion source, have been completely converted from hardwired operation to computer operation. This involved disconnecting existing interlock wires from three panels in different locations, conditioning some signals, adding some new two-state sense parameters, connecting to the available controller ports, and incorporating the changes into the software. We have found the new system to be much more flexible than the hardwired system and, with the incorporation of a built-in bypass delay timer, better fail-safe protected when used in bypass mode. Reconfiguration of the software interlock system has been accomplished in as little as 30 minutes.

A process has been incorporated into the injector deck satellite computer which polls the polarized ion source parameters and updates the LINAC μvax control computer with any changes. The present polling rate of one pass per 2.5 seconds should be an adequate refresh rate without heavily taxing the already busy satellite computer. Parameters being changed by the CSX program through the touch screens or knob boxes have a much higher refresh rate.

The design of two new knob boxes for use from locations other than the LINAC μvax control console has been completed. Access to the polarized ion source parameters, as well as all other CSX parameters, from the counting room, the caves, and the source area will be possible using these new knobs. Sixty-four parameters may be selected by a bank of 16 panel-mounted pushbutton switches each of which connect 4 different parameters to optically encoded knobs. The boxes are lightweight and small (3"x7"x13") and connected to a quasistationary panel mounted satellite computer through a single multiconductor cable to enhance portability. The ability to tune from the source area using the knob box will be a tremendous improvement over the existing system of increment and decrement keys on the front panels of the ANAC controllers which may access only one parameter at a time and must operate at some predetermined, fixed rate of change. All of the parts have been procured for this project and construction is underway.

Work is just now beginning on development of a controller for the spin precessor system. Components for use on this system and as spares have been received from Yale University which no longer uses the ANAC systems in their laboratory. Expected accomplishments this year include completion of the spin precessor system, completion and implementation of the knob boxes, and complete operation of the cesium and spin precessor systems in conjunction with CSX.

9.4 Model 860 Performance

D.J. Hodgkins and T.A. Trainor

In the initial design of the injector platform beam transport system our mass resolution goal was $m/\Delta m \sim 100$. This assumed object and image slit widths of 2 – 3 mm, a $\rho = 0.8$ m 90° magnet, a $\rho = 1$ m 45° magnet and some additional optic elements to correct for the astigmatism of this two–magnet system.

Recently we have achieved results which considerably surpass this and indicate that the Model 860 emittance is now much better than anticipated.

Figure 9.4-1 shows a beam of MoO^- on the image scanner of the mass analysis system. The four peaks from left to right correspond to A = 96 – 93 for molybdenum. The relative peak heights don't correspond to isotopic abundances because this dispersed beam has passed through a 2.5 cm circular aperture upstream of the scanner. The $m/\Delta m$ for this figure is more than 600 and the scanner wire contributes a significant fraction of the peak widths.

Figures 9.4-2, 9.4-3 and 9.4-4 show respectively analyzed beams of $^{16}O_2^-$, $^{27}Al_2^-$, $^{27}Al^{16}O^-$. Only the analysis magnets were changed between these records. The sputter sample was MgO_3 powder in an aluminum holder. One can see that oxygen is coming from the 3 mm diam. sample (cesium beam half width < 1 mm), aluminum is being produced in an annular region around the sample and AlO is being produced at the edge of the sample. These results are especially striking considering that no slits were used. Object slits were put in during beam optimization and then fully removed from the beam during the recording.

As a result of ray trace studies of cesium beam formation in the model 860,[1] new ionizer configurations are being tried with the goal of moving the cesium beam waist further upstream and possibly reducing its diameter. The former will facilitate incorporation of a rotating sample wheel at a later date, and the latter will permit use of smaller samples and reduce the source emittance.
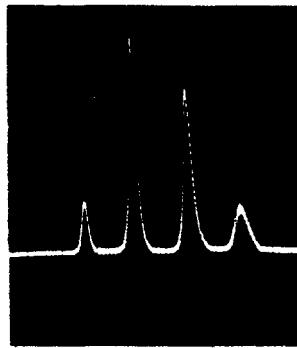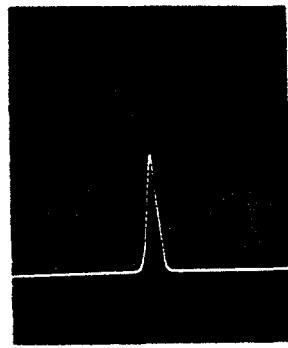
Figure 9.4-1. MoO^-.   Figure 9.4-2. $^{16}O_2^-$.   Figure 9.4-3. $^{27}Al_2^-$.   Figure 9.4-4. $^{27}Al^{16}O^-$.
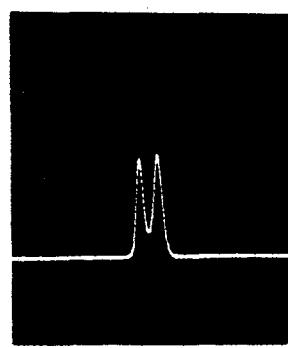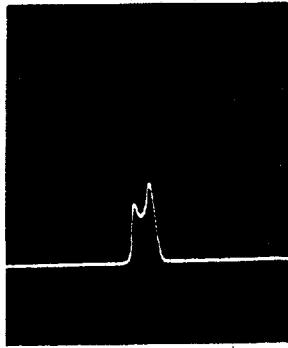
---

[1]Section 9.5, this report.

9.5 Model 860 Sputter Source Modifications Based on Computer Modelling of Cesium Trajectories

T.A. Brown, D.J. Hodgkins, and T.A. Trainor

The Model 860 Sputter Source has been significantly improved by the modifications which are described in this annual report and previously.[1] As part of efforts to further improve the source, we have computer modelled the behaviour of ionized cesium within the source with the specific goals of improving cesium focussing and minimizing difficulties in designing an automated sample-changer wheel.

The modelling program[2] performed successive relaxation calculations to determine the electric fields within an electrode geometry and then used a finite difference method to calculate the trajectories of ions in the electric fields. Comparison of computer-generated cesium trajectories with actual cesium focussing characteristics of the current ionizer geometry show that the program is able to model the behaviour of ionized cesium within the limitation that space charge effects are ignored. The modified ionizer geometry arrived at through these modelling studies (Figure 9.5-1) shows much improved cesium focussing and the sample cathode no longer intrudes into the ionizer region, which should considerably simplify the design of a sample-changer wheel. The modified ionizer geometry is being constructed and will be tested in the next months.
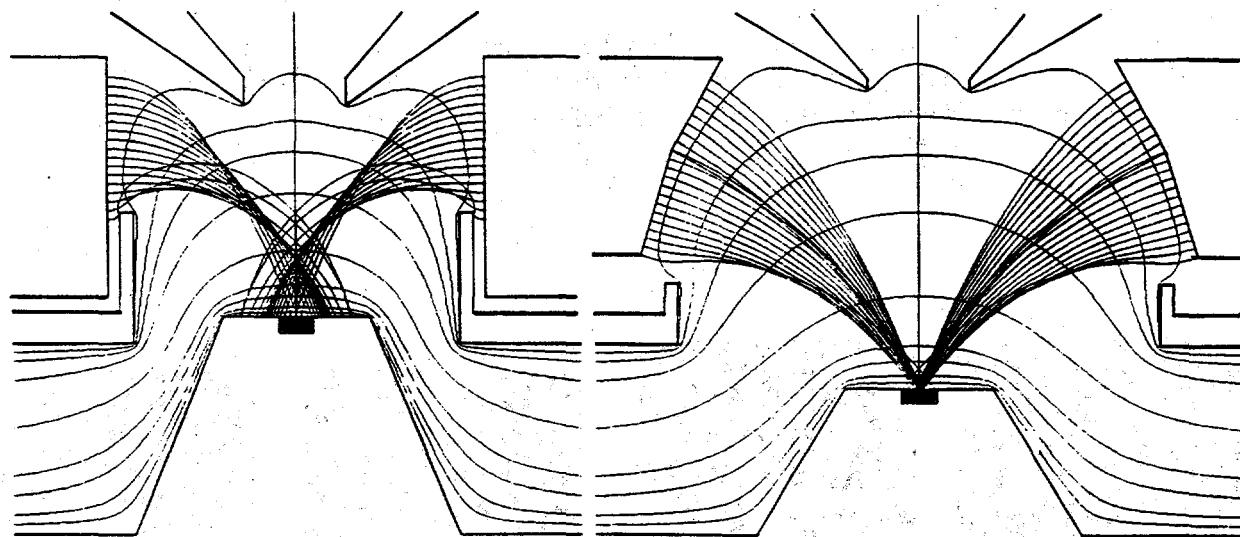
Figure 9.5-1. Ionized cesium trajectories within the current ionizer geometry (left) and the modified geometry from these modelling studies (right). The figures show the trajectories of cesium ions formed at the ionizer as they are accelerated and focussed by the electric fields within the source (which are indicated by equipotentials drawn between the electrodes).

---

[1]Nuclear Physics Laboratory Annual Report, University of Washington (1988) p. 52.

[2]Written and supplied by John Southon, Tandem Accelerator Laboratory, McMaster University, Hamilton, Ontario, CANADA L8S 4K1.

9.6 The Tandem Emittance

M.A. Howe, T.J. Irwin,* J.M. LaCroix, J.M. Stehfest and W.G. Weitkamp

As part of the superconducting booster project, we purchased a Danfysik Beam Emittance Measuring System 590 to assist in the diagnosis of beam optics problems in the booster. The first step in using this device is to characterize the tandem emittance accurately so that booster emittances, which we intend to measure in the near future, can be understood quantitatively. Consequently, we have measured the emittance of a number of tandem beams.

The emittance measuring system uses a slit and a set of parallel wires (a 'harp') both of which are mounted 38 mm offset on rotating shafts. The harp is located about 1 m downstream from the slit. Emittance is measured by rotating the slit and harp across the beam stepwise and measuring the charge intercepted by each wire of the harp during each step. The slit and harp are tilted 45° with respect to the shaft axis, so both horizontal and vertical emittances can be measured.

The interface developed to control the system and display the data using the booster computers is described in Section 12.7 of this report.

An off-line program has been written to calibrate and apply several corrections to the emittance data. One correction reduces errors introduced by the rotational geometry of the system; for example, the slit opening changes as the slit is rotated. A second correction reduces errors introduced by beam intensity fluctuations during a measurement. The final emittance number is obtained by calculating the area of the contour on the r-θ plot containing 90% of the beam.

We have completed a series of measurements of the tandem emittance. The results are given below. In all cases, we refer to the normalized emittance, i.e., the measured area in the r-θ plane multiplied by the square root of the beam energy and divided by π. The conclusions listed are based on measurements with about a 10% uncertainty.

1. The horizontal emittance is about 30% bigger than the vertical emittance. This results both from position fluctuations induced by the beam energy regulation system and from the larger beam tube aperture in the horizontal plane.

2. The emittance is independent of charge state for a given nuclear species and terminal voltage.

3. The emittance is independent of beam intensity, measured with beams of from 35 nA to 290 nA incident to the tandem. The intensity was varied by adjusting the ion source slit aperture.

4. The emittance depends somewhat on terminal voltage. It drops roughly 30% from 6 MV to 8 MV, then rises slightly above 8 MV. The drop probably results from decreasing multiple scattering in the stripper foil, but the rise above 8 MV is not understood.

5. The emittance depends on the ion source used. In particular, the emittance of ^{16}O produced by OH^- ions from the direct extraction ion source is about 15% higher than the emittance of ^{16}O produced by O^- ions from the General Ionex Model 860 sputter source. This somewhat surprising result may be caused by 'Coulomb explosions' in stripping the OH^- molecule.

6. The emittance depends on nuclear species. In the vertical plane, with 9 MV terminal voltage

---

*Now at Boeing Aerospace Company, Seattle WA 98124.

and using the 860 ion source, the values measured to date (in π mm mrad $\mathrm{MeV}^{1/2}$) are: protons, 7.7; $^{16}\mathrm{O}$, 31; and $^{28}\mathrm{Si}$, 37. The emittance values for protons compare well with calculated values for the acceptance of an FN tandem[1] (12 π mm mrad $\mathrm{MeV}^{1/2}$). Clearly, multiple scattering in the stripper foil is an important contributor to the emittance of heavy ion beams.

9.7 Tandem Energy Control—The Generating Voltmeter

T. Brown, H. Fauska, F.H. Schmidt, and T. Van Wechel

The Generating Voltmeter (GVM) has had a history of development extending over many years.[1-4] This year we discovered a surprising interaction between the GVM, 60 Hertz, and the Tandem belt.

In the course of searching for the cause of a discrepancy between the statistical accuracy of a $^{14}\mathrm{C}$ count determined by counting error, or by internal error from repeated measurements, the Accelerator Mass Spectrometry group discovered a periodicity in the $^{14}\mathrm{C}$ "beam" ($\sim$150 particles per second) with a frequency of 0.026 Hertz (39 second period). Energy control of the Tandem for such a small beam is, of course, entirely by the GVM.

It had long been thought that the GVM rotor was driven by a synchronous motor rotating at 60 Hertz; it is not. The motor is an induction motor; such motors run at less than synchronous speed, and our GVM motor spins at 58.8 Hertz. A slight asymmetry in construction of the 14-toothed rotor[4] produces a 58.8 Hertz ripple equivalent to 5.7 x 10^{-3} of the terminal potential.

A small 60 Hertz pickup caused by a ground loop in the output circuit generated a beat frequency of 60-58.8 = 1.2 Hertz. The fundamental frequency of the Tandem belt is $\sim$2.4 Hertz. Inhomogeneities in the belt charge produce a spectrum of terminal potential frequencies[6] depending on the belt quality, but the fundamental is generally predominant.

Thus, the 1.2 Hertz from the GVM—60 Hertz interaction produced a double beat frequency with the 2.4 Hertz of the belt. More careful measurements of the GVM and the belt frequencies gave a calculated final beat frequency of 0.023 Hertz, or 44 sec. period. Considering that there had been a change in the drive motor between the initial observation and the unraveling of the cause, the agreement between observation and calculation (39 sec. vs 44. sec) is remarkably good.

We have eliminated the GVM-60 Hertz interaction, and reduced the 58.8 Hertz ripple to $\sim$2x10^{-3} of the terminal potential equivalent. The 44 second period is gone, and the regulation of the Tandem terminal potential by the GVM is markedly improved. A new and more precisely machined GVM rotor is under construction. We hope to achieve "pure" GVM energy control rivalling that of slit control.

It is astonishing that we were led to all of this via a difference between counting and internal statistics.

[1]C. Lukner, G. Latzel and H. Paetz gen. Schieck, Nucl. Instr. and Meth. **146**, 139 (1977).
[2]Nuclear Physics Laboratory Annual Report University of Washington (1978) p. 119.
[3]*Ibid.*, (1979) p. 156.
[4]*Ibid.*, (1980) p. 181.
[5]*Ibid.*, (1981) p. 161.
[6]T.A. Trainor, SNEAP 1988.

9.8 FN Terminal Voltage Noise and Charging Belt Properties

T.A. Trainor

Last year I described experience with an unusually large terminal voltage fluctuation which repeatedly disrupted the operation of the energy stabilizer.[1] This was traced to transverse motion of the charging belt caused by tank gas turbulence. The belt was found to have a roughened inner surface and was replaced. This fluctuation has not recurred. Further study of the power spectra for this fluctuation indicated that the belt motion was chaotic, that the onset of chaotic motion occurred at about 175 psi tank pressure with a 20 psi hysteresis, and that the power spectrum consisted of a 1Hz wide distribution of very narrow peaks centered near 3.7Hz. The belt was acting as a microphone diaphragm for the gas turbulence.

Subsequent to these studies I have used the diagnostic techniques developed therein to analyze the remaining terminal voltage noise. I find that all remaining noise is due to loss of contact between the charge applicator and the belt surface. The contact loss is produced either by flutter of the belt edge or by bouncing of the applicator edge over thickness variations in the belt.

As diagnostics I used time and frequency domain records of the high energy column current (HECC), corona triode grid drive voltage (corona) and the stripper regulator LED current. The HECC was especially useful, and although this signal has contributions from capacitive coupling between the belt charge distribution and the column as well as ohmic currents from the terminal potential, it is possible to separate these components based on frequency content.

The belt edge flutter occurs because the belt tension drops off quickly near the belt edges due to the conical ends of the pulleys. Contact between belt and screen varies at the belt fundamental frequency f_o(2.4Hz) and causes charge fluctuations as high as 10–20%. These fluctuations have been reduced by $\sim$10x by replacing stainless steel screens with flexible 5 mil shim stock, and maintaining very firm contact between belt and applicator.

The principal thickness variations are caused by the belt rubber cure pattern and occur at 12x the belt fundamental (12 f_o). The charge applicator bounces over these bumps and momentarily loses contact with the surface, leaving strips of uncharged belt. In the HECC, corona and LED signals the 12 f_o spikes are clearly present. This noise contribution could be eliminated by slanting the cure boundaries at 45° with respect to the belt.

---

[1]Nuclear Physics Laboratory Annual Report, University of Washington (1988) p. 50.

10 COMPUTER SYSTEMS

10.1 Acquisition System Developments

C.A. Gossett, M.A. Howe, C. Hyde-Wright, H.P. Readdy, R.J. Seymour

This year saw the demise of our 11-year old PDP 11/60. We had been testing TUNL's XSYS acquisition software on a VAXStation II/GPX as its replacement. A CPU failure of the 11/60 simply chose the date of the final switchover. Since then we have replaced the VAXStation II/GPX with a VAXStation 3200. The VAXStation 3200 has a Q-bus problem which required some rewriting of MBD-11 code from the VAXStation II/GPX version.

Our principal data acquisition system is now a DEC VAXStation 3200 with a BiRa MBD-11 controlled CAMAC crate. The VAXStation has an 8 megabyte memory, a 19 inch monochrome screen and a Q-bus extension cable to a BA23-CC expansion box containing a 760 megabyte Maxtor disk drive on an Aviv DFC 904 controller, another Aviv controller for a Telex 9251 6250 bpi tape drive, a DEC IEQ11 IEEE-488 bus controller, a DEC DRV11-J and an MDB DWQ11 Q-bus to UNIBUS converter. The other end of the DWQ11 converter is in one of the 11/60's UNIBUS cabinets, where the MBD-11, a DR11-C and our Printronix's lineprinter controller are still attached. A second acquisition system is being assembled for the Time Projection Chamber project (see Section 11.3).

The principal changes we have made to TUNL's XSYS include: expansion of the XDATA histogramming space to over 8 megabytes and the addition of programs to access our special scalers, experiment control electronics and IEEE-488 hardware. We have made a VAXStation (VWS/UIS) compatible version of their DISPlay program, featuring multiple windows, integral full VMS-help, contour plots, grey-scale two-D, optional mouse-selection of commands and redefinition of the commands along the lines of Neil Yoder's IUCF version of XSYS. The forced rapid implementation prevented the installation of IUCF's verson of XSYS (we had TUNL's running, and kept with it). As time allows, more IUCF-like features will migrate into our system. The TUNL XSYS Help files are being extensively restructured to fit VMS's HELP environment.

The VAXStation 3200 is about three times faster than the VAXStation II/GPX. This is quite visible in plot updates and the amount of CPU power still available to the user during high data rates. As mentioned above, DEC admits to an error in the Q-bus implementation of all 3000-family members. It is described in a letter included with each machine, and they provided knowledgeable product managers at the Fall 1988 DECUS Symposium at Anaheim. Among the problems are: (1) failures if two devices communicate via the Q-bus without involving the CPU or main memory, (2) failures of DATIO Q-bus cycles, (3) failure to restore the CPU state under certain UNIBUS-valid interrupt cycles, and (4) a potential bus latency problem if user-written drivers directly write to the Q-bus mapping registers.

We were seeing problems when we had the MBD-11 do read-modify-writes to histograms in memory, even as separate RDR/WTR cycles. The symptoms included: bad data being received by the MBD-11 and failure of the Q-bus to respond to MBD-11 NPR requests. The first symptom would often appear during screen updates (heavy virtual paging activity), and the second would occur about once every 100,000 read/write MBD-11 cycles. On the VAXStation II/GPX, we had implemented our 11/60's fast SINGLES method of having the MBD-11 do direct histogram

incrementing, instead of the normal XSYS fill-an-event-buffer technique. The VAXStation 3200 has forced us back to the normal XSYS method, but with the MBD-11 code modified to provide an ADC CAMAC slot number along with its channel data. We also removed the need for specific LAMs to cause the SINGLES MBD-channel program to run. The slot number allows the XSYS EVAL code to determine which spectrum should be incremented for each reading in the buffer. All of the SINGLES ADCs share the same MBD-channel program, and may still be simultaneously used as part of other coincident events.

With our new system we can take event data directly to the VAXStation's 760 megabyte disk. We are also able to casually increase the number of parameters acquired with each event. For equivalent multiparameter events, we see about twice the throughput compared to our old 11/60 system. All told, we have approximately quadrupled the rate of data getting to tape.

We have used the IEEE-488 interface to read and control the inflection and analyzing magnets for the Accelerator Mass Spectrometry system (see Section 7.2).

10.2 Analysis and Support System Developments

C.A. Gossett, M.A. Howe, C. Hyde-Wright, H.P. Readdy, R.J. Seymour

Our principal interactive system is still an 8 megabyte VAX 11/780 with connections to thirty-odd local terminals. It is connected via ethernet to the nine VAXStation 3200's in our building, and via fiber optic ethernet to the rest of the campus.

As a consequence of converting to XSYS for acquisition, we are now using XSYS programs for off-line sorting and analysis. We have modified our standard spectrum print/plot program HIST to accept XSYS data areas. We have also given our spectrum manipulation program HP[1] the ability to deal with XSYS spectra. Some incompatibility arises from TUNL's XSYS carrying less information in its data structures than we maintained in our 11/60 system.

We have replaced all of our MicroVAX II's and VAXStation II/GPX's with VAXStation 3200's. This was done at little cost due to the resale value of the older machines compared with the educational price of the 3200's. The enhanced data collection offered by XSYS demonstrated the severe constraints of our VAX 11/780's processing speed and disk space available for event files and sorted spectra. We added a Maxtor 760 megabyte disk drive to our 11/780 when one of its disks developed write errors. This was cheaper and faster than repairing the old disk drive. Planning for the eventual retirement of the 11/780, the Maxtor is on a Q-bus controller connected to the 11/780 via an MDB Unibus-to-Qbus converter. As the cost of such large-capacity disk systems dropped below $6000., we have added them to most of the VAXStations to provide adequate off-line analysis power and space.

We still provide site management for the Nuclear Theory group's computers, which are also now all VAXStation 3200's.

Adding an Apple LaserWriter II/NTX to the 11/780 has allowed us to use TEX and LATEX for our document generation. We are still integrating and simplifying access to these packages.

We are using DECnet-DOS on two of our IBM PC-AT's for file access and conversion.

Linac-related computer items are covered in Section 12.

---

[1]Nuclear Physics Laboratory Annual Report, University of Washington (1981) p. 213.

11 INSTRUMENTATION

11.1 The Plastic Wall: An Array of Phoswich Counters

M. Bryce, D.D. Leach,* T. Nirider,† D. Prindle, and R. Vandenbosch

The Plastic Wall, constructed during the past year, consists of twelve individual phoswich counters. A phoswich counter consists of a thin scintillator acting as a δE counter attached to a thicker scintillator acting as an energy counter, both viewed by a single photomultiplier tube (PMT) attached to the back. The δE versus E measurement allows one to identify particle types. Using a single PMT allows one to pack the detectors close together.

An individual counter presents a square face to a particle coming from the target. Each counter is 17.5 inches from the target and is 2.13 inches (or 6.96 degrees) wide. Nearest the target is a 14 mil thick scintillator (BC400) with a short time constant (1.8 ns) acting as a δE counter. Behind this is a thick scintillator (BC444) with a long time constant (180 ns) used to measure the particle energy. Next is a lucite light guide (to decrease position sensitivity of light collection efficiency) and then the PMT. The BC444 is tapered so that its edges project back to the target. A particle depositing energy in the counter gives rise to a 'fast' pulse (due to the thin scintillator) on top of a much longer 'slow' pulse (from the thick scintillator). Measuring the charge in the fast pulse and the charge in a section of the slow pulse enables one to identify protons and alphas and measure their energy. The minimum energy to make it through the thin scintillator is 6 MeV for protons and 24 MeV for alphas. The energy to punch through the thick scintillator is about 55 MeV for protons and 220 MeV for alphas.

The counters are held in a support designed to be placed in the sixty inch scattering chamber. There are thirteen positions in the reaction plane, five positions 7 degrees above the reaction plane and three positions 14 degrees above the reaction plane. This support can be placed at virtually any angle from the beam and leaves the two arms free.

The charge from the PMT is measured in two 12-channel charge sensitive ADCs, one of which is a LeCroy 2249SG and the other is a LeCroy 2249A. The 2249SG has separate gates for each of the analog inputs. This allows us to ensure that the 'Fast Gate' is timed correctly for all counters. The 2249A has a common gate for all analog inputs, but the timing here is not critical. A signal from a counter is first split into three with a Phillips 740 linear fan–out. The first signal is delayed about 20ns using a Phillips 792 delay module and used as the analog input to the 2249SG. The delay is adjusted so the 'Fast Gate' is in coincidence with the leading edge of the analog pulse. The second signal from the linear fan–out is used as the input to the 2249A. The last signal from the linear fan–out is used to create the gates. First it goes through a Phillips 715 constant fraction discriminator used to create the 20ns wide 'Fast Gate'. This gate, in addition to being used by the 2249SG, is sent to a LeCroy 429A logical fan–in. This common signal is used to create a 'Slow Gate' 150ns wide which is delayed so its leading edge is 100ns after the leading edge of the analog signal at the input to the 2249A. The result is that for an event in which more than one counter has a signal the 'Fast Gates' will all be 20ns wide and timed to their pulses. The 'Slow Gate' will be 150ns wide and will start 100ns after the start of the first pulse. This electronics takes 1–1/2 NIM bins and 3 CAMAC slots.

---

*John Fluke Mfg Co Inc, Everett, WA 98206.
†Boeing Aerospace Company, Seattle, WA 98124.

During initial runs with ^{16}O beams we find that protons and alphas are well separated. In fact all nuclei up to ^{16}O can be identified. Protons and deuterium are not completely separated, but there is a clear deuterium signal. The counters have been calibrated with proton and alpha beams and we can measure the particle energy to about 10%.

11.2 Study of Electron Track Properties in Methane

J.G. Cramer, C.E. Hyde–Wright, D. Prindle, and <u>T.A. Trainor</u>

Pursuant to design of a TPC for study of e^+/e^- pairs in heavy ion collision we have made estimates of electron track properties in various gases. The purpose was to determine whether sufficient position and momentum resolution and data rate could be achieved to provide useful information about the e^+/e^- production mechanism.

Early in our study we realized that multiple scattering would be the principle limitation to position and energy resolution. Thus it was essential to use a light (low Z) gas. Methane is an excellent compromise in terms of low Z, high speed and low diffusion. We have concentrated on methane for design studies and have contrasted methane with isobutane performance in actual wire chamber performance tests.

The proposed drift field value for the TPC is 150 – 200 V/cm at 150 Torr, for which the drift speed should be a maximum at 10 cm/μs. At this field value the longitudinal diffusion (rms) should be $\sqrt{4.0\mu \cdot Z}$ after a drift distance Z, resulting in a track FWHM after 16 cm drift of 1.9 mm. We observe a 3 mm FWHM. Corrections due to finite wire chamber thickness may reduce this slightly.

The drift speed for methane should rise to a maximum of 10 – 11 cm/μs at an E/p value of 1.3 V/cm–Torr and then fall off. Our data agree very well with this expectation. This high speed is important because the data rate is limited primarily by how fast the tracks from a nuclear scattering can be cleared from the TPC volume. With a drift length of 17 cm this means that an event can be cleared in under 2μs and scattering rates up to 500kHz are possible.

Multiple scattering was investigated with Molière's theory of multiple scattering, both to determine statistical quantities such as θ_{rms} and to perform Monte Carlo calculations of electron trajectories. Typical results for design conditions (150 Torr Methane) were $\theta_{rms} = 0.06$rad (3.5°) and y$_{rms}$ (displacement)= 3.5 mm after 10 cm. This should be compared with multiple scattering of electrons in the target of 5–10°.

The Molière distribution departs significantly from the normal distribution at larger angles and, under our design conditions, the total number of scatterings is small, so actual multiple scattering effects are underestimated by these rms values.

These design studies serve to indicate that sufficient momentum and position resolution are possible with the TPC technique to provide useful information on e^+/e^- production, but continued study of actual trajectories with a prototype TPC will be the best source of information on limitations due to multiple scattering.

11.3   A Continuum Positronium Time Projection Chamber

J.G. Cramer, J.H. Gundlach, C.E. Hyde-Wright, F. Kurth, D. Prindle, H. Schwarze,* K. Swartz, T.A. Trainor, S.P. VanVerst, and F. Walter

We are developing a Time Projection Chamber (TPC) for studies of low energy e^+e^- coincidences produced in heavy ion collisions near the coulomb barrier. Narrow lines have been observed at a total e^+e^- energy near 1.6 MeV.[1]

The TPC is illustrated below. The TPC axis is perpendicular to the beam axis. The entire TPC is filled with 150 Torr methane. A field of 500 Gauss confines electrons of $T \leq 1$ MeV to helical orbits of radius ≤ 10 cm. Electron tracks are accepted for angles from 45° to 75° from the TPC axis. A pair of Parallel Plate Avalanche Counters (PPACs) detect the scattered heavy ions. The drift regions between the PPACs and the readout wire arrays constitute the active regions of the TPC.

We are presently prototyping wire chambers with combined anode and cathode wire readout. This scheme makes the wire chamber transparent to the primary electrons. The electrons and positrons can then be transported further from the target. The electrons and positrons are then stopped in an array of scintillator vanes. Each vane is a scintillator-absorber-scintillator sandwich, with the plane of the vane parallel to the TPC axis. The helicities of the orbits of electrons and positrons are opposite. Thus positrons will be absorbed on one face of each vane, electrons on the other. The scintillator array measures the orbit helicity, and particle charge. Behind the scintillator array is a BaF$_2$ or NaI array to detect positron annihilation quanta. The event trigger consists of a coincidence between the PPAC (heavy ion), the positron vanes, and the annihilation detector.

a. Plastic absorber
c. Solenoid coils
d. Drift volume
g. Gamma-ray detector
p. Parallel plate avalanche counters
s. Scintillator vanes
t. Target
v. Beam-line vacuum window
w. Multiwire proportional counter
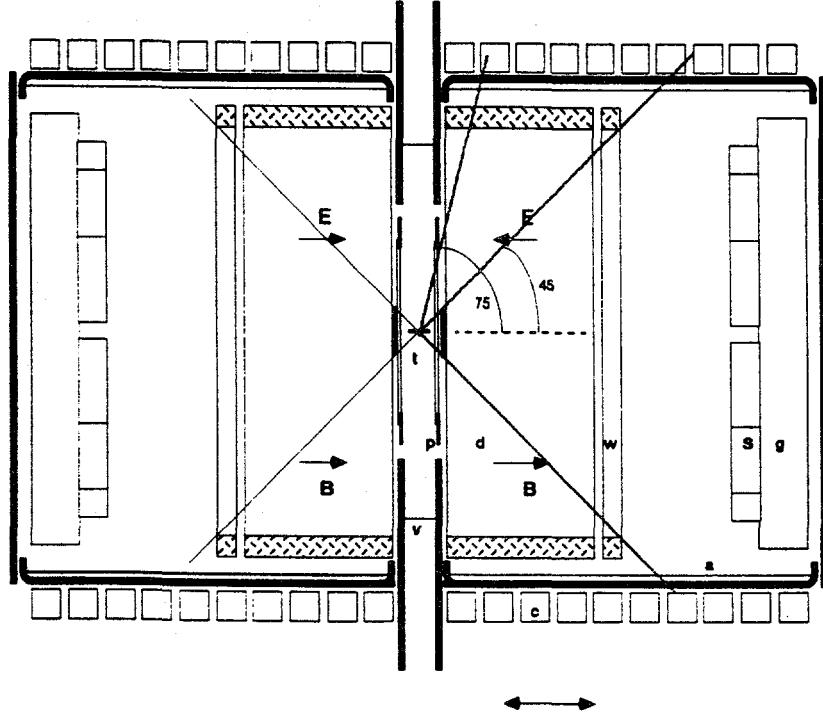
*Visiting student, Justus Liebig University, Giessen, FRG.
[1]T. Cowan, et al., Phys. Rev. Lett. **56** (1986) 444.

11.4 Prototype 2–D Wire Chamber for TPC Readout

C.E. Hyde–Wright, F.U. Kurth,* H. Schwarze,† T.A. Trainor, S.P. Van Verst, and F.H. Walter*

We are developing a time projection chamber (TPC) system to investigate narrow lines seen in e^+/e^- production in heavy ion collisions at GSI.[1] For several reasons, including economics, it is desirable to read out tracks with a wire chamber system rather than the standard pad array if this is feasible. We also need precise data on electron drift speeds, diffusion and multiple scattering for the specific conditions of this TPC design.

The chamber has a 12 cm square active area. Wires are mounted on 1.6 mm PC board. The anode board alternates anode and field wires (20μ and 50μ diam.) with a spacing of 5 mm. The upper cathode board terminates the drift field above. Wires (50μ) are positioned 5 mm above and parallel to anode board field wires. The lower cathode board carries 50μ wires spaced 5 mm apart, 5 mm below the anode plane and perpendicular to those wires.

Above the chamber is a 17 cm high field cage. A negative voltage (0–4 kV) is applied to the top of the cage to provide a uniform drift E–field above the wire chamber.

Anode wire and bottom cathode wire pair signals are brought out on RG–174/u coax to 10x broad band preamps. These signals then go to CAMAC TDC and ADC units for track reconstruction, or to a 350 MHz channel plate scope (Tektronix 2467) for studies of wire chamber operation.

The system has been operated with 150 Torr methane or isobutane to observe ^{241}Am α particles and ^{90}Sr β particles. Anode signals up to one volt are achieved with α particles. Present gain limit is photoelectron production on the aluminum base of the chamber. A simple suppression scheme should eliminate this.

To study track properties we position the α source or β spectrometer[2] and a collimated scintillator on opposite sides of the field cage. The scintillator PMT signal then triggers the wire chamber electronics. We have observed track widths (due to longitudinal diffusion over 5 – 15 cm) of 2 – 3 mm for α particles and drift speeds of 10 – 11 cm/μs for methane. Proper 2–D operation of the wire chamber has been confirmed.
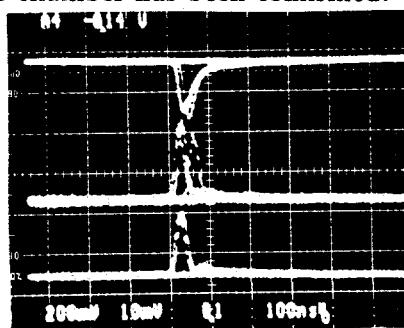

Figure 11.4-1. Anode and two cathode signals in 2-D operation.
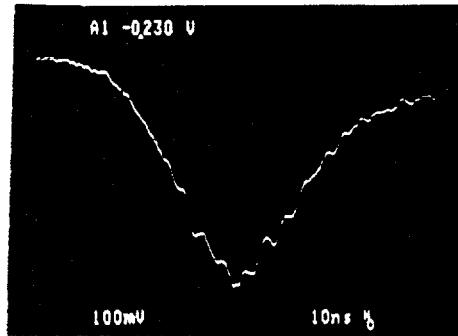
Figure 11.4-2. Anode signal showing 3 mm longitudinal diffusion after 15 cm track drift.

11.5 X–Y Beam Position Monitor Using Parallel Plate Avalanche Counters

T.A. Trainor

The PPAC–based beam profile monitor (BPM) described in last year's annual report[1] has been brought to LEAR at CERN and successfully installed for use in the apparatus developed to make a precise comparison of proton and antiproton masses as a test of CPT invariance for hadrons.[2]

The BPM is required to profile 105 MeV/c (5.9 MeV) proton and antiproton beams in space and time. It must serve as a start detector (500ps resolution) for a TOF system used to measure particle energies down to $\sim$300 eV. And it is used to calibrate in time the start signal used to actuate the Penning trap high voltage supplies.

The BPM consists of two PPAC's, each with a segmented anode. The four electrodes (2 cathodes, 2 anodes) are each aluminized $250\mu g/cm^2$ mylar. The cathodes are stretched over contoured lucite bosses to achieve high gain. The gaps are 1.25 mm and operate at 900V at 20 Torr isobutane. The total device is 5 cm in diameter and 3.5 cm long with a 1.8 cm diameter aperture. Two $9\mu m$ mylar windows supported on 90% transparent molybdenum grids withstand a 1 atm external pressure. Signals are brought out on RG–174/u and after gain–100 broadband amplifiers are fed to discriminators and ratemeters. Ten analog ratemeter signals are continuously displayed on bar displays for horizontal and vertical beam profiles. Alternatively, the ten PPAC anode signals are fed to fast ADC's to obtain a snapshot of the beam profile in pulse mode.

Figure 11.5-1 shows the bar displays for a continuous (slow extraction) beam. The resolution is 2.5 mm and the bandwidth is $\sim$10 Hz. For tuning purposes this bandwidth is superior to the 1 Hz refresh rate of the standard CERN wire chamber.

Figure 11.5-2 shows a signal from one anode strip during a fast extraction beam pulse. The PPAC's are operated at reduced bias (200–300v) in this mode as ion chambers. The pulse is $\sim$200 ns long and contains $\sim$10^8 $\bar{p}$. These signals are integrated by ADC's, and a computer display of the fast extraction pulse profile very similar to that for the ratemeters is developed.

This system has been in operation for both beam extraction modes over a seven month period.
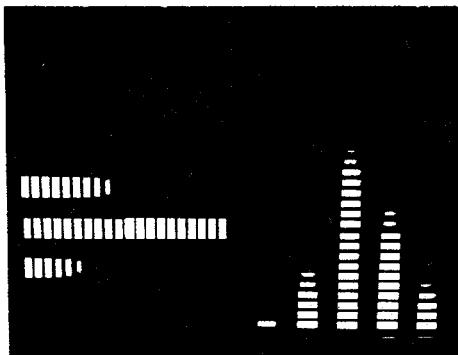
Figure 11.5-1. X-Y bar display.
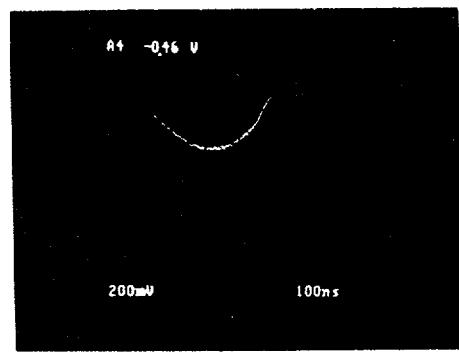
Figure 11.5-2. Center anode signal during fast extraction pulse.

---

[1]Nuclear Physics Laboratory Annual Report, University of Washington (1988) p. 79.
[2]Section 4.4, this report.

11.6 Small β Spectrometer for Track Studies in a TPC

H. Schwarze,[*] K. Swartz and <u>T.A. Trainor</u>

We are presently developing a prototype time projection chamber (TPC) as part of a program to study production of e^+/e^- pairs in heavy ion collisions.[1] A central issue is the character of electron tracks generated in the TPC, and whether sufficient resolution can be obtained in the track reconstruction to make a significant statement about the details of the pair production. To accomplish this end we needed a source of ~500 keV electrons with limited energy range ($\Delta P/P$ ~0.1) and reasonable rate (100Hz).

We have used a 50μCi ^{90}Sr source and small magnetic spectrometer as the required electron source. The ^{90}Sr source consists of a Sr salt sealed between two 75μm aluminum foil disks. These disks are sealed inside a 2 cm diameter aluminum cylinder by a 3 mm thick aluminum cover plate with a 4 mm diameter aperture.

The magnetic spectrometer has a bend angle of $90°$ and radius of 5 cm. The entrance edge angle is $60°$ and the exit face is normal. The gap is 0.5 cm and the field on center is about 500 G. Excitation is by permanent magnets in a C geometry. The object distance is 2.5 cm and image distance is 18 cm (from effective edges).[2]

The solid angle expected is roughly 30 mSr. With a 3μCi source we observed ~5 Hz in a 10% momentum slice at 500 keV. The expectation was a rate of 10 – 15 Hz. Electrons were detected by a plastic scintillator collimated by polyethylene. For the TPC track studies the electron source and scintillator will be placed on opposite sides of the TPC field cage and the scintillator (PMT) signal will serve as a start trigger for the TPC wire chamber.

We thank Robert Vandenbosch for producing the ^{90}Sr β sources.

---

[*]Visiting student, Justus Liebig University, Giessen, FRG.
[1]Section 11.3, this report.
[2]J.J. Livingood, The Optics of Dipole Magnets, p. 62, Academic Press, New York, 1969.

11.7   Optimal Tuning of a 3–harmonic Buncher

G.C. Harper and T.A. Trainor

For each ion species and injected beam energy the 12.5 or 50 MHz 3–harmonic buncher must be adjusted to minimize bunch widths at the entrance to the LINAC. There are five parameters (two phases, three amplitudes), and considerable time is saved by avoiding systematic searching. We describe two methods for directly obtaining near-optimal buncher adjustment.

1. Scaling from V_{crit}. For each individual harmonic the amplitude is adjusted to minimize the bunch width at the LINAC entrance. The resulting widths should be approximately equal and reflect the longitudinal emittance of the beam. The amplitudes obtained are $V_{crit}(n)$, n = 1,2,3, where n=1 is for the fundamental frequency. These amplitudes are then multiplied by empirical factors which depend only on the probe used to monitor the buncher wave form and are directly related to the Fourier decomposition of the desired ramp. For the 50 MHz buncher these factors are 1.6, 1.0, 0.6 for n=1, 2, 3 respectively. For the 12.5 MHz buncher the factors are 1.6, 1.0, 0.35. This method automatically accounts for transit time effects. The phases are then adjusted to eliminate any time–odd component in the monitor wave form. The buncher is then very nearly optimized. The resulting bunch width should be larger than that for single harmonic bunching because of the nonideal structure of the buncher wave form.

2. Dead Reckoning. If the buncher has been calibrated for a variety of beams by method 1), these data can be reduced to a standard ion (say hydrogen) using the scale factor $(E^3/m)^{1/2}$. There results a set of three standard amplitudes (e.g., for hydrogen at 50 keV) which can be scaled back to the desired beam species and energy. A correction must be made from a standard table for each harmonic because of the finite transit time in the buncher gap. The two phases are adjusted as in method 1).

For heavier beams these methods yield optimized beams immediately. For lighter beams (especially hydrogen) some additional optimization is possible because of the smaller longitudinal emittance.

11.8 Design and Construction of Electronic Equipment

R. Barry, J.M. LaCroix, J.M. Stehfest, R.E. Stowell and T.D. Van Wechel

The following major electronic projects were carried out and are described in detail in the indicated sections of this report.

a. A beam profile monitor integrator was designed and constructed for the linac (see Sect. 11.9).

b. A power supply and control electronics chassis for the injector deck beam chopper system was designed and built (see Sect. 12.5).

c. A low energy buncher rephasing circuit was designed and constructed (see Sect. 12.4).

d. A continuing effort was put into completing and debugging the emittance monitor for the linac (see Sec. 12.3).

Several additional electronics projects were undertaken.

a. Four 10-amp. constant current computer controlled steering magnet power supplies were constructed for the linac.

b. A separate public address paging system was installed for the linac areas.

c. A continuing effort was put into updating schematics and documentation for the linac.

d. A four-amp. constant current computer-controlled power supply was built for the polarized ion source trim field coil.

e. Design was started on a new upcharge control system for the tandem..

f. The image/object beam scanner chassis was expanded from two channels to six to allow inclusion of a newly installed scanner located immediately off the injector deck.

g. An in-house capability was developed for repairing the 100 and 200 watt r.f. amplifiers used on the linac.

h. The radiation system described last year[1] was expanded and updated, including installation of new gamma monitors for the tandem areas.

i. Multi-pin molex connectors were installed on all 36 of the linac r.f. controller modules to allow rapid removal and or replacement.

j. The second bank of 16 scalers described last year[2] was installed in the counting room.

k. A chassis was designed and built to allow computer reading of the metered currents from the variable slits and four jaw aperture on the linac.

[1]Nuclear Physics Laboratory Annual Report, University of Washington (1988) p. 66.
[2]*Ibid.*, p.78.

11.9 Beam Profile Monitor Integrator

T.D. Van Wechel

An integrator circuit was added to each of the two channels of the beam profile monitor (BPM) scanner display electronics. Its purpose is to provide a relative indication of the beam current at the displayed scanner to the Linac host control computer.

The BPM integrator receives two signals from the BPM scanner display circuit. One is a timing pulse that occurs once for each rotation of the scanner wire. The other is a signal that is proportional to the instantaneous beam current picked up by the scanner wire.

The circuit consists of a resettable integrator with a switched input, a sample and hold circuit, and a 4-bit binary counter. The binary counter is incremented one count for each revolution of the scanner wire. The BPM current is integrated for the first 15 out of each 16 revolutions. On the 16th revo- lution the input of the integrator is turned off, the output level of the integrator is transfered to the sample and hold circuit, and the integrator is then reset to zero. On the next revolution the input of the integrator is turned on and the sequence above is repeated. Since the BPM rotation frequency is approxiamately 19 Hz, the BPM integrator is updated approximately every 840 msec. The output of the sample and hold is read by a DAC in the Linac host control computer.

11.10 A New Gas-Handling System

A.W. Charlop, S. Gil[*], D.D. Leach,[†] and S.J. Luke

A new absolute pressure gas-handling system (APGHS) has been developed for use with low pressure gas detectors. The APGHS consists of a control box, manometer, proportional electromagnetic control valve, stainless steel gas reservoir and tubing, and mechanical pump all mounted on a rolling rack to allow easy movement between scattering chambers. The APGHS is currently at the end of the electrostatic deflector[1] beamline for use with the Breskin detector[2] there.

The controller is switchable to regulate over the ranges 0–0.1 V, 0.1–1 V, and 1–10 V. It has three modes, automatic, manual, and external. The automatic mode allows the regulator to maintain the set point pressure by adjusting the flow through the control valve. The manual mode allows the operator to open the control valve to a desired flow and lock it in that position. And the external mode allows the controller to be controlled remotely through a computer link. The controller also has a process limit option which shuts off gas flow if the pressure exceeds a set percentage above the set-point value.

The manometer measures the absolute pressure of the system. The current manometer, an MKS Baratron type 122A, is sensitive over a 0.1–100 torr range and produces an output voltage between 0 and 10 VDC over this range. It is connected to the gas reservoir by a Quick-Flange thus allowing easy replacement by other manometers with ranges from 2 torr full-scale to 1000 torr full-scale which may be purchased from MKS.

The proportional electromagnetic control valve is adjusted by the controller to keep constant pressure in the gas reservoir in automatic mode or held at a specific flow setting in manual mode. The controling signal is a 0 to 5 VDC signal. These proportional electromagnetic control valves are contructed so that the valve seat can be easily changed for different full-scale flow ranges from 30 sccm to 5000 sccm without removing the valve from the gas-line. The present control valve is set up for a maximum flow of 200 sccm.

The rest of the system is constructed of stainless steel tubing and manual valves. The gas reservoir has a capacity of about 1/2 L and is between the gas inlet and the detector to dampen pressure spikes and allow pressure measurments. The mechanical pump is a TRIVAC dual stage pump with an antisuckback valve to limit pump oil from getting into the system and has a pumping speed of 190 L/min.

[*]Present address TANDAR, Departmento de Física, Comisión Nacional de Energía Atómica, Buenos Aires, Argentina

[†]John Fluke Mfg Co Inc, Everett, WA 98206.

[1]Nuclear Physics Laboratory Annual Report, University of Washington, (1988) p. 73.

[2]*Ibid.*, p. 75

11.11 Single-Wire Proportional Counter Performance with Methane and Isobutane Counter Gasses

C.E. Hyde-Wright, T.A. Trainor and <u>S.P. Van Verst</u>

A single wire proportional counter has been built to investigate signal properties associated with the use of methane and isobutane in the counter. This work is part of a search for suitable operating parameters of a time projection chamber which will be used to study anomalous positron lines produced in heavy ion collisions near the Coulomb barrier.

The counter consists of a 1 cm diameter stainless steel cathode tube with a 20 micron, gold plated tungston anode wire along its axis. A 1/8 inch hole at the midpoint of the tube allows incident radiation to enter the detector. The counter resides in a vacuum housing which is connected to a gas handling system to allow gas pressure and flow rate to be adjusted. The gas pressure was typically held at 150 Torr with a flow rate of 200 cc/min. The cathode was biased from -1200 to -1800 V while the signal was read out from the grounded anode wire. A Tektronix 2467, 350 MHz oscilloscope observed the signal from a Phillips 776 fast amplifier (10X gain).

A typical anode wire signal, obtained with methane gas and a 5 MeV alpha source is shown in the figure. The alpha particles generate about 10,000 ion pairs while passing through the detector and the ionization electrons drift toward the anode under the influence of the radial electric field, where they avalanche. The signal shapes are understood as a folding of the expected shape due to a single ionization electron with the arrival time distribution of electrons from the alpha particle track. The latter is obtained from the drift velocity of the electrons in the gas, which is a function of radial position in the tube. Great care was taken to minimize noise and distributed inductance. The signal rise time is about 3 ns and is dominated by finite amplifier bandwidth. The oscillations in the trace are due to statistical fluctuations of the gas ionization process.

Signals with a flat trace after the initial peak are due to alpha particles which travel along a diameter of the counter. In this case, the signal is from ionization electrons which drift into the anode from all possible radial distances, and the width of the pulse is therefore the time for electrons created at the tube wall to drift to the anode. For alpha tracks corresponding to other chords of the tube cross section, the difference in arrival time amoung various electrons will be smaller, and the width of the pulse will decrease.

The average drift speed for methane gas was found to be about three times greater than for isobutane, which is important for the final TPC requirements. However, the isobutane was found to be a more stable gas. Investigations will be carried out with various mixtures of the two gasses. The understanding of the signals from this single-wire chamber has aided in the development of more complicated multi-wire systems.

Figure 11.11-1. Typical anode wire signal from the single-wire proportional counter filled with methane gas at 150 Torr and biased to 1500 V.

12 BOOSTER LINAC

12.1 Booster Operation

J.F. Amsbaugh, D.T. Corcoran, G.C. Harper, M.A. Howe, <u>D.W. Storm</u>, and D.I. Will

During the last year the booster was scheduled for 18 different experimental runs. The total time scheduled and run was 80 days. The beams provided are listed with the corresponding maximum energy and energy per nucleon. Asterisks indicate maximum energies which met the experimenter's requirements without requiring the full Linac.

^{4}He	^{12}C	^{13}C	^{16}O	^{18}O	^{28}Si	^{58}Ni	
64	164	132*	225	140*	148*	340	MeV
16	13.7	10.1*	14.0	5.3*	7.8*	5.8	MeV/nucleon

When the maximum Linac energy was desired, we were regularly able to operate all but one resonator (which has its coupler stuck in such a way that only very low fields can be obtained). In general, the booster operated stably and reliably. As a result of accumulated experience as well as improvements in the control system, down time for repairs decreased during the year, and the amount of time required for tuning the Linac also decreased. The main sources of down time have been failures of rf amplifiers, failures with rf controllers, and a tendency for one of three particular resonators to multipactor. The history of these problems during the year will be described below.

Early in the year there were occasional failures of rf power amplifiers. Such a failure would typically cause down time of less than an hour, since the dead amplifier could be replaced. Apparently the weak amplifiers have been broken and repaired, as by the end of the year the failure rate had improved so that only one amplifier failed in the last four months of the year.

Failures of the rf controllers were more subtle. One symptom would typically be an increase of noise in the control loop, leading to loss of amplitude and phase lock in the resonator. Another symptom could be drifting of the beam energy, due to a failure in the rf monitoring circuitry of one of the controllers. As with the amplifiers, the poor controllers have been repaired and this failure mode is becoming rare.

During several runs, time was lost when one of three different resonators would begin multipactoring. We have performed additional multipactor conditioning with these resonators, but two of them are not free of multipactor problems. We are pursuing this effort. In addition, more of the staff members are learning how to start up resonators which exhibit a tendency to multipactor.

The final failure mode that we have experienced (although it has not shut down a run) is loss of cooling water. On two occasions we have lost the primary cooling water in the cooling tower. As a result, the water that circulates through the accelerator and which cools the helium compressors has overheated. We are in the process of putting some alarms on the primary water as well as on the temperature of the secondary water, so that such problems can be avoided.

Our main focus last year has been on making the system more reliable and easier to operate, rather than putting a big effort into improving resonator performance. This approach was consistent with the demands of the experimenters, who, in many cases, did not require the full machine energy. During extended running periods we were regularly able to obtain 2.8 MV/m average fields in the

low-β resonators and 2.4 MV/m in the high-β ones. During the past year we have not opened any cryostats.

We have not had a mechanical failure in the cryogenic system that required shutting down the Linac. Furthermore, we have not had to cancel any runs due to failures of the Linac.

Most experimenters have not been concerned with optimum resolution of beam energy or time. Consequently we have usually not used the rebuncher. In one case, however, an experimenter was able to measure a 0.46-nsec bunch width (FWHM) with the rebuncher off. (This was for a 221-MeV oxygen beam.) Setting the rebuncher to a relatively arbitrary field produced a 0.22-nsec width. From these figures, which include the (unknown) time resolution width of the experimenter's equipment, we can conclude that the energy resolution of the Linac beam was better than 0.2% before using the rebuncher. However, we do not have enough information to determine details of the energy and time widths from this single measurement.

A considerable effort has been spent trying to improve the transmission of the beam through the linac. We observe a substantial loss of beam between the entrance to the linac and the middle of the 180 degree bend. An additional loss is observed between the end of the linac and the beam line after the final 90 degree bend. The first of these losses is somewhat more than 50%, while the second is typically 40% (of the current at the end of the Linac) or more. We have carried out various efforts to understand and correct these losses. This work is described in the section on beam dynamics. The net result, however, is that we have not substantially reduced the losses.

A number of improvements have been made in the control system software. These will be described below (Section 12.7). The main goal of this work is to make the operation of the Linac both easier and more automatic.

Finally, the other hardware improvements (which will be discussed in subsequent sections) include 1) construction of a stripper foil mechanism (Section 12.10) that is located before the dogleg (to permit transmission of heavy beams, such as nickel), 2) construction of a chopper (Section 12.5) that is located on the injector deck (to permit operation of the deck at higher elevation than with the old chopper), and 3) commissioning of the 12.4-MHz buncher driver (Section 12.3) with the associated electronics (which also will control the old 49.6-MHz buncher driver). The new buncher electronics also provides computer control and monitoring of the buncher.

For the next year we look forward to even more reliable operation of the booster as well as toward improving average resonator performance by replacing and/or replating the resonators with the lowest fields. In conjunction with this effort, we are pursuing studies of improved plating techniques.

We are beginning to train the graduate students in the operation of the Linac. We still use the experienced Linac staff for tuning the machine. However it runs stably enough that continuous attendance by experienced staff is not generally necessary. We expect that in the future the students will be able to change energy and perform minor tuning adjustments.

12.2 Beam Dynamics

J.F. Amsbaugh, G.C. Harper, <u>D.W. Storm</u>, D.J. Hodgkins and D.I. Will

We have pursued several different approaches to improving the transmission of the beam through the Linac. These are 1) calculations to better understand the focusing, 2) construction and installation of vertical steering magnets, and 3) alignment studies and adjustments.

As reported last year,[1] we use the inter-cryostat quadrupoles to give a 90° phase rotation, and calculate the required settings. This technique seems to work reliably. We have automated the determination of resonator fields (needed for the defocusing calculation) and have integrated the calculation and setting of the quadrupole fields into the resonator tuning procedure. The matching of the beam to the acceptance of the periodic focusing system is done empirically, and we have not been able to reach agreement between empirical and calculated settings for the quadrupoles upstream of the Linac. The situation is similar regarding matching the beam leaving the Linac to the final beam transport. It is apparent that part of the problem with these regions results from misalignment of the beam with the focusing elements or with the Linac axis. We hope to be able to use the emittance monitor to unravel some of these puzzles.

Because we observed various focusing elements steering the beam vertically, we built four small steering magnets and power supplies (capable of about 10 mr bend for a typical beam). These magnets were located before the dogleg, before the linac, in the 180° bend, and at the exit of the Linac. We find these magnets helped with the transmission, but the amount of steering required is very small (except for the magnet right after the Tandem), so there is apparently no large net vertical misalignment of the main sections of the Linac.

Since both resonators and quadrupoles were observed to steer, we have been working on studying and correcting misalignments of these elements. First, a repeat of the surveying of the cryostats indicated that the floor has sagged somewhat less than one mm. Second, we found that by using one quadrupole doublet at a time to focus the beam to a spot on the scanner at the end of the relevant half of the linac, we could easily determine whether the beam was off axis in the doublet. Several doublets were adjusted to put them onto the beam axis. Finally, studies of resonator misalignment were done by phasing each resonator at the bunching phase to observe beam displacement. Some cryostat misalignment was discovered and corrected using this technique. When the adjustments are made, we first check the surveyed position of the relevant item, then we move it to correct the steering, and finally we record the displacement from the nominal position.

We have improved the transmission from the Linac exit through the final beam transport system, but only to about 70% at best. A larger loss occurs in the first 90° bend following the first half of the Linac. Since the buncher captures only 60 to 70% of the beam, without the chopper we would expect to have 30 to 40% losses here, since that much beam is accelerated through the Tandem but is not in the bunch. With the new chopper, however, we should be able to remove this part of the beam and then to study the transmission of the first half of the Linac itself. At present, the transmission from the end of the dogleg to the middle of the 180° bend is usually 30 to 50%, although the transmission through the South half of the Linac (but not around the first 90° bend) is nearly 100%, as is the transmission from the middle of the 180° bend to the Linac exit. The problem of transmission requires more study, which we will pursue in the coming year.

---

[1]Nuclear Physics Laboratory Annual Report, University of Washington (1988) p. 70.

12.3 Completion and Operation of the 12.4-MHz Driver for the Low-Energy Buncher and of the New Controller for 12.4- and 49.6-MHz Bunching

D.P. Rosenzweig, <u>D.W. Storm</u>, and T.D. Van Wechel

The buncher and driver form a resonant circuit. The rf power is provided by a unit which synthesizes a ramp from either three frequencies which are 1, 2, and 3 times 12.4 MHz or four frequencies which are 1, 2, 3, and 4 times 49.6 MHz. The design of this device was described last year.[1] It provides feedback control of the buncher waveform. It also controls the overall phase of the buncher wave to phase lock the beam itself to the Linac clock. With the new unit, all the buncher parameters are under computer control. This controller was installed early in the year and has performed very well.

At the same time we completed the 12.4-MHz driver described briefly in last year's Annual Report.[2,3] It consists of several coils and two vacuum variable capacitors. It resonates simultaneously at 12.4, 24.8 and 37.2 MHz, with the maximum voltage appearing across the buncher grids. The three signals generated by the new controller are combined before being fed into a single wideband power amplifier (200 Watt). The rf power is transmitted on a coaxial cable which terminates in two coupling loops adjacent to coils of the resonator. These loops provide nearly critical coupling of the lower two frequencies, and for the highest frequency about half the forward power is coupled. The resonator is in a copper box with connectors that fit into the vacuum feedthroughs that connect to the buncher grids. Installation is very simple. Fine adjustment of the resonant frequencies is done using the vacuum variable capacitors and by moving a sheet of copper that intersects magnetic flux around one coil. One or two iterations of these adjustments may be required whenever the resonator box is installed.

About 60 Watts is required to bunch 130-keV carbon beams. The ion energy has been limited by the chopper; now that the on-deck chopper is available we may want to raise the deck potential. The required buncher power scales as the cube of the ion energy and inversely with the mass. Consequently we would expect to reach the buncher power limit with 190-keV carbon, 250-keV silicon, or 290-keV calcium ions. Present indications are that these energies are more than adequate to achieve optimum bunch width.

The unit has performed stably during the year, except that we observed a drop in Q (by about a factor of 2) during February. This deterioration was attributed to some corrosion around solder joints connecting some of the coils. These joints were redone in a manner which permitted better cleaning, and the Q's returned to the original values of about 300 for all three frequencies.

Near the Linac entrance, the 12.4-MHz buncher has regularly provided bunch widths (FWHM) of 0.8 nsec for oxygen beams leaving the deck at 130 keV. For nickel (also 130-keV initial ion energy), we obtained a width of 1.1 nsec. We capture between 60 and 70% of the beam into the bunch. From the bunching waveform that captures this fraction of the beam, one expects a bunch width of about 0.7 nsec. Thus other contributions to the bunch width appear to be small. In particular, the need for higher ion energies from the deck, to reduce the contribution to bunch width of the initial ion energy spread, is not obvious, at least for the moderately light ions.

[1] Nuclear Physics Laboratory Annual Report, University of Washington (1988), p. 56.

[2] *Ibid.*, p. 60.

[3] K. Johnson, Dual Frequency Buncher, Argonne Bldg. 211 Design note.

12.4 Low Energy Buncher Rephasing Circuit

D.W. Storm and <u>T.D. Van Wechel</u>

Along with 12.4-Mhz operation of the low-energy (LE) buncher (see Section 12.3) it was necessary to provide a 12.4-MHz timing signal. This signal is needed as a timing reference signal for experiments and for the time structure monitor. The 12.4-MHz signal generated in the LE buncher controller could not be used directly since its phase is varied to keep the bunched beam at the resonant phase detector synchronous to the linac. Since the phase detector is resonant at 49.6 MHz, the 12.4-MHz bunched beam harmonically excites the phase detector and phase lock occurs at 49.6 MHz. The frequency is divided down to 12.4 MHz after the phase lock circuit. Parallel dividing of the 49.6-MHz clock to 12.4 MHz is risky due to the possibility of the two dividers getting out of step.

A different scheme was devised where a timing signal could be generated that is synchronized to an edge of the 49.6-MHz clock coincident to a timing window synchronous to the 12.4-MHz LE buncher. This is shown in figure 12.4-1. When the chopper is in use we divide the 12.4-MHz buncher signal down further. This lower frequency signal is then used to generate the window. The inputs and outputs are level shifted between NIM and ECL levels.

The timing window is created by a pair of one-shots. The first one-shot is started by a negative transition of the 12.4-MHz signal from the LE buncher. Its time determines the start time of the timing window. The second one-shot is started at the trailing edge of the first one-shot and determines the width of the timing window. The output of this one-shot is the timing window. A NIM output of the timing window is provided for setup purposes. By adjusting the time width of the first one-shot, the window can be set to be roughly symmetric about a negative edge of the 49.6-MHz signal. The 49.6-Mhz signal is applied to the clock input of the negative-edge-triggered D-type flip-flop. The flip flop generates a timing pulse for each occurance of the window.
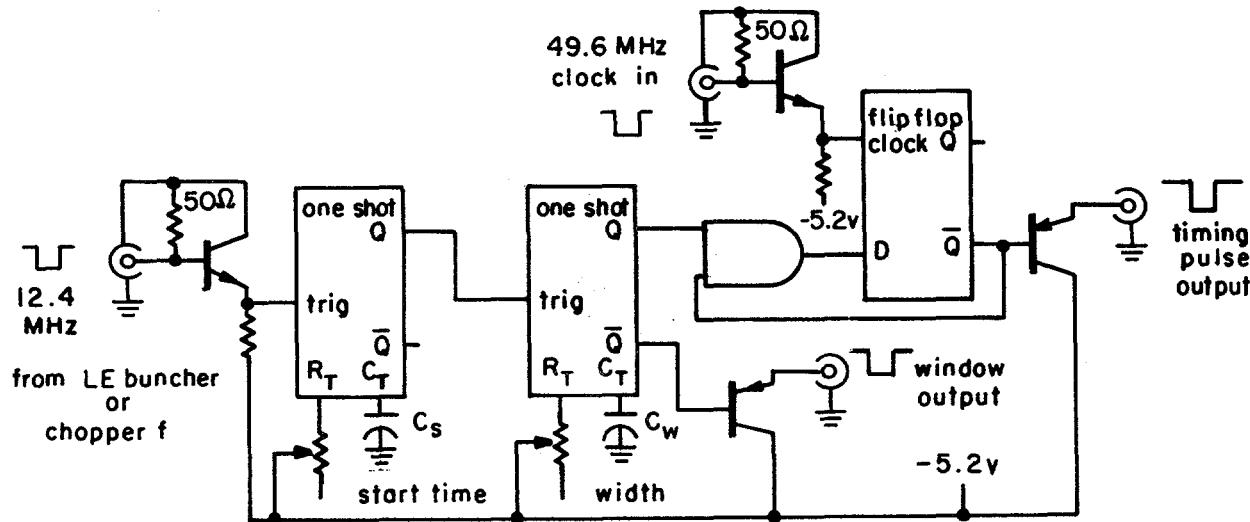

Figure 12.4-1. Timing pulse circuit.

66

12.5 Injector Deck Beam Chopper System

G.C. Harper, D.J. Hodgkins, T.A. Trainor, and T.D. Van Wechel

A high frequency, freon-cooled beam chopper system has been developed for use on the injector deck. It consists of a chopper plate assembly, a wiper slit assembly, two high voltage plate drivers, a power supply, a controller, and a fiber-optic link.

The plate assembly, mounted on the output port of the 90-degree bending magnet, houses vertical deflection plates 1.5 cm by 3.0 cm with the longer dimension perpendicular to the beam axis. The spacing between the plates can be continuously varied from 0 to 2.0 cm. A 1.5-cm diameter aperature immediately precedes the plates. There is a wiper slit assembly located 1 m downstream from the plates which has vertical travel permitting a slit width up to 10.0 mm.

The high voltage drivers are mounted on the plate assembly and housed in sealed aluminum enclosures which provide electrical shielding and permit submersion in a freon bath for cooling. These include on and off switching stacks each consisting of 10 cascode-connected bipolar switching transistors and a preamp with 50 ohms input impedance which accepts a +5 volt pulse. They operate at 400 volts each and, when cooled, can be operated at a 6.2 MHz repetition rate with rise and fall times of 25 nsec and a flat bottom pulse width of 25 nsec.

The controller provides timing pulses to the chopper drivers synchronous to the Low-Energy Buncher. The controller is divided into two sections, one at ground and the other at the elevated injector-deck potential, coupled by a fiber optic link. At the ground potential section the frequency is determined by an 8-bit divide by n counter, whose input is a 12.4-MHz clock from the LE Buncher. The frequency is set by an 8-bit word from the deck computer. The output of the divider drives a fiber-optic transmitter. The fiber-optic link was constructed with HP components that have a rated bandwidth of 25 MHz. The drift of the fiber-optic system after initial warm up was measured to be less than 100 psec.

The pulses from the output of the fiber-optic receiver start a one-shot whose time determines the relative delay of the chopper with respect to the LE Buncher. This delay can be set over a range of 150 nsec. A second one-shot is started at the end of the delay time. The time of this one-shot determines the width of the chopper pulse. Width can be set from 10 to 250 nsec. Delay and width can be set locally on the injector deck or by computer through the ANAC controller. The output of the one-shot drives a +10-volt, 50-ohm line driver. The output of the line driver is resistively split between the two chopper driver inputs.

A fast Faraday cup consisting of a 1.5-cm radius copper disk covered by a grounded aperature with a molybdenum mesh front cover has been developed to measure the rise time of the beam deflection. The output of the cup is connected directly to a 50-ohm coaxial cable and is fed to the input of 2 cascade-connected instrumentation amplifiers, each with a gain of 10. Prior tests of a 400-volt, 20-nsec rise time, single plate unit using this assembly have shown beam deflection times ranging from 5-10 nsec for 45 kev ^{1}H$^-$ to 50 nsec for 30 kev ^{63}Cu$^-$ at the entrance to the tandem. The final freon cooled version has been installed and some preliminary tests done. Using the direct extraction source, pulses of 10-nsec rise and fall times with duration of 20 nsec have been observed on the fast Faraday cup and the time structure monitor for 45-kev ^{1}H$^-$ at a 4.1-MHz repetition rate. Identical pulses have been observed at the fast Faraday cup for 45 kev ^{16}OH$^-$. Tests for 30 kev ions from the 860 sputter ion source are underway.

12.6 Cryogenic Operations

D.I. Will, and J.A. Wootress

The cryogens used to cool the Linac are liquid helium and liquid nitrogen. The helium is purchased as high purity (less than 10 ppm impurities) bulk gas. Usage of 82,000 SCF in 1988 was 22,000 SCF more than that in 1987 due to an increase in the frequency of purging contaminants from charcoal beds. Purging beds deters ice formation in expanders and valves. The nitrogen is purchased as bulk liquid in 6000 gallon lots. In 1988 consumption increased from 150,000 to 200,000 gallons as the result of a decision to use liquid nitrogen precool for the refrigerator when the Linac was not in use. Precooling with liquid nitrogen permits maintaining liquid helium levels with only one compressor during idle periods.

Most routine maintenance is directed at rotating machinery on our helium refrigerator and its compressors.[1] The major unplanned maintenance was replacing a broken crankshaft (and two damaged cams) on the middle expander.

Item	Hours ON	Major Services	Times Performed
Refrigerator			
Cold Box	>99%	warm/derime	2
Top Expander	~6500 Hrs	main seals	4
	~120 RPM	wristpin bearings/pins	2
		crankpin bearings	1
		valve seals	2
		crosshead/guide replace	2
		flywheel bearings	1
Middle Expander	~7200 Hrs	main seals	4
	~130 RPM	wristpin bearings/pins	2
		crankpin bearings	2
		valve seals	1
		crosshead/guide replace	2
		flywheel bearings	2
Wet Expander	~3500 Hrs	main seals	1
	~30 to 70	wristpin bearings/pins	1
	RPM	crosshead/guide replace	1
Screw Compressors			
RS 1	7100 Hrs	replace charcoal	1
		replace sight tube seals	1
		replace load/unload seals	1
RS 2	8100 Hrs	none	
RS 3	5000 Hrs	none	
Distribution System		warm/derime	4

---

[1] Nuclear Physics Laboratory Annual Report, University of Washington (1988) p. 64.

12.7 Improvements to the Main Control System

G.C. Harper, <u>M.A. Howe</u>, H.P. Readdy, R.J. Seymour

The Booster computer hardware was upgraded from a MicroVAX II to a MicroVAX III. There are now eight Mbytes of system memory. This system is roughly three times as fast as the old MicroVAX II. In general, this increase in speed is not noticeable to booster users since the control system speed is driven by external events and the bandwidth of the RS-232 links to the satellite computers. However, compilation and link times are now much faster during the development cycle of software. In addition, version 4.7 of the VMS operating system was installed.

The main control system (CSX) was modified to allow multiple users. This modification has proved very useful in letting staff members in charge of the cryogenic system gain access to the control system from remote sites while CSX is already running from the main console.

Work continues in areas of automating some of the booster setup and operation activities. For example, the program that calculates the inter-cryostat quadrupole settings was integrated into CSX. Now during resonator tuning the quadrupole settings can be calculated using the touch screens rather than having to run a separate stand-alone program.

Another stand-alone program that is now integrated into CSX is a program to scale dipole and quadrupole settings by a ratio. The ratio can be input from the console keyboard or calculated from the old and new fields of a selected dipole magnet. A selected group of magnets are then scaled by this ratio. Thus it is now possible to use the touch screens to change a group of magnets to transport a different energy beam.

A major area of effort was the development and debugging of control software for the emittance monitor[1] and integrating that software into CSX. The software consists of the touch screen interface and a control program that runs the emittance monitor during data collection. From CSX an experimenter can set the sensitivity of the current integrator, select a horizontal or vertical scan, pick a coarse or fine scan, set the center positions and step size for the stepper motors, and start (or stop) data collection. Once started, the control portion of the software steps the slit and detector across the beam, takes data from the current integrator, stores the data, and watches for errors. The data being taken is displayed in real time on the touch screen monitors to provide a visual feedback to the experimenter. The data is stored for offline analysis.

The first steps were taken to provide a software interface across the network into CSX. This will allow programs running on the data acquisition system to make booster parameter adjustments and record booster parameters during data collection. One of the first uses of this system will be to let the data acquisition computer control some parameters on the polarized ion source during set up of that source.

Internal 'hooks' were added to CSX to allow for a remote knob box which will be used exclusively for the polarized ion source. The hardware and software for the new knob box is under development.

Work continues on adding polarized ion source control to CSX as the hardware is completed. Controls for the cesium beam and atomic beam source sections of the polarized source are complete with the spin precessor to follow.

---

[1]See Section 9.6, this report.

12.8 Improvements to the Vacuum System

J.F. Amsbaugh and H.P. Readdy

The Linac vacuum-satellite computer is a PDP-11/23+ with a 40 Mbyte disk and is configured to reboot, load and then run the control program from this disk after power up. The control code, written in Micropower Pascal, processes a linked list of constraints and actions which can be changed during run time. An event is a list of actions and constraints that control a portion of the system and have a purpose, e.g. Event 20 starts the buncher cryostat pump station. Many different events are loaded into the computer's memory and a task chooses which events are linked into a list to provide the vacuum system control. Several standard tasks are loaded into memory. These events and tasks are stored on the satellite disk and on the VAX disk.

A utility program, **Vaccmd**, provides VAX to satellite-disk transfers, task or event loading and deletion from memory, manual control of the vacuum system, and debugging functions. A customized version of the VAX Text Processing Utility, **Vactpu**, does numeric or english editing of the events and can interpret between the two. Both **Vaccmd** and **Vactpu** run on the VAX where development of the task and events is done.

The satellite control code was modified to display the unmet constraint that prevented an action requested by an operator from occurring. If multiple constraints were unmet, the operator may request an additional monitor page which lists all unmet constraints along with the action and event to which they belong. This list guides the operator in satisfying the constraints thus enabling the previously requested action.

Modifications also were made to both the satellite controller and **Vaccmd** so that log files are created and maintained to keep track of which versions of events and tasks are loaded into the satellite's memory and onto the satellite's disk. These log files are updated as to the location, version and creation time of any task or event data files which are copied to the satellite disk or loaded into memory; these log files are updated also when satellite disk files are renamed or deleted and when tasks or events are unloaded from memory. **Vaccmd** can detect if the satellite was recently booted and automatically sets up new memory log files. If its old log file indicates that tasks or events had been loaded from the VAX into the satellite's memory, instead of from the satellite disk, **Vaccmd** presents the option of whether to load these files automatically from the VAX; if asked to do this it loads the correct version from the directory as specified in the log file.

Changes were made to **Vactpu** to improve its flexibility in interpreting text input lines, for example in converting mTorr or Torr entries to adc units using a table.

The limited memory addressing of the PDP requires subdividing the list processor code into sections each addressing different memory segments of < 14,000 bytes. A fourth such sublist processor was added along with careful documentation so that this can readily be done when needed. Numerous miscellaneous changes were made in the logic and in the monitor display. The display changes reflect three minor changes in the vacuum hardware.

First, two automatic valves were installed in the foreline of the turbo-molecular pump on the beamline before the linac. The Linac stripper foil wheel is located in this beamline which is roughed out through the turbo-molecular pump. The new valves allow isolation of the mechanical pump with a small aperture bypass (1/8 inch) for controlled gentle pumpdown from atmospheric pressure.

Second, a purge gas valve with a gas heater and regeneration pumpout valve sensing were added to the cryopump on the switching magnet. Messages appropriate to the pump's regeneration status are now displayed. Third, indication of the status sensing of the six scattering chamber valves was added and is now displayed.

We now have up to three years of operating experience with three different models of Leybold-Heraeus turbo-molecular pumps, TMP-150, TMP-360, and TMP-360CSV. The two TMP-360CSV are oil lubricated and were bought as additional backups since the grease lubricated pumps were failing often. Experience with them is limited to 4580 and 400 hours. The rest fall into two groups, the first are 2 TMP-150s and 9 TMP-360s which have operated since installation. The average operating time was 17,000 hours with a standard deviation of 6,000 hours.

The pumps of the second group all have a history of multiple failure and factory repair. This group consists of 3 TMP-150s and 7 TMP-360s. All of these have had bearing failure and there was one motor short in a TMP-360. Leybold-Heraeus attributes this problem to a retooling by the bearing manufacturer. The average life is 2000 ±1400 hours. The two following tables summarize this experience. An asterisk indicates currently operating pump time. Many repaired pumps will be approaching the average time to failure during the coming year.

Operation To Date		
Tmp-150	12,766	hrs
Tmp-150	21,390	hrs
Tmp-360	4,889	hrs
Tmp-360	12,607	hrs
Tmp-360	13,854	hrs
Tmp-360	16,070	hrs
Tmp-360	16,539	hrs
Tmp-360	17,464	hrs
Tmp-360	19,204	hrs
Tmp-360	20,786	hrs
Tmp-360	27,910	hrs
Table 12.8.1		

Operating Time Between Failures (hrs)				
Type	First	Second	Third	Fourth
Tmp-150	395	1,646	590*	–
Tmp-150	764	1,995	3,507	7,140*
Tmp-150	904	–	–	–
Tmp-360	2,203	12,607*	–	–
Tmp-360	?	717	2,636	–
Tmp-360	2,585	4,567	–	–
Tmp-360	3,040	5,837*	–	–
Tmp-360	1,647	890	120*	–
Tmp-360	2,022	4,641	261*	–
Tmp-360	7,248	1,041	2,121	–
Table 12.8.2				

12.9 Diagnostics Improvements: New Scanner and Reduced Slit Noise

J.F. Amsbaugh

New Scanner: Early linac operating experience showed that a beam-profile scanner after the last 90° bending magnet would be very useful for phasing high-β resonators. The beam transport to the next 4-sector aperture or next beam-profile scanner was complicated by a quadrupole doublet, a narrow tandem analyzing-magnet vacuum chamber and the long flight path. A National Electrostatics Corporation BPM-80 was purchased and installed. Extra satellite computer interface positions made the addition straightforward. The high-β resonator phasing procedure that evolved is as follows:

- Start with beam centered on a scanner after the last bending magnet.

- Record magnet field.

- Turn on resonator and find the reference phase that recenters beam ($\Delta E = 0$) and where $\frac{\Delta E}{\Delta \phi} < 0$ (bunching phase).

- Reduce reference phase by 70° .

- Increase magnet current to center beam and record field.

The resonators, at the bunching phase, defocus the beam radially which made phasing difficult. The new scanner enables two to three cryostats to be phased before quadrupole adjustment.

Reduced Slit Noise: A pair of National Electrostatic Corporation BDSR-10 single jaw slits were installed horizontally at the image of the tandem analyzing magnet. These replaced slits which had been used previously. The new slits are offset by 4 inches and enclosed in a biased tube with apertures bracketing the slits to suppress crosstalk and secondary electrons. These slits are part of the tandem terminal-voltage regulation. Two types of large noise were sometimes seen at the logarithmic current amplifier outputs.

The old slits were cooled with coolanol because when cooled with compressed air the discharge of built up static electricity was observed. The new slits were air cooled since this discharge was not seen. Later this discharge was seen, probably from seasonal changes in the make up air. Reinstalling the overhauled coolanol system fixed this problem.

The displacer of a cryopump near the slits introduced noticeable noise. This motion coupled to vibration modes of each slit and the bias shield. The capacitively induced currents generate slit noise. In the NEC slit design, slit vibration is unavoidable. Reducing the bias from 300 volts to 90 volts reduces the induced current yet is sufficient to suppress secondaries. Anchoring the cryopump to the large mass of the switching magnet, planned but not yet done, should further reduce this noise. Shield movements induce out-of-phase envelopes in the slit signals. Tightening the shield mounts and stiffening the spring loaded electrical connection effectively eliminated shield movement.

The slit noise was reduced from 120-150 mV peak to peak to 25 mV. The equivalent RMS current is <0.1 nA for a beam of 1 nA.

12.10 Post-Tandem Stripper

D.T. Corcoran and H. Simons

A post-tandem stripper was added between the tandem and the dog leg magnet system to permit the transmission of heavy ion beams to the linac. Since there was no empty beam line space between the tandem and the first dipole magnet of the linac, a fast-acting valve sensor just upbeam from the dipole was removed to make room. (The sensor was incorporated into the the stripper housing.) Because of the limited space (five inches) a rack and pinion system with a manual rotary vacuum feed-through was made to move the foil ladder in and out of the beam line. The foil ladder will hold eight 3/4" foils or four 1-3/4" foils. To prevent thermal damage to the ladder, the foil holders and ladders are made entirely of tantalum, and to prevent thermal conduction to the rotary feed-through, the rack is made of stainless steel. The stripper has been used successfully with a nickel beam.

13 APPENDIX

13.1 Nuclear Physics Laboratory Personnel

Faculty

Eric G. Adelberger, Professor
John G. Cramer, Professor; Director, Nuclear Physics Laboratory
George W. Farwell, Professor Emeritus
Cynthia A. Gossett, Research Assistant Professor
Pieter M. Grootes, Joint Senior Research Associate, Geological Sciences
Isaac Halpern, Professor
Charles E. Hyde-Wright, Assistant Professor
Fred H. Schmidt, Professor Emeritus
Kurt A. Snover, Research Professor
Derek W. Storm, Research Professor; Director, Superconducting Booster Project
Thomas A. Trainor, Research Associate Professor
Robert Vandenbosch, Professor
William G. Weitkamp, Research Professor; Technical Director, Nuclear Physics Laboratory

Research Staff

Salvador Gil, Research Associate[1]
Wilhelm R. Hering, Visiting Scientist[2]
S. Kailas, Research Associate
Warren F. Rogers, Research Associate[3]
Kenshi Sagara, Visiting Scientist[4]
Christopher W. Stubbs, Research Associate
Scott Van Verst, Research Associate

Predoctoral Research Associates

John A. Behr	Diane Markoff
Cecilia Bitz	Brian McLain
Thomas A. Brown	Douglas P. Rosenzweig
Aaron Charlop	Gregory Smith
Ziad M. Drebi	Yue Su
Jon Eisenberg	Kenneth Swartz
Patricia B. Fernández[5]	Ryoji Watanabe[6]
Alejandro García	Philip Williams
Jens H. Gundlach	Peter Wong
S. John Luke	Valdis J. Zeps[7]

---

[1]Now at TANDAR, Comisión de Energía Atómica, Av. de Libertador 8250, Buenos Aires, ARGENTINA 1429.
[2]University of Munich, Sektion Physik, Schellingstrasse 4, D-8000 Muenchen 40, W. Germany.
[3]Now at Department of Physics, SUNY, Geneseo, NY.
[4]Permanent address: Department of Physics, Kyushu University, Fukuoka, Japan.

Professional Staff

John F. Amsbaugh, Research Engineer
David Balsley, Research Engineer
Gregory C. Harper, Research Engineer
David J. Hodgkins, Research Engineer
Mark A. Howe, Research Engineer
Duncan Prindle, Research Scientist
H. Pamela Readdy, Computer Systems Engineer
Richard J. Seymour, Computer Systems Manager
Rod E. Stowell, Electronics Engineer/Electronics Shop Supervisor
H. Erik Swanson, Research Physicist
Timothy D. Van Wechel, Electronics Engineer
Douglas I. Will, Research Engineer

Technical Staff

Robert L. Cooper, Instrument Maker
Dean T. Corcoran, Engineering Technician
Louis L. Geissel, Instrument Maker, Student Shop Leadman
John M. LaCroix, Electronics Technician
Carl E. Linder, Engineering Technician
George E. Saling, Accelerator Technician[8]
Hendrik Simons, Instrument Maker, Shop Supervisor
John M. Stehfest, Electronics Technician[6]
John A. Wootress, Accelerator Technician

Administrative Staff

María G. Ramírez, Administrative Assistant
Ida M. Tess, Technical Secretary

Part Time Staff

Richard Barry	Kevin McMurry
David P. Brockington[6]	Leane Nakamoto[6]
Melanie Bryce	Darren Paschke[6]
Joseph Caggiano	Jack S. Prestrud
Celia Champagne[6]	John A. Rogers
W. Brian Christman	Patrick J. Santos
David Hamann	Kevin S. Sarver[6]
Mark Lemmon	Eric C. Torrence

---

[5]Now at: Physics Division, Argonne National Laboratory, Argonne, IL.

[6]No longer associated with the Nuclear Physics Laboratory.

[7]Now at: Department of Physics, Carnegie-Mellon University, Pittsburgh, PA.

[8]Retired—part time employee; no longer associated with the Nuclear Physics Laboratory

13.2 Degrees Granted, Academic Year 1988-1989

Ph. D. Degrees:

"Gamma Decay of the 5.17 MeV Level in ^{14}O and the Hot CNO Cycle," Patricia B. Fernández, Ph. D. Thesis, University of Washington (1988).

"Parity Mixing of the 0^+,0^-; T=1 Doublet in ^{14}N," Valdis J. Zeps, Ph. D. Thesis, University of Washington (1989).

13.3 List of Publications

Published Papers:

"(γ,n) Studies of the Giant Isovector E2 Resonance in Lead, Cadmium, and Calcium", D.W. Storm, I. Halpern, C.A. Gossett, T. Murakami, D.P. Rosenzweig, and D.R. Tieger, Can. J. Phys. Vol. 65, 677 (1987).

"Alpha Scattering from ^{209}Bi", A. Chatterjee, S.K. Gupta, S. Kailas, and S.S. Kerekatte, Phys. Rev. **C37**, 1420 (1988).

"Excited–State Giant Resonances in Proton Capture", G. Feldman, J.A. Behr, D.H. Dowell, C.A. Gossett, J.H. Gundlach, M. Kićinska–Habior and K.A. Snover, Inst. Phys. Conf. Series, No. 88, IOP Publishing Ltd, Bristol, England (1988).

"Optical Model Analysis of ^{90,92,94,96}Zr + ^{4}He Elastic Scattering at 35.4 Mev", P. Singh, S. Kailas, and A. Navin, Z. Phys. **A331**, 309 (1988).

"Photoneutron Studies of the Giant Isovector Quadrupole Resonance in Calcium, Cadmium and Lead", T. Murakami, C.A. Gossett, I. Halpern, D.P. Rosenzweig, D.W. Storm, D.R. Tieger, P.T. Debevec, A. Freytag L.J. Morford, S.A. Wender, and D.H. Dowell, Inst. Phys. Conf. 88, J. Phys. G: Nucl. Phys. 14 (1988).

"Giant Nuclear Resonances", K.A. Snover, McGraw–Hill Yearbook of Science of Technology, 1989.

"Electroexcitation of the Δ Resonance in the (e,e'p) Reaction", H. Baghaei, W. Bertozzi, K.I. Blomqvist, J.M. Finn, J. Flanz, C.E. Hyde–Wright, N. Kalantar–Nayestanaki, R.W. Lourie, J. Nelson, W.W. Sapp, C.P. Sargent, P. Ulmer, L. Weinstein, B.H. Cottman , P.K. Teng, E.J. Winhold, M. Yamazaki, J.R. Calarco, F.W. Hersman, C. Perdrisat, V. Punjabi, M. Epstein, and D.J. Margaziotis, Phys. Rev. **C39**, 177 (1989).

"Improved Collagen Extraction by Modified Longin Method", T.A. Brown , D.E. Nelson, J.S. Vogel, and J.R. Southon, Radiocarbon, **30(2)**, 171 (1988).

"Search for ℓ–forbidden β decay ^{207}Tl→ ^{207}PB (570 kev)", M.M. Hindi, E.G. Adelberger, S.E. Kellogg and T. Murakami, Phys. Rev. **C38**, 1370 (1988).

"Systematic Behaviour of the Giant Dipole Resonance in Highly Excited Nuclei", C.A. Gossett, J.A. Behr, G. Feldman, J.H. Gundlach, M. Kićinska–Habior and K.A. Snover, J. Phys. G: Nucl. Phys. **14**, S267 (1988).

Comment on "A New Approach to the Question of the Fifth Force", E.G. Adelberger and C.W. Stubbs, Phys. Lett. **A132**, 91 (1988).

"Constraints on Proposed Spin–0 and Spin–1 Partners of the Graviton", C.W. Stubbs, E.G. Adelberger and C. Gregory, Phys. Rev. Lett. **61**, 2409 (1988).

"Fifth Force Remains Elusive", C.W. Stubbs, Nature **338**, 301 (1989).

"Hard Photon Production in the Nucleon–Exchange Transport Model", J. Randrup and R. Vandenbosch, Nucl. Phys. **A490**, 418 (1988).

"Limits on Composition–Dependent Interactions Using a Laboratory Source: Is there a "Fifth Force" Coupled to Isospin?", C.W. Stubbs, E.G. Adelberger, B.R. Heckel, W.F. Rogers, H.E. Swanson, R. Watanabe, J.H. Gundlach, and F.J. Raab, Phys. Rev. Lett. **62**, 609 (1989).

"Shielding the Fifth Force?", R. Watanabe, C.W. Stubbs, and E.G. Adelberger, Phys. Rev. Lett. **61**, 2152 (1988) (Comment).

"Searching for New Macroscopic Forces", E.G. Adelberger and C.W. Stubbs, Physics News in 1988, Physics Today **42**, S–53 (1989).

"Velocity Reversal and the Arrows of Time", J.G. Cramer, Foundations of Physics, Vol. 18. No. 12 (1988).

Papers to be Published or Submitted:

"Density Dependence in the Two–Nucleon Effective Interaction at 135 MeV", J.J. Kelly, W. Bertozzi, T.N. Buti, J.M. Finn, F.W. Hersman, C.E. Hyde–Wright, M.V. Hynes, M.A. Kovash, B. Murdock, B.E. Norum, B. Pugh , F.N. Rad, A.D. Bacher, G.T. Emery, C.C. Foster, W.P. Jones, D.W. Miller, B.L. Berman, J.A. Carr, and F. Petrovich, accepted for publication in Phys. Rev. C (1989).

"Direct Observation of the Barhas Effect Using Antiprotons and Protons", G. Gabrielse, X. Fei, L.A. Orozco, S.L. Rolston, R.L. Tjoelker, T.A. Trainor, J. Haas, H. Kalinowsky and W. Kells, accepted for publication in Phys. Rev. A.

"Giant Nuclear Resonances", K.A. Snover, McGraw–Hill Encyclopedia of Science and Technology, 7th Edition, to be published.

"Importance of Biospheric CO_2 in a Subcanopy Atmosphere Deduced from ^{14}C AMS Measurements", P.M. Grootes, G.W. Farwell, F.H. Schmidt, D.D. Leach, and M. Stuiver, Radiocarbon **30**, No. 3 (1989), in press.

"T–violation Experiments Using Mössbauer Transitions", E.G. Adelberger and A. Schäfer, Physical Review C (to be submitted).

"Electroexcitation of Normal–Parity States in ^{18}O", D.M. Manley, B.L. Berman, W. Bertozzi, T.N. Buti, J.M. Finn, F.W. Hersman, C.E. Hyde–Wright, M.V. Hynes, J.J. Kelly, M.A. Kovash, S. Kowalski, R.W. Lourie, B. Murdock, B.E. Norum, B. Pugh, and C.P. Sargent, Phys. Rev. C (1988) (submitted).

"Radiocarbon Dating of Pollen by Accelerator Mass Spectrometry", T.A. Brown, D.E. Nelson, R.W. Mathewes, J.S. Vogel, and J.R. Southon, Quanternary Research (in press).

"Capture cross sections of ^{232}Th", R.P. Anand, H.M. Jain, S. Kailas, S.K. Gupta, and V.S. Ramamurthy, Annals of Nuclear Energy (in press).

"Excitation of Giant Resonance Region in ^{58}Ni and ^{208}Pb by Inelastic Scattering of 270 MeV Helions", S. Kailas, A. Saxena, P.P. Singh, Q. Chen, P. Schwandt, and E.J. Stephenson, Nucl. Phys. A (in press).

"High–Sensitivity Hillside Results from the Eöt–Wash Experiment", E.G. Adelberger, Proceedings of the 1989 Moriond Workshop, Editions Frontiers (to be published).

"Giant Resonances in ^{90}Zr and ^{116}Sn", S. Kailas, A. Saxena , P.P. Singh, Q. Chen, D.L. Freisel, P. Schwandt, and E.J. Stephenson, Pramana-Journal of Physics (submitted).

"Continuum Background in the Giant Resonance Region of Excitation", A. Saxena, S. Kailas, P.P. Singh, P. Schwandt, E.J. Stephenson, Q. Chen, and D.L. Freisel, Phys. Letts. B (submitted).

"Proton Energy Dependence of Deformation Length", S. Kailas, Phys. Rev. C (submitted).

"Searches for Forces Weaker than Gravity", E.G. Adelberger, 1989 Yearbook of Science and Technology, McGraw–Hill, J. Weil, Editor (to be published).

Conference Presentations, Proceedings, and Invited Talks:

"Constraints on Composition Dependent Interactions from the Eöt–Wash Experiment", E.G. Adelberger, Proceedings of the XXIIIrd Rencontre de Moriond, p. 445, ed. by O. Fackler and J. Tran Thanh Van, Editions Frontiers (1988).

"γ Decay of the 5.17 MeV Level of ^{14}O and the Hot CNO Cycle", P.B. Fernandez, Bull. Am. Phys. Soc., **33**, 1598 (1988).

"Giant Dipole Resonances in Hot Nuclei", K.A. Snover, Proc. of the Texas A&M Symposium on Hot Nuclei, S. Shlomo et al., eds., World Scientific, p.72 (1988).

"Searching for New Macroscopic Forces," C.W. Stubbs, XXIV International Conference on High Energy Physics, Munich, August, 1988.

"The Experimental Status of the Fifth Force", C.W. Stubbs, Bull. Am. Phys. Soc., **33**, No. 4 (1988).

"Exclusive and Inclusive Virtual Compton Scattering", C.E. Hyde– Wright, Topical Conference on Electronuclear Physics with Internal Targets, January 1989, S.L.A.C., CA. To be published by World Scientific, R. Arnold, ed.

"Status of and Operating Experience with the University of Washington Superconducting Booster Linac", D.W. Storm, J.F. Amsbaugh, D.T. Corcoran, G.C. Harper, M.A. Howe, R.E. Stowell, W.G. Weitkamp, T.D. Van Wechel, and D.I. Will, International Conference on Electrostatic Accelerators and Associated Boosters, Strasbourg, France, and Heidelberg, W. Germany, May 1989.

"A Foil Stripper and Terminal Steering Assembly for an FN Tandem", W.G. Weitkamp, SNEAP, October 1988.

"Charging Belt Noise in a Van de Graaff Accelerator", T.A. Trainor, SNEAP, October 1988.

"Sub–Barrier Heavy Ion Fusion", R. Vandenbosch, lectures presented at the 20th International Summer School on Nuclear Physics, Mikolajki, Poland, September 1988.

"The Giant Dipole Resonance and the Deformation of Heated Nuclei", K.A. Snover, Joint

CAP/APS Congress, Montreal, Bull. Am. Phys. Soc. **33**, 1176 (1988).

"The Model 860i: a Turbo Sputter Source", T.A. Trainor, SNEAP, October 1988.

"The Giant Dipole Resonance and the Deformation of Highly Excited Nuclei", K.A. Snover, Proc. of the International Conference on Contemporary Topics in Nucl. Structure Physics, Cocoyoc, Mexico, R.F. Casten et al., eds., World Scientific, 1988, p.251.

"Fundamental Symmetries in the Nuclear Arena", E.G. Adelberger, International Conference on Contemporary Topics in Nucl. Structure Physics, Cocoyoc, Mexico, 1988.

"Fission: The First 50 Years", R. Vandenbosch, International Conference on Nuclear Reaction Mechanism, Calcutta, India, January 3 – 9, 1989.

"High Energy Gamma Emission Following Heavy Ion Collisions", C.A. Gossett, Proceedings of the 26th International Meeting on Nuclear Physics, ed. I. Iori, Ricerca Scientifica ed Educazione Permanente, Supplemento N. 63 (1988).

"Parity Mixing of the 0^+-0^-; T=0 Doublet in ^{14}N", V.S. Zeps, E.G. Adelberger, A. Garcia, C.A. Gossett, H.E. Swanson, W. Haeberli, R.A. Quin and J. Sromicki, Proceeding of the 3rd Conference on the Intersection Between Particle and Nuclear Physics.

"Nuclear Fission: What have we Learned in 50 Years?", R. Vandenbosch , International Conference on Fifty Years Research in Nuclear Fission, Berlin, W. Germany, April 3 – 7, 1989.

"Probing the Spin Distribution in Near–barrier Fusion Reactions", A. Charlop, A. Garcia, S. Gil, S.J. Luke and R. Vandenbosch, Symposium on Heavy Ion Interactions around the Coulomb Barrier, Legnaro, Italy, June, 1988.

"Searches for a Composition–Dependent 'Fifth Force' ", E.G. Adelberger, Bull. Am. Phys. Soc. **34**, 1199 (1989).

"The Giant Dipole Resonance in Highly Excited Nuclei", C.A. Gossett, American Chemical Society Symposium on the Interface Betwen Nuclear Structure and Reactions, Los Angeles, California, September 26 – 29, 1988.

"An Isotopic Biogeochemical Study of Tundra Methane and its Exchange with the Atmosphere", P. Quay, S. King, J. Staley, P.M. Grootes, G.W. Farwell, and R. Gannon, NASA Upper Atmosphere Research Program: Research Summaries, 1986–1987, pp.317–318.

Abstracts:

"Comparison of π^+ and π^- Inclusive Scattering at 100 MeV", D. Rosenzweig, I. Halpern, M. Khandaker, D.W. Storm, (Univ. of Wash); J. Nelson, D. Tieger, S. Wood (MIT Bates); K. Doss, (U. of Sask); J. Amann, R. Boudrie, and D. Drake (LANL), Bull. Am. Phys. Soc., **34**, 1204, 1989.

"Dispersive Contribution to ^{6}Li + ^{12}C, ^{58}Ni Real Potential", S. Kailas, Bull. Am. Phys. Soc. **34**, 1244 (1989).

"Beam Diagnostics for the University of Washington Superconducting Booster", W.G. Weitkamp, R.C. Connolly, H. Fauska, T.J. Irwin. M.A. Howe, J.M. LaCroix, D.D. Leach and H.P. Readdy,

Interational Conference on Electrostatic Accelrators and Boosters, Strasbourg, France, May 24 – 30, 1989.

"High Energy Gamma Production at E/A = 10 MeV", C.A. Gossett, J.A. Behr, S.J. Luke, B.T. McLain, D.P. Rosenzweig, and K.A. Snover, Bull. Am. Phys. Soc. **33**, 1601 (1988).

"Determination of Gamma Mulitplicities using an Electrostatic Deflector", Bull. Am. Phys. Soc., **33**, 1561 (1988).

"A Prototype Continuum Positronium Time Projection Chamber", S.P. Van Verst, C.E. Hyde–Wright, J.G. Cramer, D. Prindle, K. Swartz, T.A. Trainor, and J. Gundlach, Bull. Am. Phys. Soc., **34**, 1173 (1989).

"Giant Dipole γ–rays and Dynamic Shape Changes in Highly Excited Nuclei near A = 90, J.H. Gundlach, K.A. Snover, J.A. Behr, C.A. Gossett, M. Kićinska–Habior (Univ. of Wash); K.T. Lesko (LBL), Bull. Am. Phys. Soc., **34**, 1154 (1989).

"Giant Dipole Gamma–Rays and Dynamic Shape Changes in Highly Excited Nuclei Near A = 90", J.H. Gundlach, K.A. Snover, J.A. Behr, C.A. Gossett, M. Kićinska–Habior; K.T. Lesko (LBL), International Nuclear Physics Conference, São Paulo, Brazil, August 20 - 26, 1989.

"The University of Washington Polarized Ion Source", C.A. Gossett, D.R. Balsley, G.C. Harper, C.M. Bitz, J.K. Eisenberg, and J.A. Rogers, submitted to International Conference on Ion Sources, Berkeley, CA, July 10 – 14, 1989.
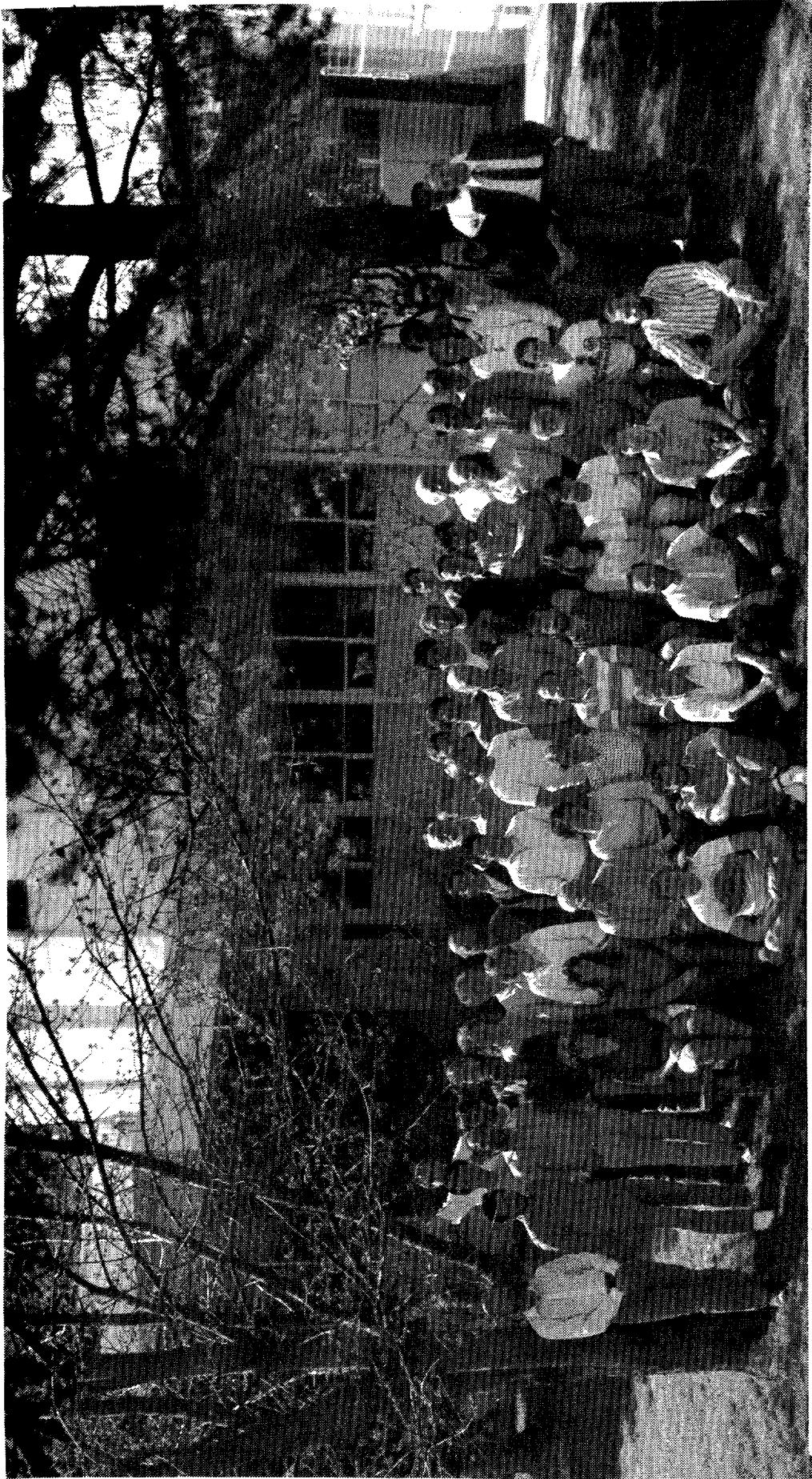
FRONT ROW: A. CHARLOP, A. GARCIA, R. STOWELL, D. WILL, J. BEHR, C. STUBBS

2nd ROW: C. BITZ, D. MARKOFF, F. SCHMIDT, M. RAMIREZ, I. TESS, J. HANNAMANN, T. TRAINOR, M. BRYCE, K. SWARTZ, L. GEISSEL, J. CAGGIANO

3rd ROW: K. SNOVER, Z. DREBI, E. ADELBERGER, S. KAILAS, C. GOSSETT, D. ROSENZWEIG, D. HAMANN, G. FARWELL, M. HOWE, T. BROWN, R. SEYMOUR, T. VANWECHEL, D. PRINDLE, R. COOPER, P. GROOTES

4th ROW: S.P. VAN VERST, J. GUNDLACH, P. WONG, R. STOUT, D. BALSLEY, E. SWANSON, D. STORM, C. HYDE-WRIGHT, W. WEITKAMP, J. EISENBERG, D. CORCORAN, G. HARPER, B. CHRISTMAN, J. ROGERS, H. SIMONS, I. HALPERN, J. LACROIX, D. HODGKINS, J. AMSBAUGH, J. LUKE

NOT PRESENT: C.E. LINDER